7-28-2015

Computation of Intrinsic Breakdown Based on Computational Quantum Mechanics

Ying Sun
University of Connecticut - Storrs, yingsun.sandy@gmail.com

Computation of Intrinsic Breakdown Based on Computational Quantum Mechanics

Ying Sun, PhD

University of Connecticut, [2015]

A first principles quantum mechanical method for estimating intrinsic breakdown field of insulating materials has been implemented based on an average electron model which assumes that breakdown occurs when the average electron energy gain from the electric field exceeds the average energy loss to phonons. The approach is based on density functional perturbation theory and on the direct integration of electronic scattering probabilities over all possible final states, with no adjustable parameters. The computed intrinsic breakdown field for many prototypical materials over a range of elemental compositions and crystal structures compares favorably with experimental data. This model also provides physical insight into the material properties that affect breakdown.

The introduction of dipoles into a polymer can enhance breakdown field as a result of dipole-induced scattering which tends to "cool" hot electrons and thereby inhibits impact ionization. A theoretical analysis of electron scattering by dipoles and phonons is presented which explains temperature dependence of the breakdown field on the basis of the dominant scattering process as a function of temperature. Electron mobility calculations in non-polar and polar polymers produce a quantitative correlation between chemical composition and intrinsic breakdown field. Calculation of dipole scattering limited electron mobility can be used to assess the effect of dipole scattering on the intrinsic breakdown field of polymers.

The problem of hot electron transport and energy loss in insulators at high electric fields is of interest in related to aging of dielectrics. Monte Carlo (MC) simulations provide the basis for a study of hot electron transport at high electric fields in thin polyethylene (PE) films with nanocavities based on energy loss to phonons computed using computational quantum mechanics. The electron trajectories, probability densities, and spatial evolution of the electron energy distribution are presented. Electrons with energy greater than the bandgap (8.8 eV) trigger impact ionization, which can cause avalanche breakdown, while electrons with energy greater than 3-4 eV can cause degradation through bond cleavage. In the presence of nanocavities, high field aging is likely to occur in the immediate vicinity of nanocavities.

Computation of Intrinsic Breakdown Based on Computational Quantum Mechanics

Ying Sun

B.A., Xi'an Jiaotong University, **[2006]**

M.A., Xi'an Jiaotong University, **[2009]**

A Dissertation

Submitted in Partial Fulfillment of the

Requirements for the Degree of

Doctor of Philosophy

at the

University of Connecticut

[2015]

APPROVAL PAGE

Doctor of Philosophy Dissertation

Computation of Intrinsic Breakdown Based on Computational Quantum Mechanics

Presented by

Ying Sun, B.A., M.A.

Major Advisor _____
Steven A. Boggs

Associate Advisor _____
Ramamurthy Ramprasad

Associate Advisor _____
S. Pamir Alpay s

University of Connecticut
[2015]

Acknowledgement

I would like to express my gratitude to my major advisor Prof. Steven Boggs, for his insightful advice, his sincere support, and his generous time and commitment. I have learned so much from his wide knowledge and long research expertise, and clearly there was no limit to how much he was always willing to provide. As his last Ph.D student, I can not say enough how lucky I am.

I would like to express my sincere gratitude to my co-major advisor Prof. Ramamurthy Ramprasad for his guidance through my Ph.D. He is the one who gave me insightful ideas to tackle the difficult problem of calculate “intrinsic breakdown” quantum mechnically. And he gave me an original recepie of calculating breakdown which is the basis of this work. Whenever I encounter difficulties in my research, he is the resource I get my questions answered, and he can always give me the right direction which is impossible without his immense knowledge in density functional theory computations. He also allows me to attend his group meetings, during which I not only get inspired by his enthusiam towards research, but also learned a lot of skills that are benifical lifeime. This work would not have been possible without her guidance, support and encouragement. My gratitude to Prof. Ramamurthy Ramprasad is far beyond what these lines can convey.

I would also like to thank Prof. Pamir Alpay, Prof. Avinash M. Dongare for their valuable comments and suggestions for my PhD study. Special thanks give to Prof. Yang Cao and JoAnne Ronzello for their continious support and kindness help.

I would like to acknowledge my labmates and friends: Kai Zhou, Wen Shu, Shanshan Qin, Lili Zhang, Dominique Bolliger, Ghanshyam Pilania, Clive Bealing, Vinit Sharma, Thinh Pham, Lihua Chen, Chenchen Wang, Zengmin Xia, Satyesh Yadav, and many others.

Special gratitude would go to my beloved family for their never changed love, encouragement and support all through the years.

Table of Contents

List of Tables

List of Figures

CHAPTER 1
INTRODUCTION TO INTRINSIC BREAKDOWN

1.1 Dielectric Breakdown Phenomena

The dielectric breakdown of insulating materials has been a subject of experimental and theoretical investigations for many decades as a result of its technical importance [1]. Whether breakdown is measured using a.c., d.c. or impulse voltage, the breakdown field of solid materials is affected by many factors, e.g., ambient temperature, humidity, test duration, atomic level chemical impurities, and cavities at nanoscopic and microscopic scales. As a result, engineering breakdown of solid dielectrics is highly complex, as large variety of instabilities can occur. The interplay among electrical, mechanical, chemical, and thermal effects makes a general description of engineering breakdown difficult. However, an understanding of breakdown theory is a prerequisite to any approach to the prediction of engineering breakdown.

For discussion purposes, the time over which breakdown occurs can be divided into regions in which differing breakdown processes operate, as shown in Figure 1.1[2].

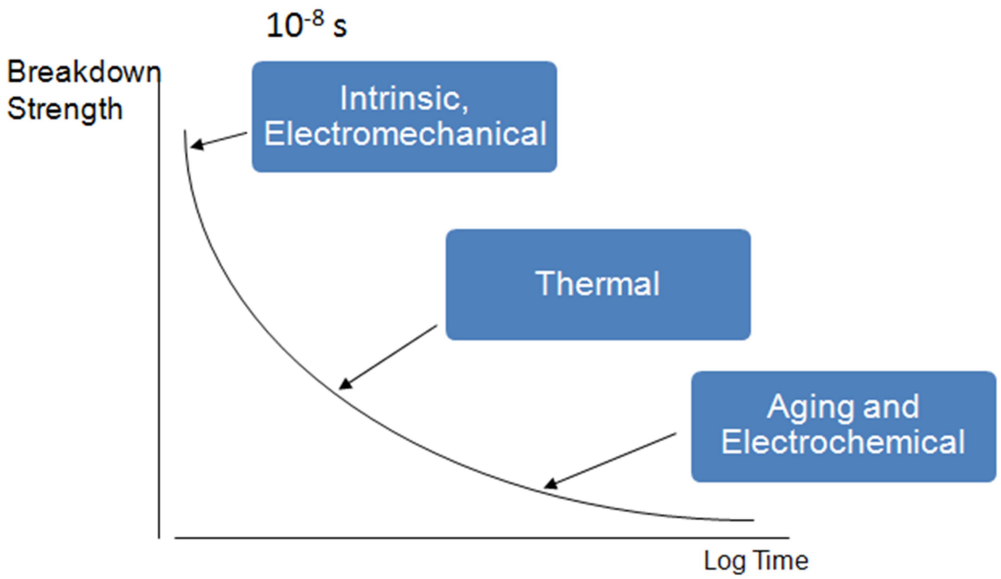

Figure 1.1 Variation of breakdown process with time to breakdown after application of voltage.

1.1.1 Intrinsic Breakdown

If the dielectric material is pure and homogeneous and if the temperature and environmental conditions are controlled suitably, the short time breakdown field of a solid dielectric reaches an upper limit called the intrinsic electric strength, which is an intrinsic property of the material. Experimentally, this highest dielectric strength can be obtained only under ideal experimental conditions when all extraneous influences have been removed, so that the breakdown electric field depends only on the structure of the material and the temperature. Intrinsic breakdown occurs on a time scale of order 10 ns and is therefore considered electronic in nature. The electric field for intrinsic breakdown typically ranges from 100 to 1000 MV/m depending on the material under test [2].

During intrinsic breakdown, the kinetic energy of the electrons and the total number of free electrons increase with the electric field as a result of impact ionization and field emission. Thus the conductivity and the rate at which the electrons gain energy during intrinsic breakdown is an explicit function of electric field.

1.1.2 Thermal Breakdown

Heat is generated continuously by conduction current and dielectric losses in electrically stressed insulation, the heast is transferred to the surrounding medium by thermal conduction through the dielectric and by radiation from its surfaces. If the heat generated exceeds the heat lost to the surrounding medium, the temperature of the insulation increases. The electrical conductivity increases with temperature, and instability is reached when no equilibrium between heat generated and heat dissipated is possible. Thermal effects impose an upper limit of electric field for an insulating material, beyond which instability will occur. The theory of thermal breakdown is macroscopic, involving the generation and transfer of heat in the classical sense.

1.1.3 Electromechanical Breakdown

When solid dielectrics are subjected to high electric fields, failure can occur from electrostatic compressive forces which exceed the mechanical compressive strength. The electrical strength, like the mechanical strength, depends very strongly on cracks and other crystal imperfections.

1.1.4 Electrochemical Deterioration

In the presence of air and other gases or liquids, some dielectric materials undergo chemical changes when subjected to electric fields. Progressive electrochemical degradation of insulating materials can occur from a variety of processes such as chemical instability at high temperatures, electro-oxidation, cracking in the presence of air, ozone, or surfactants, and hydrolysis from moisture and heat.

1.1.5 Local Discharge

In a small gas-filled cavity within a solid dielectric, the field is greater than the average field in the dielectric. Under an a.c. voltage, continuous discharge is likely within such a cavity. Electrons and ions from the discharge bombard the inner surface which can break chemical bonds and eventually initiate an electrical tree. Other breakdown processes include surface breakdown, electrolytic breakdown, electrical treeing, high field aging, etc.

1.2 Historical Overview of Intrinsic Breakdown Theory

In 1932, von Hippel [3] postulated that breakdown occurs when the “average electron” gains energy more rapidly from the electric field than it loses energy to the lattice (i.e., to phonons) for all electron energies less than that needed to produce impact ionization, which is often called von Hippel’s low energy criterion for breakdown [4]. Von Hippel explained breakdown theory qualitatively, e.g., he did not give an expression for the electron-lattice collision rate or electron energy loss rate.

Zener (1934) proposed an alternative mechanism which assumes that breakdown occurs as a result of field emission, e.g., that in an electric field, electrons can tunnel from the valence band to

the conduction band without changing energy [5]. He also derived an expression for the probability that an electron will make a transition to the conduction band; however, Zener's approach is not consistent with the temperature dependence of the intrinsic breakdown field [6].

In 1937 Fröhlich [7] proposed a theory of intrinsic breakdown based on impact ionization which differs from von Hippel's approach primarily in the condition postulated for breakdown. Fröhlich postulated that breakdown occurs when the electric field is sufficiently large that electrons in the high energy tail of the electron energy distribution, which have sufficient energy to cause impact ionization, gain more energy from the field than they lose to phonons (Fröhlich's high energy criterion). Fröhlich made a quantitative calculation of the breakdown field which assumes that only longitudinal optical phonons interact with electrons. His calculation is based on a quantum mechanical derivation of the electron relaxation time. Both von Hippel and Fröhlich neglect the interaction of electrons with nonpolar (i.e., acoustic and transverse optical phonon) modes of vibration.

In 1981, Sparks [8] proposed a breakdown model based on analytical approximations which agrees well with experimental laser breakdown data, including the magnitude and temperature dependence of the breakdown field, pulse-duration dependence, material dependence, and wavelength dependence. The good agreement with measured breakdown field is the result of more realistic electron-phonon scattering rates used in his calculation than had been used by previous investigators, e.g., both acoustic and optical phonons are included. Quantitative calculations of breakdown field by both Fröhlich and Sparks were performed only for alkali halides, since the simple structure of these materials eases the derivation of analytical solutions.

In 1994, D. Arnold from IBM presented a detailed theoretical study of impact ionization related to transport phenomena in SiO_2 thin films [10], in which the Boltzmann transport equation is integrated with the Monte Carlo method using electron-phonon scattering rates derived from photo-induced electron transmission experiments. The study shows that acoustic phonon scattering

accounts for the high energy tail in the electron energy distribution, and breakdown in SiO_2 thin films might be caused by the cumulative degradation of the thin film structures near interfaces, primarily by hot electron-induced hydrogen chemistry. In the last few years [11], first principles quantum mechanical methods for calculation of electron-phonon scattering rates have been pursued. Development of the intrinsic breakdown theory is summarized in Table 1.1.

Table 1.1 Summary of theories of intrinsic breakdown

Year	Contributor	Materials	Brief description
1932	Von Hippel [3][4]	Alkali halides	Qualitative description of avalanche breakdown.
1934	Zener [5]	One dimension lattice	Field Emission Breakdown; tunneling probability for one dimension lattice is given.
1937	H. Fröhlich [7]	Alkali halides	Quantitative calculation of breakdown field; only polar phonons are considered.
1981	M. Sparks *et al*. [8]	Alkali halides	Quantitative calculation of the laser induced breakdown field. Both polar and non-polar phonons are included.
1986	E. Cartier, *et al.* (Brown Boveri) [9]	Organic dielectrics ($n\text{-}C_{36}H_{74}$)	Investigated the transport and relaxation of hot electrons by using electron phonon scattering rates derived from experiments.
1994	D. Arnold *et al*. (IBM) [10]	SiO_2 thin film	Investigated the transport of hot electrons by Monte Carlo method using electron phonon scattering rates derived from experiments.
2007-2010		GaAs and GaP[11], Si[12], Graphene [13]	Electron phonon scattering rates are calculated from first principles
2012	Y. Sun et al. [14]	Ionic and Covalent Crystals	Computational quantum mechanical implementation of von Hippel's low energy criterion.
2014	Y. Sun et al. [15]	Amorphous Materials	Inclusion of dipole scattering in the context of intrinsic breakdown.

1.3 Intrinsic Breakdown Theory

Prediction of intrinsic breakdown requires calculating the number of free electrons and their energy and momentum distributions as a function of applied electric field. Many mechanisms can contribute to the number of conduction band electrons as shown in Figure 1.2 [16].

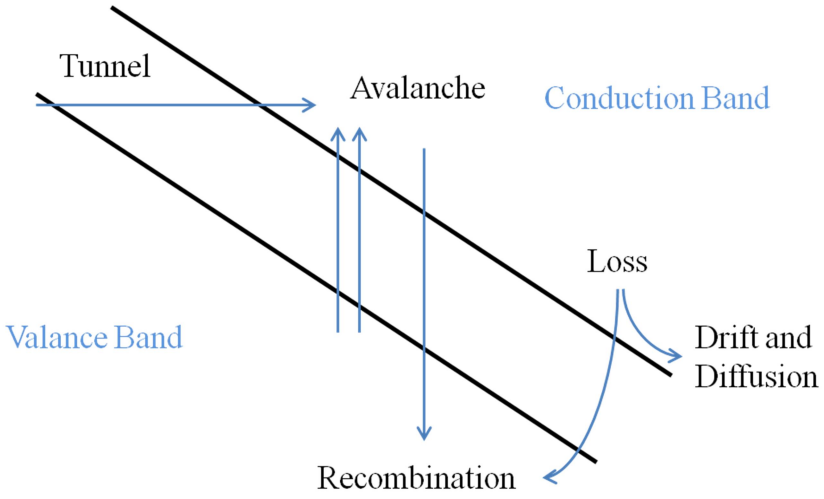

Figure 1.2 Mechanisms which contribute to conduction band electrons.

One of the first systematic theoretical developments along modern lines is that of Zener [5], who proposed that breakdown occurs when the electrostatic field becomes sufficiently strong to ionize the atoms of the insulator by field emission. In effect, an electron in the bulk solid tunnels from the filled valence band to the conduction band without changing its energy. The energy distribution function of the free electrons remains unaltered except that the total number of electrons in the conduction band increases rapidly. The rate at which electrons tunnel from the valence band to the conduction band under the influence of electric field is independent of the thermal motion of the lattice. Zener gave the probability, p, per unit time that an electron tunnels from the filled band to the empty conduction band in the presence of electric field F for a one-dimensional lattice,

$$p = \frac{eFa}{2\pi\hbar}\exp\left(-\frac{maE_g^2}{4\hbar^2 eF}\right). \tag{1.1}$$

where a is the lattice constant, E_g is the energy gap, e and m are the elementary charge and mass respectively. However, calculations based on Zener's field emission theory predict an order of magnitude larger of breakdown field relative than is measured experimentally for sodium chloride [17]. Also, measurements of Buehl and von Hippel [6] show that the breakdown field in alkali halides increases with increasing temperature in the range below room temperature whereas Zener's theory predicts a decrease in breakdown field with temperature, which seems to rule out field emission. The strong breakdown field dependence with temperature measured experimentally is explained very naturally from avalanche theory (as temperature increases, greater numbers of phonons are available to interact with electrons and transfer energy to the lattice, which increases the breakdown field).

1.4 Avalanche Breakdown Theory

Electron avalanche breakdown is the prevalent theory for intrinsic breakdown and is supported by many investigations (e.g., von Hippel [3], Fröhlich [7], Sparks [8], Seitz [17], *etc.*) The general features of electron avalanche breakdown theory include the acceleration of conduction electrons by the electric field, the loss of energy from electrons to phonons, the generation of a secondary conduction electrons accompanied by a loss of kinetic energy of the exciting electron through impaction ionization, and the repetition of impact ionization until the electron concentration is sufficient to damage the material.

Descriptions of electron behavior below and above the threshold electric field for impact ionization are presented in Figure 1.3. As shown in Figure 1.3a, when the electric field is less than the avalanche threshold electric filed （$F<F_{th}$）, the electron energy distribution achieves steady state, as the energy gain from the external electric field is balanced by energy loss from collisions with phonons, which inhibit electron energy gain from the field by scattering in momentum space which sometimes changes momentum to the opposite direction from that imparted by the electric filed. As a result of such collisions, the heated lattice is shown vibrating about its equilibrium

position. This process will not cause avalanche breakdown, but the phonons created by collisions will result in a steady increase in the lattice temperature which must be balanced by heat loss to the environment.

At a sufficiently high electric field, (Figure 1.3b), the electron energy achieves the threshold at which high-energy electrons ionize the lattice. An electron with initial velocity V_i undergoes an collision with the lattice and creates a second free electron with velocity V_{f2}. These two electrons then undergo collisions with the lattice resulting in a total of four electrons, and the repetition of this process leads to carrier multiplication. As long as the electrons can repeat this process before electron-hole recombination or electron diffusion, the process will generate enough electrons to damage the material.

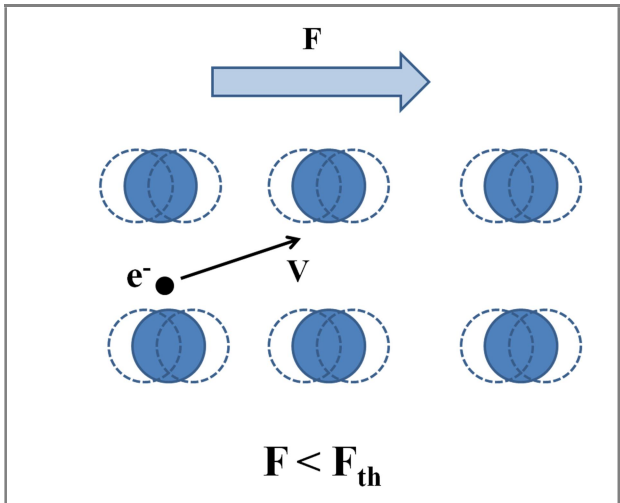

Figure 1.3(a) Energy balance of a free electron when the electric field is less than the avalanche threshold electric field (F<Fth).

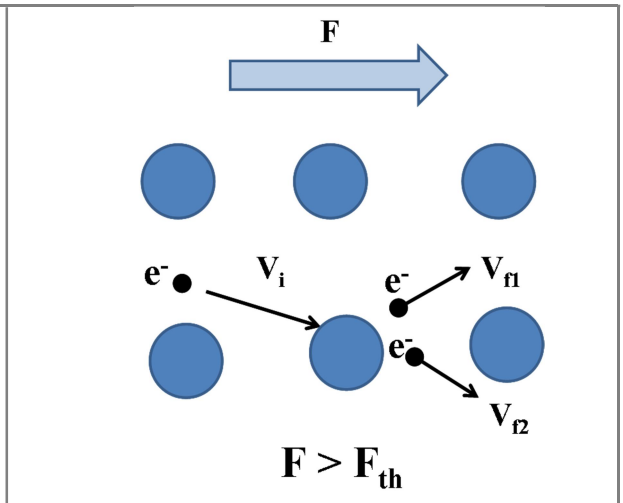

Figure 1.3(b) Onset of avalanche when the electric field is larger than the avalanche threshold electric field (F>Fth).

1.4.1 von Hippel's Low Energy Criterion and Fröhlich's High Energy Criterion

In 1932, von Hippel [3] proposed that breakdown in solids is a by-product of the production of electron avalanches through impact ionization. He pointed out that any free electrons in a solid under the influence of electric field are subject to two opposing influences. The electrons tend to be accelerated by the field and retarded by the "friction" resulting from interaction with the

vibrational waves of the lattice. He postulated that breakdown occurs when the average electron gains energy more rapidly from the field than it loses energy to the lattice for all electron energies less than that needed to produce impact ionization. Von Hippel's theory is not a quantitative treatment (e.g., he did not give an expression for the rate at which a conduction electron would lose energy to the lattice), but provides the correct order of magnitude for the intrinsic breakdown field, explains the occurrence of avalanches, and the temperature dependence of intrinsic breakdown.

In 1937 Fröhlich [7] proposed a theory based on impact ionization which differs from von Hippel's hypothesis primarily in the condition postulated for breakdown. Fröhlich also postulated that breakdown occurs as a result of acceleration of electrons through a friction barrier arising from interaction between electrons and lattice waves. Fröhlich's high energy criterion is based on the high energy tail of the electron energy distribution which, quite logically, should precipitate breakdown. However, he pointed out that the critical conditions are determined by the behavior of electrons which have energy sufficient to ionize the atoms of the solid. In essence, his theory rests on the assumption that when the breakdown field is reached, the distribution function describing the spread of electron energies will have a maximum well below the ionization energy but will possess a tail in the region of the ionization energy. The behavior of the electrons in this tail determines breakdown.

Based on the assumption that only longitudinal polarization waves interact with the electrons, Fröhlich derived the electron relaxation time of alkali halides using quantum mechanics by calculating the interaction of electrons with longitudinal polarization waves. Fröhlich's quantitative calculation of the breakdown field for alkali halides based on the balance between electron energy gain and energy loss agrees with experimental results of von Hippel.

Figure 1.4 shows a schematic of von Hippel's low energy and Fröhlich's high energy criteria [1]. The red lines represent the rate of energy transfer from the field to electrons as a function of

electron energy and applied field F, while the black line represents the rate of energy loss to phonons as a function of electron energy E.

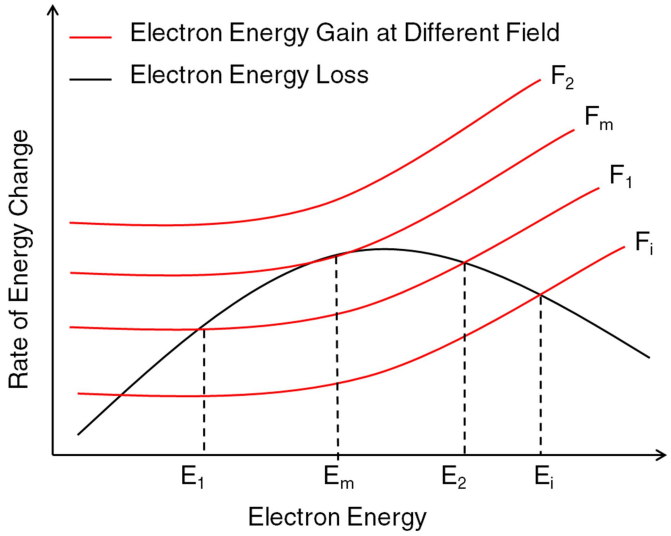

Figure 1.4 Schematic of von Hippel's low energy and Fröhlich's high energy criteria.

When the electric field, F is sufficiently low, i.e., F_1 in **Error! Reference source not found.**4, the energy gain and loss balance at two electron energies, E_1 and E_2. As the field increases, a field F_m is reached where the two solutions merge into one E_m. For higher values of the field, e.g., F_2, no solution exists. Thus if $F>F_m$, the energy gain will larger than the energy loss for all E so that every free electron will increase its energy to the threshold of impaction ionization. This led von Hippel to define F_m as the breakdown field.

Following Fröhlich, even if $F<F_m$, equilibrium is not possible. Consider an electron in field F_1, for which two solutions are possible. Solution E_1 represents a stable equilibrium, while E_2 is unstable, since for $E>E_2$, electron energy increases indefinitely. Suppose that the energy for ionization (E_i) is such that $E_2>E_i$, in which case the electrons which have energies in excess of E_2 can ionize lattice atoms and thus reduce their energy. However, if $E_2<E_i$, electrons with energy interval E_2 to E_i will increase their energy on average which results in a continuous increase in the total energy of the electron system, and steady state is impossible. Thus the maximum field for a steady state (i.e., the "critical" field) corresponds to $E_2=E_i$. Once electrons achieve energies in

excess of E_2, they can accelerate rapidly to energies of order E_i. Perhaps the best that can be said of Fröhlich's high energy criterion is that it provides a lower limit for fields which give appreciable ionization, while the intrinsic breakdown field is determined by the degree of ionization which is required to produce avalanche breakdown.

1.4.2 Spark's Average Electron Model and Diffusion Model

In 1981, Sparks proposed an average electron and diffusion model based on avalanche breakdown theory which agrees well with laser induced breakdown data for alkali halides in terms of the breakdown field dependence, temperature dependence, pulse-duration dependence, wavelength dependence, and material dependence [8]. The good agreement is obtained as a result of improved energy dependent estimates of the electron-phonon relaxation frequencies relative to previous investigators, e.g., the contributions of both optical and acoustic phonons to electron energy loss and diffusion in energy space are included. The breakdown field is calculated by solving an eigenvalue equation obtained from a diffusion transport equation in energy space, i.e., in Sparks' model, electron energy gain from the field and loss to phonons contributes to diffusion of electron energy in a classical approximation, the instability of which indicates breakdown.

The average electron model affords the simplest mathematical treatment of intrinsic breakdown, in which breakdown occurs when the energy gain from the electric field exceeds the energy loss to phonons for all electron energy less than that to produce impact ionization. The limitations of the average electron model stem both from the difficulty of treating the energy dependence of energy gain and loss properly, and from the neglect of electron diffusion in energy space. Holway and Fradin [18] demonstrated that avalanche breakdown cannot be truly an "average electron" phenomenon. Breakdown can occur without having electric fields so strong that every electron below the ionization energy is gaining energy on the average. An electron typically gains energy over part of the energy range by diffusion to greater energy while, on average, electrons loose

more energy than they gain. Spark's energy diffusion model is a classical approach to approximating the effect of electron–phonon interaction on the electron energy distribution.

The simple crystal structure of alkali halides allows an analytical solution of electron relaxation time (the reciprocal of which is electron–phonon scattering rate) and electron energy loss rate. Sparks derived an analytical solution for both of these parameters by treating the contribution of both polar (longitudinal optical phonons) and nonpolar (acoustical and transverse optical phonons) phonons to electron–phonon scattering. Inaccuracy of the theoretical calculation may stem from various approximations made in order to obtain these analytical expressions. The greatest limitation of Sparks' model is that the analytical expression for electron relaxation time and energy loss rate is derived only for alkali halides and cannot be extended to other more complex materials, which makes the theoretical investigation of many technically important materials (such as SiO_2 and PE) impossible.

1.5 Carrier Scattering Mechanisms

1.5.1 Electron Phonon Scattering

The electron relaxation time (the reciprocal of which is the scattering rate) determines the time interval over which electrons gain energy from the field before a collision with the lattice. The scattering rate also determines the rate of energy loss per unit time. The electron-phonon scattering rate controls both the electron energy gain and energy loss, the balance of which determines the breakdown field. As a result, the proper interpretation of electron-phonon scattering rate is a key factor in predicting the breakdown field.

The simple crystal structure of alkali halides facilitates an analytical derivation of electron-phonon scattering rates based on reasonable approximations. Fröhlich derived the electron LO-phonon scattering rates for alkali halides by calculating the interaction of electrons with longitudinal polarization waves. Fröhlich's polar interaction describes only part of the relevant interaction for the hot electrons involved in the avalanche development. Sparks provided an

analytical solution for electron phonon scattering rates by treating the contribution of both polar (longitudinal optical phonons) and non-polar (acoustical and transverse optical phonons) phonons to electron-phonon scattering respectively. The contribution of polar phonons (longitudinal optical phonons) is inherited from Fröhlich's electron LO-phonon scattering expression. Sparks derived the electron-phonon scattering rates from non-polar phonon modes, which is the essential to compute realistic scattering rates.

Analytical expressions of electron phonon scattering rates can only be obtained by various approximations which are only appropriate for alkali halides (e.g., masses and charges of each sort of ion should be uniformly distributed [7]). The scattering rates of more complex materials can be obtained by photon-induced electron transmission experiments as developed at Brown Boveri Research (later ABB). Investigations of hot electron transport and impact ionization were carried out based on electron-phonon scattering rates derived experimentally. Similar research was carried out by IBM [10] (mostly on SiO_2), and Brown Boveri [9] (mostly on organic dielectrics).

The First principles quantum mechanical methods for calculation of electron-phonon scattering rates have been pursued only in the last few years with the development of computational quantum mechanics. Jelena Sjakste et al. [11] calculated electron-phonon scattering times for excited electrons interacting with short-wavelength phonons in semiconductors GaAs and GaP. Restrepo et al. [12] calculated the electron-phonon scattering rate in silicon from density functional perturbation theory (DFPT), and Borysenko et al. [13] investigated electron-phonon interaction in graphene from first principles.

1.5.2 Dipole Scattering

Dipoles also influence charge carrier mobility through dipole scattering, i.e., the Coulomb field associated with the dipoles interacts with charge carriers to change their motion, which reduces electron mobility. The effect on the breakdown field of small mole fractions of fluorine atoms incorporated into plasma-polymerized polyethylene has been studied by applying rectangular

voltage pulses. The increased breakdown field after incorporation of fluorine atoms into the film for pulse widths less than 5 μs was explained on the basis of electron scattering by C-F dipoles [19]. Work of Austen and Pelzer [20] on polyethylene and vinylite showed that the dipoles act as scattering centers which increase the breakdown field at low temperature. The very high breakdown field of atomically flat, amorphous aromatic polythiourea films suggests that the randomly oriented dipoles (thiourea group) and the glass-phase structure provide strong scattering of charge carriers which results in greater breakdown field and reduced conductivity compared with nonpolar polymers [21]. Such experimental evidence demonstrates that dipoles play an appreciable role in determining the dielectric breakdown field of polar polymers. Frohlich's early theoretical work demonstrated that polar groups in polymers act as scattering centers for hot electrons and thereby decrease the electron mean free path, which increases the breakdown field at low temperature [7]. Understanding the effect of dipole scattering on breakdown field at a fundamental level can provide guidance for the design of dielectrics with improved breakdown field.

1.6 Thesis Organization

Chapter 1 provided an overview of intrinsic breakdown theory and carrier scattering mechanisms with a brief introduction of the complex dielectric breakdown phenomenon. Previous intrinsic breakdown theories were described, including Zener's field emission theory, Von Hippel's Low Energy and Fröhlich's High Energy Criterion, Spark's average electron model and energy diffusion model.

Chapter 2 provides a brief introduction to the computational methods used in the present work, which includes density functional theory (DFT), density functional perturbation theory (DFPT) and phonon calculations using DFT.

Chapter 3 presents a predictive, parameter-free, first principles method for estimating the intrinsic breakdown strength of crystalline insulators based on electron-phonon scattering.

Chapter 4 addresses the effect of dipole scattering on the intrinsic breakdown field of polymers by performing electron mobility calculations based on electron interactions with dipoles and phonons in non-polar and polar polymers.

In Chapter 5, Monte Carlo (MC) simulations are described to examine the electron energy distributions as a function of field and nanocavity size as a first step down the path from intrinsic breakdown to engineering breakdown.

The last chapter provides a summary and proposes extensions to the work described in this thesis.

1.7 Summary of Contributions

Next generation insulating materials require high dielectric constant, high thermal stability, high breakdown field, and low loss. The overarching goal of this work is to study the breakdown process with the focus on the intrinsic breakdown, in order to identify (or develop an intuition for) the fundamental (chemical) factors that control the breakdown field and which provide a basis for search strategies for insulating materials (especially in polymers) with a potential for high breakdown field. The main contributions of this study are summarized as follow:

A predictive, parameter-free first principles method for estimating the intrinsic breakdown field of dielectrics was developed which produced good agreement with literature values for intrinsic breakdown for a wide range of ionic and covalent bonded inorganic materials. Intrinsic breakdown can be correlated with both bandgap and phonon cutoff frequency, although the relationships differ with crystal structure.

A theoretical analysis of electron scattering by dipoles and phonons is presented which provides the basis for explaining temperature dependence of breakdown field on the basis of the dominant scattering process as a function of temperature. By performing electron mobility calculations in non-polar and polar polymers, a quantitative correlation between chemical composition and intrinsic breakdown field can be established. Calculation of dipole scattering limited electron

mobility can be used to assess the effect of dipole scattering on the intrinsic breakdown field of polymers.

A MC simulation method was developed to examine the electron energy distributions as a function of electric field and the likely effect of nanocavities on high field aging and breakdown. Nanocavities increase the number of high energy electrons, which should accelerate the high field aging. The electrons with energy greater than the bandgap (8.8eV) trigger impact ionization, which can lead to avalanche breakdown, while electrons with energy larger than 3-4eV can cause degradation of the dielectric.

1.8 References

[1] R. Stratton, "Progress in Dielectrics", vol. 3, J. B. Birks and J. Hart, Ed. New York, NY: Wiley, pp. 235-292, 1961.

[2] Ravindra Arora & W. Mosch, "High Voltage Insulation Engineering", New Age International, 2005.

[3] A. von Hippel, "Electronic conduction in insulating crystals under very high field strength", Phys. Rev., vol 54, pp.1096-1102, 1938.

[4] A. von Hippel, "Electric breakdown of solid and liquid insulators," J. App. Phys., vol. 8, pp. 815-832, 1937.

[5] C. M. Zener, "A theory of the electrical breakdown of solid dielectrics," Proc. Roy. Soc., 145, pp. 523-529, 1934.

[6] R. C. Buehl and A. von Hippel, "Electric breakdown. Strength of ionic crystals as a function of temperature", Phys. Rev., vol. 56, pp. 941-947, 1939.

[7] H. Frohlich, "Theory of electrical breakdown in ionic crystals," Proc. Roy. Soc., 160, pp. 230-241, 1937.

[8] M. Sparks, D. L. Mills, R. Warren, T. Holstein, A. A. Maradudin, L. J. Sham, E. Loh Jr., and D. F. King, "Theory of electron-avalanche breakdown in solids", Phys. Rev. B, vol. 24, pp. 3519-3536, 1981.

[9] E. Cartier and P. Pfluger, "Transport and relaxation of hot conduction electrons in an organic dielectric", Phys. Rev. B, vol. 34, no. 12, pp.8822-8827, 1986.

[10] D. Arnold, E. Cartier, and D. J. Dimaria, "Theory of high-field electron transport and impact ionization in silicon dioxide", Phys. Rev. B, vol. 49, pp.10278-10297, 1994.

[11] J. Sjakste, N. Vast, and V. Tyuterev, "Ab initio method for calculating electron-phonon scattering times in semiconductors: Application to GaAs and GaP", Phys. Rev. Lett., vol. 99, pp. 236405-1-4, 2007.

[12] O. D. Restrepo, K. Varga, and S. T. Pantelides, "First-principles calculations of electron mobilities in silicon: Phonon and Coulomb scattering", Appl. Phys. Lett., vol. 94, pp. 212103-1-3, 2009.

[13] K. M. Borysenko, J. T. Mullen, E. A. Barry, S. Paul, Y. G. Semenov, and J. M. Zavada, "First-principles analysis of electron-phonon interaction in graphene," Phys. Rev. B, vol. 81, pp.121412 (R) - 1-4, 2010.

[14] Y. Sun, S. A. Boggs, R. Ramprasad, "The intrinsic electrical breakdown strength of insulators from first principles", Appl. Phys. Lett. 101, 132906, 2012.

[15] Y. Sun, S. A. Boggs, R. Ramprasad, “The Effect of Dipole-Induced Scattering on the Intrinsic Breakdown Field of Polymers”, IEEE Transactions on Dielectrics and Electrical Insulation (accepted June 06, 2014).
[16] Gary L. Wood and Edward J. Sharp, Laser Induced Optical Damage in Solids, final report CECOM Center for Night Vision & Electro-Optics July1991.
[17] F. Seitz, “On the theory of electron multiplication in crystals”, Phys. Rev., vol. 76, pp. 1376-1393, 1949.
[18] Lowell H. Holway and D. W. Fradin, “Electron avalanche breakdown by laser radiation in insulating crystals”, J. App. Phys, vol.46, No.1, pp.279-291, 1975.
[19] T. Nakano. M. Fukuyama, H. Hayashi, K. Ishii and Y. Ohki, “Effect of polar groups on the electrical breakdown strength of plasma-polymerized films”, IEEE Trans Dielectr. Electr. Insul, vol. 25, No. 6, 1085, 1990.
[20] A. E. W. Austen, H. Pelzer, “Electric strength of vinylite and its temperature dependence”, E.R.A. Report Ref. L/T 149, 1944.
[21] Shan Wu , Weiping Li , Minren Lin , Quinn Burlingame , Qin Chen , Andrew Payzant , Kai Xiao , and Q. M. Zhang, “Aromatic polythiourea dielectric with ultrahigh breakdown field strength, low dielectric loss and high electric energy density”, Adv. Mater, 25, pp. 1734-1738, 2013.

CHAPTER 2
DFT AND PHONON CALCULATION IN DFT

2.1 Introduction to Density Functional Theory (DFT)

Density Functional Theory (DFT) is presently the most successful and also the most promising approach to compute the electronic structure of matter. The only required inputs for DFT calculation are the electronic and ionic charges and masses, which make it parameter-free, i.e., free from any experimental input. Such methods are also referred to "first-principles" or "ab initio" techniques.

DFT can predict a variety of molecular properties, including molecular structure, vibrational frequencies, atomization energies, ionization energies, electric and magnetic properties, reaction path, etc. Its applicability ranges from atoms, molecules and matter made therefrom, to nuclei and quantum and classical fluids. For the past 30 years, density functional theory has been the dominant method for the quantum mechanical simulation of periodic systems as shown in Figure 2.1.

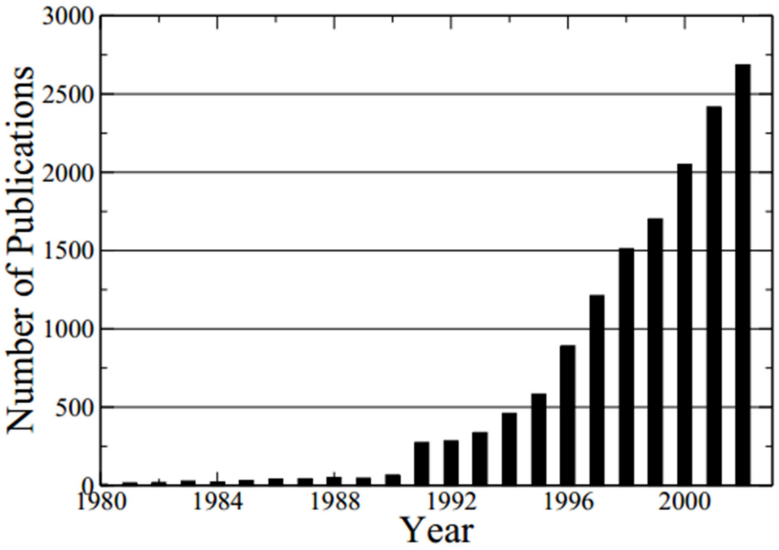

Figure 2.1 The number of publication where the phrase "density functional theory" appears in the title or abstract (taken from the ISI Web of Science)

This chapter provides a very brief introduction to the basic concepts underlying density functional theory and outlines the features that have led to its widespread adoption. A detailed description is avoided, as conventional DFT is well established and documented in the literature. A number of reviews and books describe DFT in detail is available [1][2][3].

2.1.1 The Schrödinger Equation

The basic equation which all computational quantum mechanical methods aspire to solve is the Schrödinger equation. One simple form of the time independent, nonrelativistic Schrödinger equation is

$$H\psi = E\psi \,. \tag{2.1}$$

In this equation, H is the Hamiltonian operator and ψ is a set of solutions, or eigenstates, of the Hamiltonian. Each of these solutions ψ_n, has an associated eigenvalue, E_n, a real number that satisfies the eigenvalue equation. The detailed definition of the Hamiltonian depends on the physical system being described by the Schrödinger equation. For several well-known physical systesm, such as the particle in a box or a harmonic oscillator, the Hamiltonian has a simple form, and the Schrödinger equation can be solved exactly. Properties of the hydrogen atom can be determined by solving the Schrödinger equation (2.1) analytically for the single electron of the hydrogen atom subjected to the electrostatic field of the nucleus. In larger atoms, electrons interact, which prohibits analytical solutions. Solving a system of interacting quantum mechanical particles is referred to as the "Many Body" problem, which, in spite of its simple formulation, is among the most complicated problems in computational physics.

2.1.2 Many Body Problem

The Many Body problem is the problem of determining the wavefunctions and energies of a system consisting of *N* electrons and *M* nuclei which form a molecule or a solid. According to the Born-Oppenheimer approximation, the much heavier nuclei can be considered fixed classical particles while studying electron dynamics [4]. Thus, the Many Body problem is reduced to

determining the behavior of N electrons, as described by the time independent Schrödinger equation [5]

$$\left[-\frac{\hbar^2}{2m}\sum_{i=1}^{N}\nabla_i^2+\sum_{i=1}^{N}V(\mathbf{r}_i)+\sum_{i=1}^{N}\sum_{j<i}U(\mathbf{r}_i,\mathbf{r}_j)\right]\psi=E\psi \qquad (2.2)$$

where m is the electron mass. The three terms in brackets in equation (2.2) define, from the left, the kinetic energy of each electron, the interaction energy between each electron and the collection of atomic nuclei M, and the interaction energy between electrons. For the Hamiltonian we have chosen, ψ is the electronic wave function, which is a function of each of the spatial coordinates of each of the N electrons, so $\psi = \psi(\mathbf{r}_1,\ldots, \mathbf{r}_N)$, and E is the groundstate energy of the electrons. The physical interpretation of the wave function $\psi(r)$ is the square of its absolute value $|\psi|^2$ provides the probability of finding the particle at the location $\mathbf{r}_1, \mathbf{r}_2,\ldots, \mathbf{r}_N$.

If we could solve the Schrödinger equation, we could predict the behavior of any electronic system. However, it is very challenging to solve the Schrödinger equation for practical materials. First, many electron wave functions $\psi(\mathbf{r}_1,\ldots, \mathbf{r}_N)$ is a function of $3N$ variables, where N is the number of electrons. For example, in a single molecule of CO_2, the full wave function is a 66-dimension function (3 dimensions for each of the 22 electrons) [5]. Second, the Schrödinger equation is a many-body problem where N electrons interact with each other. As shown in equation (2.2), the third term in the Hamiltonian describes electron–electron interactions is the most problematic. The form of this contribution means that the individual electron wave function cannot be found without simultaneously considering the individual electron wave functions associated with all the other electrons.

Solution of many body problems generally requires the use of approximations, of which the most basic is the independent electron approximation, the Hartree theory and Hartree–Fock (HF) theory. The Hartree-Fock equations describe non-interacting electrons under the influence of a mean field potential consisting of the classical Coulomb potential and a non-local exchange

potential. The lack of proper representation of electron correlation and its large computation scaling with the system size ($\propto N^4$) renders HF a poor method for studying solids [6][7]. Other methods have been developed to solve the Many Body problem with a better representation of electron correlation than used in the HF formulation. Some of these methods, such as the Configuration Interaction (CI) and the Couple Cluster (CC) methods, are similar to HF in starting with an assumption of Ψ and proceeding through a variational principle, while others are based on perturbation theory such as Møller–Plesset (MP) method [6][8][9]. What is common among the methods mentioned so far is that they solve for Ψ directly. The CI, CC, and MP methods are more accurate than HF. However due to the computational expense, the routine application of such methods to realistic models of systems of interest is not practical and not likely to become so despite rapid advances in computer technology.

2.1.3 DFT- From Wave Functions to Electron Density

Density Functional Theory (DFT) has the double advantage of being able to treat many problems to a sufficiently high accuracy, as well as being computationally simple (simpler even than the Hartree scheme).

Solving the Schrödinger equation is the fundamental problem of quantum mechanics; however, the wave function for any particular set of coordinates cannot be observed directly. The quantity of physical interest is the probability that a set of N electrons in any order have coordinates $\mathbf{r}_1,\ldots,\mathbf{r}_N$. Representing the full wave function by a product of individual one electron wave functions, $\psi(\mathbf{r}_1,\ldots, \mathbf{r}_N)= \psi_1(\mathbf{r})\ \psi_2(\mathbf{r})\ \psi_N(\mathbf{r})$ is a good approximation, which is known as a Hartree product. A closely related quantity is the density of electrons at a particular position in space, $n(\mathbf{r})$, which can be written in terms of the individual electron wave functions as

$$n(\mathbf{r}) = 2\sum_i \psi_i^*(\mathbf{r})\psi_i(\mathbf{r}) \qquad (2.3)$$

The factor of 2 appears because electrons have spin, and the Pauli exclusion principle states that each electron wave function can be occupied by two separate electrons provided they have different spins. The work of Hohenberg and Kohn (HK) in 1964 [10] and the derivation of a set of equations by Kohn and Sham (KS) in 1965 [11] establish the theoretical basis of DFT. The work of HK and KS maps the problem of N interacting electrons (in general fermions) subjected to an external potential into a problem of N non-interacting electrons subjected to an effective potential. The basic idea of DFT is to solve the Many Body problem in terms of electron density $n(\mathbf{r})$.

(i) The first Hohenberg and Kohn theorem: The ground-state energy from Schrödinger's equation is a unique functional of the electron density.

This theorem states that there exists a one-to-one mapping between the ground-state wave function and the ground-state electron density. Another way to interpret Hohenberg and Kohn's result is that the ground-state electron density determines uniquely all properties, including the energy and wave function, of the ground state, which means that we can think about solving the Schrödinger equation by finding a function of three spatial variables (3 variables), the electron density, rather than the wave function ($3N$ variables). Although the first Hohenberg–Kohn theorem proves that a functional of the electron density exists that can be used to solve the Schrödinger equation, the theorem do not provide a basis for determining the functional. The second Hohenberg–Kohn theorem gives the form of the functional.

(ii) The second Hohenberg–Kohn theorem states: The electron density that minimizes the energy of the overall functional is the electron density which corresponds to the full solution of the Schrödinger equation.

In practice, this variational principle is used with approximate forms of the functional. According to the two HK theorems, determining the ground state energy, ground state electron density, and, consequently, the ground state properties of N interacting electrons subjected to an

external potential is reduced to the problem of minimizing a functional of electron density. The energy functional described by the Hohenberg-Kohn theorem can be written in terms of the single-electron wave functions, $\psi_i(\mathbf{r})$, as

$$E\left[\{\psi_i\}\right] = E_{known}\left[\{\psi_i\}\right] + E_{XC}\left[\{\psi_i\}\right], \tag{2.4}$$

where the functional has been split into a collection of terms which can be written in a simple analytical form, $E_{\text{known}}[\{\psi_i\}]$, and everything else E_{XC},

$$E_{known}\left[\{\psi_i\}\right] = -\frac{\hbar^2}{m}\sum_i \int \psi_i^* \nabla^2 \psi_i d^3r + \int V(\mathbf{r}) n(\mathbf{r})\, \mathrm{d}^3 r + \frac{e^2}{2}\iint \frac{n(\mathbf{r})n(\mathbf{r}')}{|\mathbf{r}-\mathbf{r}'|} d^3r d^3r' + E_{\text{ion}} \tag{2.5}$$

The terms on the right of equation (2.5) are, in order, the electron kinetic energies, the Coulomb interactions between the electrons and nuclei, the Coulomb interactions between pairs of electrons, and the Coulomb interactions between pairs of nuclei. The other term, $E_{\text{XC}}[\{\psi_i\}]$, is the exchange–correlation functional, which includes all the quantum mechanical effects that are not included in the "known" terms. The approximation of the unknown term $E_{\text{XC}}[\{\psi_i\}]$, plays a central role in DFT [12].

In 1965 Kohn and Sham (KS) showed that the task of finding the correct electron density can be expressed as the solution to a set of equations, each of which involves only a single electron, The Kohn–Sham equations have the form,

$$\left[-\frac{\hbar^2}{2m}\nabla^2 + V_{ext}(\mathbf{r}) + V_H(\mathbf{r}) + V_{XC}(\mathbf{r})\right]\psi_i(\mathbf{r}) = \varepsilon_i \psi_i(\mathbf{r}). \tag{2.6}$$

The Kohn–Sham equations are single electron wave functions that depend on only three spatial variables $\psi(\mathbf{r})$. The main difference between the Kohn–Sham equations and the full Schrödinger equation (2.2) is the lack of summations over all electrons. The left-hand side of the Kohn–Sham equations contain three potentials, V_{ext}, V_H, and V_{XC}. The first term V_{ext} is the "known" part of the total energy functional given above (equation(2.5)), which defines the interaction between an electron and the collection of atomic nuclei. The second term V_H is the Hartree potential defined by

$$V_H(\mathbf{r}) = \mathrm{e}^2 \int \frac{n(\mathbf{r}')}{|\mathbf{r}-\mathbf{r}'|} d^3r'. \tag{2.7}$$

This potential describes the Coulomb repulsion between the electron considered in one Kohn–Sham equation and the total electron density defined by all electrons in the problem. The Hartree potential includes a self-interaction contribution because the electron in each Kohn–Sham equation is also part of the total electron density, so part of V_H involves a Coulomb interaction between the electron and itself. The self-interaction is unphysical, and the correction for it is one of several effects that are lumped together into the final potential in the Kohn–Sham equations, V_{XC}, which defines exchange and correlation contributions to the single electron equations. V_{XC} can be defined formally as a "functional derivative" of the exchange–correlation energy:

$$V_{XC}(\mathrm{r}) = \frac{\delta E_{XC}(\mathbf{r})}{\delta n(\mathbf{r})} \tag{2.8}$$

The Kohn-Sham approach achieves an exact correspondence of the density and ground state energy of a system consisting of non-interacting Fermions and the "real" many body system described by the Schrödinger equation as shown in Figure 2.2.

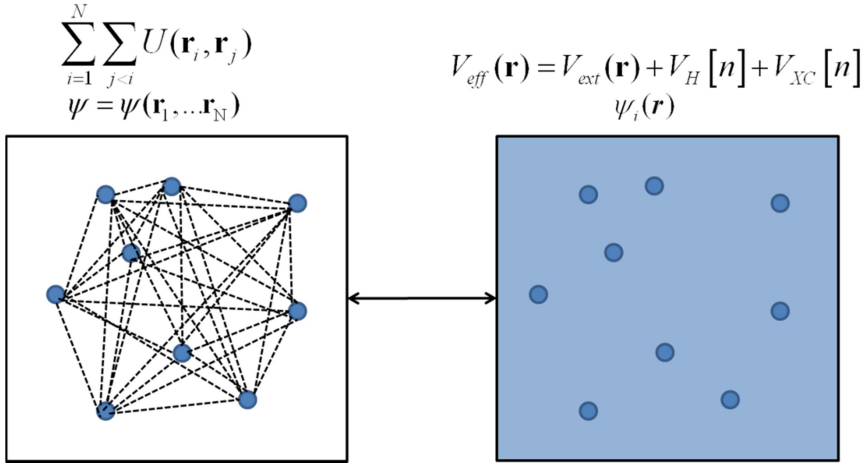

Figure 2.2 The relationship between the "real" many body system (left) and the non-interacting system of Kohn Sham density functional theory (right).

Solving equations (2.6)(2.7) and (2.8) self consistently provides an exact solution of the Many Body problem of *N* interacting electrons subject to an external potential [11]. Figure 2.3 gives the self-consistent calculation flowchart of DFT. The numerical implementation of the self-consistent algorithm involves many approximations. Some approximations are dictated by the discrete nature of numerical methods, such as the need for a basis set to represent the wavefunctions, and some are related to the numerical techniques used to solve the system of equations. The main conceptual approximations used in the implementation of DFT are: the exchange-correlation approximation $V_{XC}(r)$, basis set approximation (to represent the wavefunctions), and pseudopotentials approximation (to represent the interaction of the nuclei and core electrons with valence electrons).

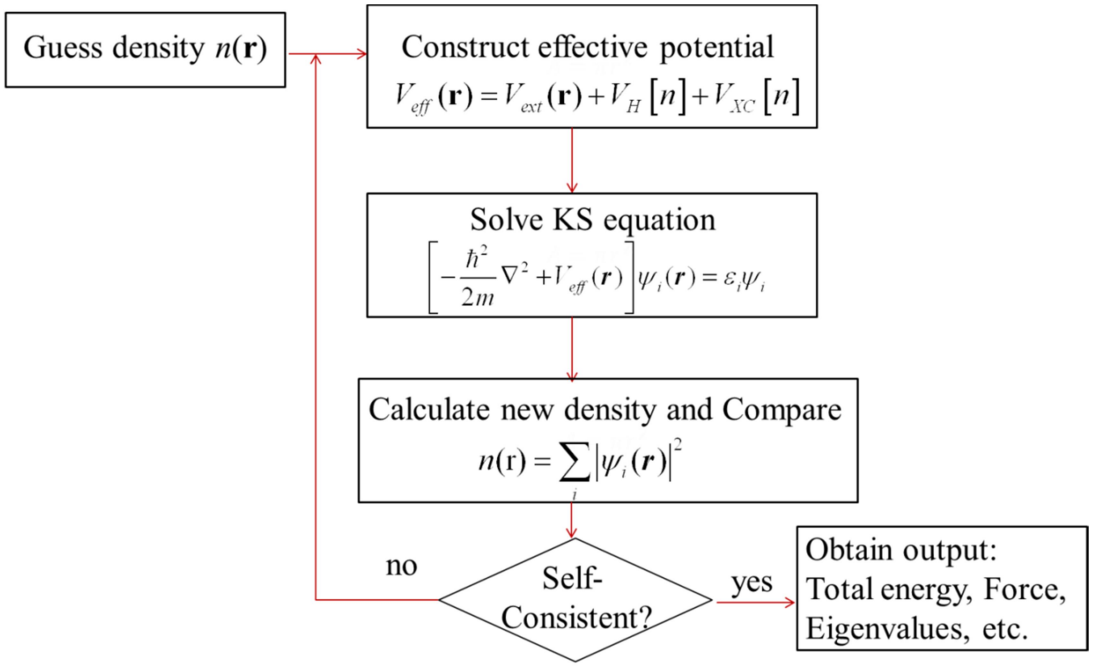

Figure 2.3 Self consistent calculation procedure of DFT.

The accuracy of DFT calculations depends on the approximation for the exchange-correlation energy functional. The local density approximation (LDA) is the basis of all approximate exchange-correlation functionals and is based on an electron density which is constant at all points in space, i.e, n(**r**) = constant. This describes a system in which electrons move on a positive background charge distribution such that the total ensemble is neutral [13]. The LDA has proveda

remarkably fruitful approximation. Properties such as structure, vibrational frequencies, elastic moduli, and phase stability (of similar structures) are described reliably for many systems [14]. In general, LDA gives ionization energies of atoms, dissociation energies of molecules and cohesive energies with a fair accuracy (typically 10-20%), and gives bond lengths of molecules and solids with a typically accuracy of ~2% [14]. The LDA performs well in structural studies of isolated chains and crystals of polymers such as PE [15][16]. The deficiency of the LDA approximation is most evident for strongly correlated materials [17]. A more accurate functional, the generalized gradient approximation (GGA) use information about the local electron density and the local gradient in the electron density. Significant advances have been made in recent years in the quality of exchange correlation functionals as dependence on local density gradients, semi-local measures of the density, and nonlocal exchange functionals have been introduced.

2.2 Phonon Calculation in DFT

The calculation of vibrational properties of materials from their electronic structure is an important goal for materials modeling. A wide variety of material properties depend on the dynamical behavior of the lattice, including specific heat, thermal expansion, and thermal conduction. Phenomena related to the electron-phonon interaction include the resistivity of metals, superconductivity, and the temperature dependence of optical spectra. Vibrational spectroscopy is a very important tool for the characterization of materials. Vibrational frequencies are measured using infrared and Raman spectroscopy, as well as inelastic neutron scattering. The resulting vibrational spectra are a sensitive probe of the local bonding and chemical structure. Accurate calculations of vibrational frequencies and displacement patterns yield a wealth of information on the atomic and electronic structure of materials.

Phonons are characterized by a vibrational frequency $\omega(\mathbf{q})$ and by the displacements of the atoms in one unit cell. The $\mathbf{q}$ wave-vector is the equivalent of the Bloch vector for the electronic states and is inside the first Brillouin zone, i.e., the unit cell of the reciprocal lattice. Phonon

frequencies form “dispersion bands" in quite the same way as electronic states form band structures. A system with N atoms in the unit cell has $3N$ phonons for a given $\mathbf{q}$. The dynamical matrix contains information on the vibrational properties of a crystal, for example, the phonon frequencies are the square roots of its eigenvalues while the atomic displacements are related to its eigenvectors. The calculation of vibrational properties of materials from their electronic structure is an important goal for materials modeling. Two alternative methods are used to calculate phonons in crystals within the framework of DFT. The two methods are generally known as the small displacement and the linear response methods.

The small displacement method is more direct and easier to understand [18][19] as it is based on the force constant matrix which expresses the proportionality between displacements and forces for displacements that are sufficiently small for this relationship to be linear. In principle, the force matrix can be determined by displacing a single atom in the unit cell in one Cartesian direction, while all other atoms are fixed at their equilibrium positions. The forces on all the atoms give directly the elements of the force constant matrix for the given displacement. All the elements of the force-constant matrix can be obtained after this procedure is repeated for all other displacements. Translational invariance implies that the number of separate calculations required is at most three times the number of atoms in the primitive cell, but for most materials symmetry relations can be used to reduce this number substantially. Since calculations on condensed matter often use periodic boundary conditions, the repeating cell (the super-cell) must be large enough so that the force constant matrix elements have all fallen off to negligible values at the boundary of the super-cell. One advantage of the small displacement method is that it is an add-on that can work with any code, including non-density functional theory codes. All is needed is the ability of the external code to compute forces. For example, small displacement method implemented in software such as phonopy [20] and PHONON [21] can be used in conjuction with VASP and WIEN2K to calculate phonon dispersion curves.

Density functional perturbation theory (DFPT) [22][23][24] provides a second elegant strategy for the calculation of phonons in crystals (also known as the “linear response method”). The main idea in DFPT (Baroni et al. [22]) is to exploit the Hellmann-Feynman theorem to show that a linear order variation in the electron density upon application of a perturbation to the crystal is responsible for a variation in the energy up to second (in fact, third [25]) order of the perturbation. Using standard perturbation theory, this linear order variation of the electronic charge density can be calculated using only unperturbed wave-functions, which therefore only require calculations on the ground state crystal. If the perturbation is a phonon wave with wave-vector **q**, calculation of the density change to linear order in the perturbation can be used to determine the dynamical matrix at wave-vector **q**. This can be carried out for any arbitrary wave-vector, without the need for a super-cell, which is computationally more efficient than the small displacement method. In systems where the phonon dispersion behaves in an anomalous way (such as systems with Kohn anomalies), the linear response method is more suitable, because it is capable of calculating the exact phonons at the requested points. Finally, the linear response method provides a natural way of dealing with the LO-TO splitting of the phonon frequencies in polar materials.

2.3 The Quantum ESPRESSO Code

Quantum ESPRESSO (QE) is an integrated suite of Open-Source computer codes for electronic-structure calculations and materials modeling at the nanoscale. It is based on density-functional theory, plane waves, and pseudopotentials [26]. Quantum ESPRESSO calculates the dynamical matrix of a solid using DFPT [23]. This approach calculates the charge response to lattice distortions of a definite wave vector **q**. The starting point is the electronic structure of the undistorted crystal, obtained from a conventional DFT self-consistent (scf) calculation. The charge response must be calculated for each of the $3N$ independent atomic displacements, or for any equivalent combination thereof. QE uses atomic displacements along symmetry-dependent patterns the irreps (shortend for “irreducible representations"). The irreps are sets of displacement

patterns that transform into themselves under small group of **q**, i.e. the symmetry operations that leave both **q** and the crystal unchanged. Since the irreps of the small group of **q** are typically 1 to 3-dimensional, only a few displacement patterns belong to one irrep and only the responses to these patterns need to be calculated simultaneously. This procedure exploits symmetry [26] in an effective way, while keeping the calculation of the charge response within each irrep independent from others. Once the charge response to one irrep is calculated self-consistently, the contribution of this irrep to the dynamical matrix is calculated and stored. When all atomic displacements (or all irreps) have been processed, the dynamical matrix for the given q is obtained.

In order to calculate the full phonon dispersions and thus all quantities depending on integrals over the Brillouin Zone, one needs dynamical matrices for any **q** vector. In practice, one can store the needed information in real space under the form of Interatomic Force Constants [24]. These are obtained by inverse Fourier Transform of dynamical matrices, calculated for a finite uniform mesh of **q** vectors. The number of needed **q** vectors is relatively small, since Interatomic Force Constants are short-ranged quantities or can be written as the sum of a known long-ranged dipolar terms plus a short-ranged part. Once Interatomic Force Constants in real space are available, the dynamical matrix can be reconstructed at any desired value of **q** with little effort. Alternatively, one can compute a finite number of **q** vectors and plot or interpolate the resulting phonon dispersion branches. We stress here that phonon calculations at each **q** are independent.

Crystals with unit cells that contain a few tens of atoms, up to ~100, fit into a single modern computing element and require relatively short execution time (minutes to hours) for the self-consistent field (scf) step. The memory requirement of a phonon calculation is somewhat larger than that for the scf calculation, but of the same order of magnitude. A full-fledged phonon calculation for a system of N atoms per unit cell for a uniform mesh with n_q **q** vectors requires CPU time of at least $3Nn_q$, times the CPU time for the scf step. For systems with a few tens of atoms in the unit cell, this multiplicative factor can be in the order of thousands and more.

2.4 References

[1] R. G. Parr, and W. Yang, “Density-Functional Theory of Atoms and Molecules”, OUP, Oxford, (1989)
[2] N. H. March (ed.), “Electron Correlation in the Solid State”, ICP, London, (1999)
[3] J. Callaway and N. H. March, “Density Functional Methods: Theory and Applications”, Solid State Physics, 38, 135 (1984)
[4] Max Born; J. Robert Oppenheimer (1927). "Zur Quantentheorie der Molekeln" [On the Quantum Theory of Molecules]. Annalen der Physik (in German) 389 (20): 457–484. Retrieved 28 May 2013.
[5] David Sholl, Janice A Steckel, “Density Functional Theory: A Practical Introduction”, April 2009
[6] P. R. Kent, “Techniques and Applications of Quantum Monte Carlo”, PhD Thesis, University of Cambridge, Cambridge, UK, (1999).
[7] M. J. Gillan, “The Virtual Matter Laboratory”, Contemporary Physics, Vol. 38, No. 2, pp.115-130, (1997).
[8] C. Møller and M. S. Plesset, “Note on an Approximation Treatment for Many-Electron Systems”, Physical Review, Vol. 46, No. 7, pp.618-622, (1934).
[9] J. A. Pople, J. S. Binkley, and R. Seeger, “Theoretical Models Incorporating Electron Correlation”, International Journal of Quantum Chemistry, Vol. 10, No.10, pp.1–19, (1976).
[10] P. Hohenberg and W. Kohn, “Inhomogeneous Electron Gas”, Physical Review, Vol. 136, No. 3B, pp.B864–B871, (1964).
[11] W. Kohn and L. J. Sham, “Self-Consistent Equations Including Exchange and Correlation Effects”, Physical Review, Vol. 140, No. 4A, pp.A1133–A1138, (1965).
[12] R. O. Jones and O. Gunnarsson, “The Density Functional Formalism, its Applications and Prospects”, Review of Modern Physics, Vol. 61, No.3, pp.689-746, (1989).
[13] P. Hohenberg and W. Kohn, “Inhomogeneous Electron Gas”, Physical Review, Vol. 136, No. 3B, pp.B864–B871, (1964).
[14] W. Kohn, “Nobel Lecture: Electronic Structure of Matter—Wave Functions and Density Functionals”, Reviews of Modern Physics”, Vol. 71, No. 5, pp.1253-1266, (1999).
[15] J. Kleis, “First Principle Calculations of Polymer Interactions”, PhD Thesis, Chalmers University of Technology, Göteborg, Sweden, (2005).
[16] M. S. Miao, P. E. Van Camp, V. E. Van Doren, J. J. Ladik and J. W. Mintmire, “Conformation and Electronic Structure of Polyethylene: A Density-Functional Approach”, Physical Review B, Vol. 54, No. 15, pp.10430-10435, (1996).
[17] V. I. Anisimov, F. Aryasetiawan, and A. I. Lichtenstein, “First Principles Calculations of the Electronic Structure and Spectra of Strongly Correlated Systems: the LDA+U Method”, Journal of Physics: Condensed Matter, Vol.9, No.4, pp.767–780, (1997)
[18] G. Kresse, J. Furthmüller and J. Hafner, “Ab initio Force Constant Approach to Phonon Dispersion Relations of Diamond and Graphite”, Europhys. Lett. 32, 729 (1995).
[19] D. Alfè, G. D. Price, M. J. Gillan, "Thermodynamics of hexagonal close packed iron under Earth's core conditions", Physical Review B 64, 045123 1-16 (2001).
[20] Atsushi Togo, Fumiyasu Oba, and Isao Tanaka, “First-principles calculations of the ferroelastic transition between rutile-type and CaCl2-type SiO2 at high pressures”, Phys. Rev. B, 78, 134106 (2008)
[21] K.Parlinski, Z.Q.Li and Y.Kawazoe, “First-principle determination of the soft mode in cubic ZrO2”,Phys.Rev.Lett. 78, 4063 (1997). Program available at http://wolf.ifj.edu.pl/phonon/
[22] S. Baroni, P. Gianozzi, and A. Testa, “Green’s-function approach to linear response in solids”, Phys. Rev. Lett. 58, 1861 (1987).
[23] P. Giannozzi, S. de Gironcoli, P. Pavone, and S. Baroni, “Ab initio calculation of phonon dispersions in semiconductors”, Phys. Rev B, 43, 7231 (1991).
[24] S. Baroni, S. de Gironcoli, A. Dal Corso, and P. Gianozzi, “Phonons and related crystal properties from density-functional perturbation theory”, Rev. Mod. Phys. ,73, 515 (2001).

[25] X. Gonze, and J.-P. Vigneron, “Density-functional approach to nonlinear-response coefficients of solids”, Phys. Rev. B 39 13120, 1989.
[26] P. Giannozzi, S. Baroni, N. Bonini, M. Calandra, R. Car, C. Cavazzoni, D. Ceresoli, G. L. Chiarotti, M. Cococcioni, I. Dabo, A. Dal Corso, S. Fabris, G. Fratesi, S. de Gironcoli, R. Gebauer, U. Gerstmann, C. Gougoussis, A. Kokalj, M. Lazzeri, L. Martin-Samos, N. Marzari, F. Mauri, R. Mazzarello, S. Paolini, A. Pasquarello, L. Paulatto, C. Sbraccia, S. Scandolo, G. Sclauzero, A. P. Seitsonen, A. Smogunov, P. Umari, R. M. Wentzcovitch, “Quantum ESPRESSO: a modular and open-source software project for quantum simulations of materials”, J. Phys. Condens. Matter 21, 395502 (2009). http://www.quantum-espresso.org/

CHAPTER 3
FIRST PRINCIPIPLES COMPUTATIONS OF INTRINSIC BREAKDOWN

3.1 Introduction to "Intrinsic Breakdown"

The "intrinsic" breakdown field of an insulator is a quantity determined by the physical properties of the material and temperature, and can be viewed as an intrinsic material property which provides an upper bound to the dielectric breakdown field. Experimentally, intrinsic breakdown can be obtained only under ideal conditions, when all extraneous influences have been eliminated. Developing a predictive theory of intrinsic breakdown is the first step in the path to predicting extrinsic breakdown field, as well as achieving an improved understanding of the fundamental factors that control dielectric breakdown.

Intrinsic breakdown can be explained in terms of electron avalanche theory [1], which depends on the presence and creation of charge carriers capable of migration through the dielectric. A central tenet of this theory is that the relevant scattering mechanism for charge carriers is the electron-phonon interaction, i.e., electrons gain energy from an external electric field between successive collisions with phonons. At low electric fields, the electron energy distribution achieves steady state, as the energy gain from the external electric field is balanced by energy loss from collisions with phonons. At a sufficiently high electric field, the electron energy increases indefinitely until a threshold is reached at which high-energy electrons ionize the lattice, leading to carrier multiplication. This process is referred to as impact ionization, and the ensuing carrier multiplication leads to irreversible damage (e.g., through bond breakage), and ultimately breakdown.

As discussed in Chapter 1, Fröhlich's high energy criterion is based on the high energy tail of the electron energy distribution which, quite logically, should precipitate breakdown. As a result, he requires only that the energy gain from the electric field be greater than the energy loss for phonons for electrons in the high energy tail of the electron energy distribution [2]. Since Fröhlich's breakdown criterion depends explicitly on the high energy tail of the electron energy distribution, it is not

consistent with an average electron model [1], which makes it more complex, whether approached analytically or numerically.

von Hippel's low energy criterion for avalanche breakdown is based on the hypothesis that the energy gain from the electric field must be greater than the energy loss to phonons for all energies from the conduction band minimum (CBM) to the threshold for impact ionization [3]. The physical basis of this criterion is that when the electron energy rea ches the threshold for impact ionization, an electron with the impact ionization energy is replaced by two electrons at the CBM, and the process repeats, leading to electron multiplication, avalanche formation, and breakdown. If the energy loss to phonons is greater than the energy gain from the electric field for any electron energy between the CBM and the impact ionization energy, electrons collect at that energy and never reach the energy required for impact ionization. von Hippel's criterion is consistent with an average electron model, as his criterion does not depend explicitly on the tail of the electron energy distribution. Within this framework, the breakdown criterion can be formulated following von Hippel, as the lowest field at which the average electron energy gain from the field is greater than the average energy loss to phonons for all electron energies less than that which produces impact ionization.

The electron relaxation time (the reciprocal of which is the scattering rate) determines the time interval over which electrons gain energy from the field before a collision with the lattice. The electron-phonon scattering rate controls both the electron energy gain and energy loss, the balance of which determines the breakdown field. As described in Chapter 1, the proper interpretation of electron-phonon scattering rate is a key factor in predicting the breakdown field. Analytical solution for electron-phonon scattering rates can be derived through reasonable approximations in simple crystal structure of alkali halides [1][2]. The scattering rates of more complex materials can be obtained by photon-induced electron transmission experiment which was developed at Brown Boveri Research (later ABB) [4]. Consistent work has been done by IBM group [5](mostly on SiO2), and Brown Boveri group [4][6](mostly on organic dielectrics). The First principles quantum mechanical methods for

calculation of electron phonon scattering rates have been pursued only in the last few years with the development of computational quantum mechanics[7][8][9].

3.2 First Principles Computations of Intrinsic Breakdown

While quantum mechanical descriptions of intrinsic breakdown are well over 50 years old, until recently, the estimation of the relevant parameters, such as electron-phonon scattering rates, has relied on approximations or empirical deformation potentials. The electron-phonon interaction plays a crucial role in the electron and lattice dynamics of condensed matter systems. For example, phenomena such as the electrical resistivity [10] and superconductivity [11] are a direct consequence of the interaction between electrons and lattice vibrations. Here, we present a parameter free scheme for estimating intrinsic breakdown field of crystalline materials based on electron-phonon interactions by determining the electron energy gain and loss rates using Density Functional Perturbation Theory (DFPT).

The intrinsic breakdown field, F_{bd}, is defined according to the von Hippel low energy criterion as follows [3]. If we represent the rate of energy gain of an electron of electron energy E as $A(F,E)$ at a field F, and the rate of energy loss as $B(E)$, the above criterion can written as

$$A(F,E) > B(E), \quad \text{for all } E \hat{\text{I}} \left\{ \text{CBM},\ \text{CBM} + E_g \right\}. \tag{3.1}$$

where CBM and E_g are the conduction band minimum and the bandgap of the material, respectively. The reason for choosing CBM + E_g as the upper bound is that all electrons with greater energy will impact ionize the lattice resulting in electron multiplication, i.e., CBM + E_g is assumed to be the impact ionization threshold in the present treatment.

The rate of energy gain of an electron of energy E at field F can be evaluated as [1]

$$A(F,E) = \frac{e^2 t\,(E) F^2}{3m} \tag{3.2}$$

where e and m are, respectively, the electronic charge and mass, and $\tau(E)$ is the electron relaxation time determined by scattering due to phonons. The isotropic (and purely energy dependent) form of the electron relaxation time (whose reciprocal is the scattering rate) is given by [8]

$$\frac{1}{t(E)} = \frac{1}{D(E)} \sum_{\boldsymbol{kj}} \frac{1}{t(\boldsymbol{kj})} d(e_{\boldsymbol{kj}} - E) \tag{3.3}$$

where $D(E)$ is the electronic density of states, $\varepsilon_{\boldsymbol{kj}}$ is the energy of an electron above the CBM at wave vectors $\boldsymbol{k}$ and band index j. The explicit $\boldsymbol{k}$- and j-dependent relaxation time, $\tau(\boldsymbol{kj})$ can be evaluated from Fermi's golden rule by direct integration of electronic scattering probabilities over all possible final states and is given by

$$\frac{1}{t(\boldsymbol{kj})} = \frac{2\pi}{\hbar} \sum_{\boldsymbol{q}l\,j'} \left| g^{\boldsymbol{q}l}_{\boldsymbol{k}+\boldsymbol{q}j',\boldsymbol{kj}} \right|^2 \left(n_{\boldsymbol{q}l} + \frac{1}{2} \mp \frac{1}{2} \right) d\left(e_{\boldsymbol{kj}} - e_{\boldsymbol{k}+\boldsymbol{q}j'} \pm \hbar\omega_{\boldsymbol{q}l} \right) \tag{3.4}$$

where $\hbar$ is the Planck's constant and $\omega_{\boldsymbol{q}\lambda}$ is the frequency of phonon at wave vector $\boldsymbol{q}$ and band index λ. Physically, the above expression represents the scattering of an electron initially with energy $\varepsilon_{\boldsymbol{kj}}$ to a final state with energy $\varepsilon_{\boldsymbol{k}+\boldsymbol{q},j'}$ by a phonon with frequency $\omega_{\boldsymbol{q}\lambda}$. The ± sign indicates whether a phonon is absorbed (+) or emitted (-) during this scattering process. $n_{\boldsymbol{q}\lambda}$ is the phonon occupation number which is given by the Bose-Einstein distribution. Temperature is set as 300 K for this distribution. The δ-function in the equation above ensures energy conservation during scattering [7], and $g^{\boldsymbol{q}\lambda}_{\boldsymbol{k}+\boldsymbol{q}j',\boldsymbol{k}j}$ is the electron-phonon coupling function [8] given by

$$g^{\boldsymbol{q}l}_{\boldsymbol{k}+\boldsymbol{q}j',\boldsymbol{kj}} = \sqrt{\frac{\hbar}{2M\omega_{\boldsymbol{q}l}}} \left| \left\langle \psi_{\boldsymbol{k}+\boldsymbol{q}j'} \left| \boldsymbol{\xi}_{\boldsymbol{q}l} \cdot \nabla_{\boldsymbol{R}} V_{\boldsymbol{q}} \right| \psi_{\boldsymbol{kj}} \right\rangle \right|^2 \tag{3.5}$$

where M is the atomic mass, $\boldsymbol{\xi}_{\boldsymbol{q}\lambda}$ are the phonon polarization vectors, $\nabla_{\boldsymbol{R}} V_{\boldsymbol{q}}$ is the gradient of the screened one electron potential with respect to atomic displacements from their equilibrium positions $\boldsymbol{R}$, and $\psi_{\boldsymbol{kj}}$ is the 1-electron wave function.

The net rate of energy loss $B(E)$ represents the energy exchange between an electron of energy E and the distribution of phonons (in terms of phonon emission or absorption) and can be calculated similarly to the scattering rate as

$$B(E)=\frac{2p}{D(E)}\sum_{\pm}\sum_{\boldsymbol{kj}}\sum_{\boldsymbol{ql}\,j'}\left\{\pm w_{\boldsymbol{ql}}\left|g^{\boldsymbol{ql}}_{\boldsymbol{k}+\boldsymbol{q}j',\boldsymbol{kj}}\right|^{2}\left(n_{\boldsymbol{ql}}+\frac{1}{2}\mp\frac{1}{2}\right)d(e_{\boldsymbol{kj}}-e_{\boldsymbol{k}+\boldsymbol{q}j'}\pm\hbar w_{\boldsymbol{ql}})d(e_{\boldsymbol{kj}}-E)\right\}. \tag{3.6}$$

Combining equations (3.1) (3.2) and (3.6) results in

$$F_{bd}=Max\left[\frac{\sqrt{3m}}{e}\sqrt{\frac{1}{t(E)}B(E)}\right]E\in\{\mathrm{CBM},\ \mathrm{CBM}+E_g\}. \tag{3.7}$$

The above approach provides the basis for estimating F_{bd}, [1][3][12], provided $\tau(E)$ and $B(E)$ are available.

3.3 Calculation Scheme and Modifications of QE Code

In the present work, the relevant quantities are computed using first principles density functional theory (DFT) based calculations within the local density approximation (LDA) and norm conserving pseudopotentials as implemented in Quantum ESPRESSO (QE) [13]. Phonon frequencies and the electron-phonon coupling function $g^{\boldsymbol{q}\lambda}_{\boldsymbol{k}+\boldsymbol{q}j',\boldsymbol{k}j}$ as defined in equation (3.5) were computed in the linear response regime using Density Functional Perturbation Theory (DFPT). Quantum ESPRESSO calculates directly $g^{\boldsymbol{q}\lambda}_{\boldsymbol{k}+\boldsymbol{q}j',\boldsymbol{k}j}$ which is then adapted to compute $\tau(E)$ and $B(E)$ as described by equation (3.3), (3.4), (3.5) and equation (3.6). For all the materials studied, the convergence of the calculations with respect to plane-wave cut-off energy, and the k-point and q-point meshes has been checked thoroughly.

The calculation of the electron-phonon coupling from first-principles is challenging because of the necessity of evaluating Brillouin zone integrals with high accuracy. Such calculation requires the evaluation of matrix elements between electronic states connected by phonon wavevectors [14]. Large numbers of matrix elements may be necessary to achieve numerical convergence of the Brillouin zone

intergrals over these matrix elements. As a result, accurate evaluation of $\tau(E)$ and $B(E)$ requires a very dense sampling of both the electronic ($\boldsymbol{k}$) and the phononic ($\boldsymbol{q}$) reciprocal space grids, significantly more dense than required in standard DFT computations involving the corresponding systems.

The definitions of both $\tau(E)$ and $B(E)$ involve double delta functions, which, in practice, are replaced by sharp Gaussians. A Monkhorst-pack k point mesh of 32×32×32 and q point mesh of 4×4×4 with 0.01 Ry Gaussian broadening is used for all materials to obtain converged results. In polar materials, macroscopic electric fields are present in the long-wavelength limit and induce the so called LO-TO splitting as a result of the longitudinal optical phonons having a much greater frequency than transverse optical phonons. This effect can be accommodated in the computation by adding a non-analytic term to the dynamical matrix. Longitudinal optical phonon frequencies must be computed in order to provide the correct phonon frequencies for calculation of the polar electron phonon scattering rate.

In practice, the calculation of electron-phonon scattering rate and energy loss rate requires three steps. Step 1: A self-consistent calculation with a dense k-point grid. The dense grid must contain all k and k+q grid points used in the subsequent electron-phonon calculations and should be dense enough to produce accurate electron-phonon scattering coefficients. The option "la2F=.true." instructs the code to save data into a file that is subsequently read during the electron-phonon calculation. All grids must be unshifted, i.e., include k=0. Step 2: A self-consistent calculation using a grid of coarse k points and a value of the gaussian broadening that is suitable for good self-consistency and for the phonon frequency calculation and scattering coefficients calculation. Step 3: Phonon frequencies, electron-phonon scattering rate and energy loss rate are calculated for the specified q vector. Specify "elph=.true." and the name of a file where the derivative of the potential is stored, "fildvscf". lambda.f90 read files 'filelph' produced by phonon (one for each q-point) sum over q-points to produce the electron-phonon scattering rate and energy loss rate. Appendix B provides an example of

Quantum-ESPRESSO 4.3 input script files to calculate electron-phonon scattering rate for silicon. Minor input changes exist in later Quantum-ESPRESSO versions.

Quantum ESPRESSO code (elphon.f90) can evaluate the electron-phonon coupling matrix, but the program uses the matrix to describe superconductivity of metals. The code had to be modified to calculate intrinsic breakdown field in dielectric materials. Figure 3.1 illstrates the main modifications of elphon.f90 code. See Appendix C for a version of modified elphon.f90 code. Equation 1 is the phonon linewidth of phonon mode for metals calculated by the original code, and equation 2 is the electron-phonon scattering rate and equation 3 is the enery loss rate. Main modifications in the QE code (elphon.f90) include:

- Modification 1: divide by density of states D(E).
- Modification 2: sum over phonon modes λ and phonon wave vectors **q**.
- Modification 3: add phonon occupation factor $n_{q\lambda}$ from Bose Einstein distribution, T=300 K.
- Modification 4: add the energy change $\hbar\omega_{\mathbf{q}\lambda}$ at each electron-phonon scattering event.
- Modification 5: add loop over electron energy E.
- Modification 6: add phonon frequencies $\omega_{\mathbf{q}\lambda}$ in order to calculate energy loss rate.

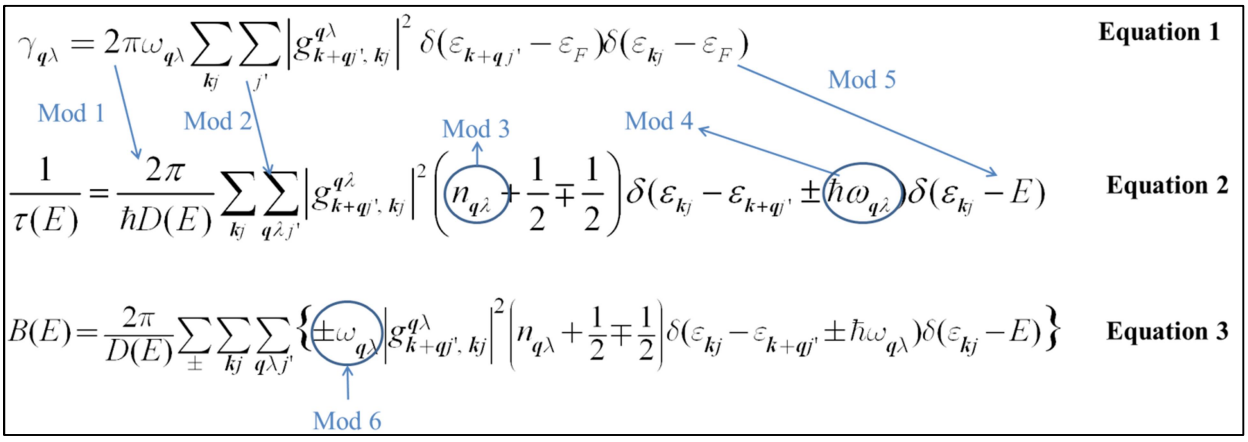

Figure 3.1 Main modifications made in QE code (elphon.f90 code). Equation 1 is the original quantity calculated, equations 2 and 3 calculate electron-phonon scattering rate and energy loss rate.

3.4 Computation Results for Intrinsic Breakdown

Figure 3.2 shows a computation of the electron-phonon scattering rate ($1/\tau(E)$) of Si along with the electronic density of states. The scattering rate follows closely the line shape of the density of states, and both quantities are generally in good agreement with prior work [8], [15]. Once the electron-phonon scattering rate as a function of electron energy has been computed, the energy loss as a function of electron energy can be calculated, shown as the red line of Figure 3.3.

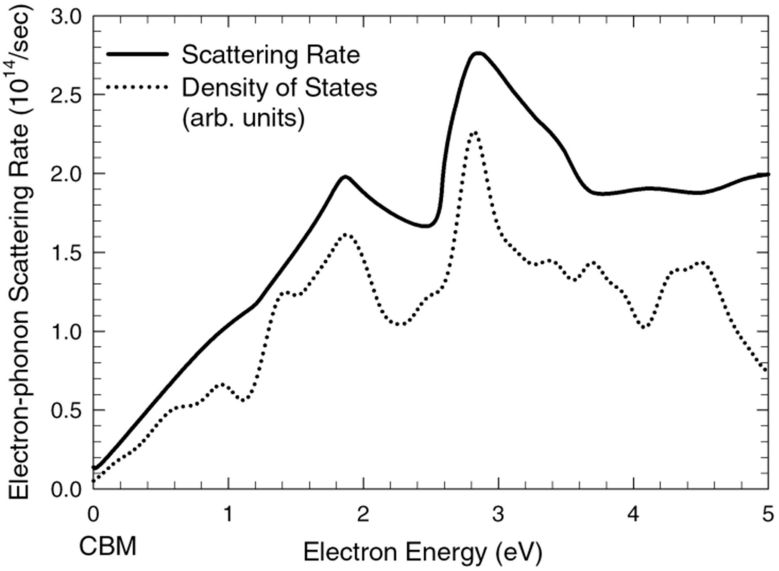

Figure 3.2 The electron-phonon scattering rate ($1/\tau(E)$) and the density of states ($D(E)$) for Si at room temperature as a function of electron energy. The electron energy scale is referenced to the conduction band minimum (CBM).

Figure 3.3 shows $A(F,E)$ and $B(E)$ for Si, the former for various values of the electric field, F, as a function of the electron energy E. As described by equation (3.1), the intrinsic breakdown field, F_{bd}, is the electric field at which the *A(F,E)* curve is greater than the *B(E)* curve over the entire energy range of interest, namely from the CBM to CBM + E_g. We use the experimental E_g value of 1.17 eV (for Si), as the LDA underestimates significantly the E_g of insulators. While advanced many-body methods can be used to compute E_g from first principles, we use available experimental E_g data for Si and other insulators considered here. The calculated F_{bd}, of Si is $8.39\text{x}10^7$ V/m compared with highest observed breakdown field of 5×10^7 V/m [16].

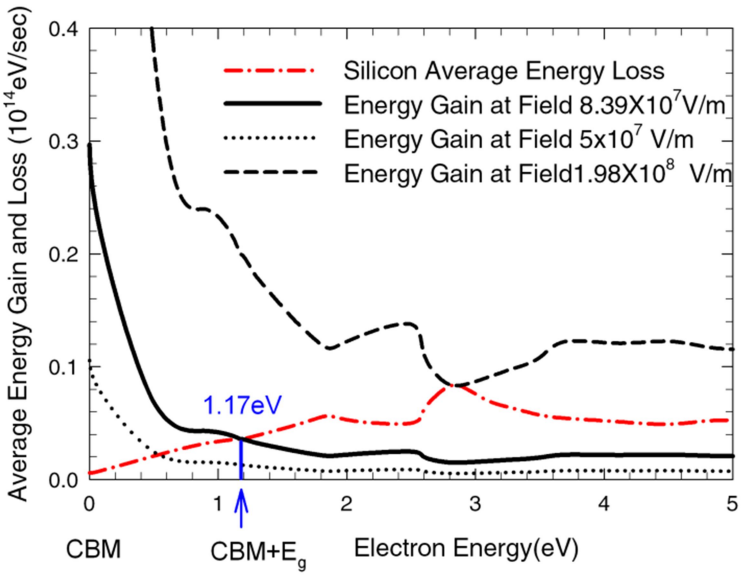

Figure 3.3 The average energy loss ($B(E)$) and energy gain ($A(F,E)$) at electric fields of 5x10^7 V/m, 8.39×10^7 V/m and 1.98×10^8 V/m for Si as a function of electron energy. The electron energy scale is referenced to the conduction band minimum (CBM). The intrinsic breakdown field of silicon is estimated as the electric field for which the energy gain curve (black solid line) is greater than energy loss curve (red dash-dot line) for all electron energies from the CBM to 1.17 eV above CBM, i.e., from the CBM to the CBM plus the bandgap (E_g) of Si.

Another example of NaCl, is presented in Figure 3.4 and Figure 3.5. Figure 3.4 shows the electron-phonon scattering rate and the density of states for NaCl at room temperature as a function of electron energy. Figure 3.5 shows energy gain $A(F,E)$ at electric fields of 2 × 10^8 V/m, 3.86 × 10^8 V/m, and 5 × 10^8 V/m as a function of electron energy and average energy loss $B(E)$ as a function of electron energy for NaCl. The electron energy scale is referenced to CBM. The intrinsic breakdown field of NaCl is estimated as the electric field for which the energy gain curve (black solid line) is greater than energy loss curve (red dash-dot line) for all electron energies from the CBM to 8.61 eV above CBM, i.e., from the CBM to the CBM plus the experimental bandgap (Eg) of NaCl. The calculated F_{bd}, of NaCl is 3.86×10^8 V/m compared with highest observed breakdown field of 2.5×10^8 V/m [1].

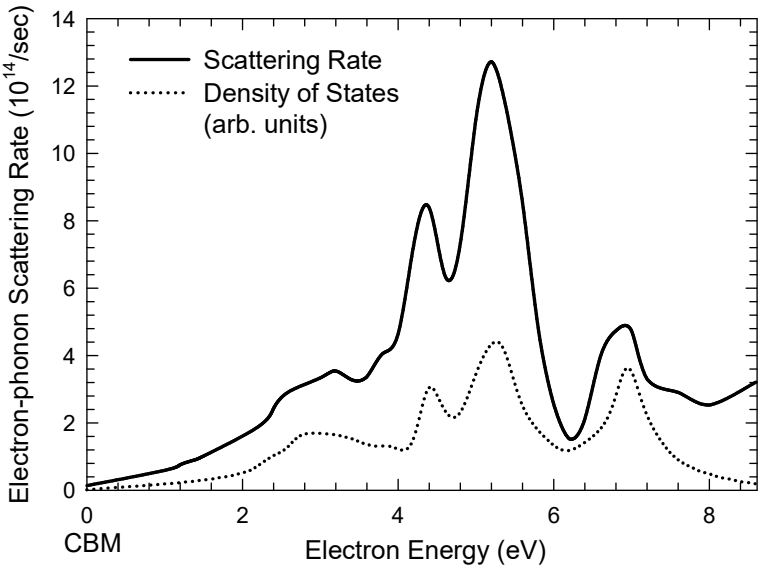

Figure 3.4 The electron–phonon scattering rate and the density of states for NaCl at room temperature as a function of electron energy. The electron energy scale is referenced to the conduction band minimum (CBM).

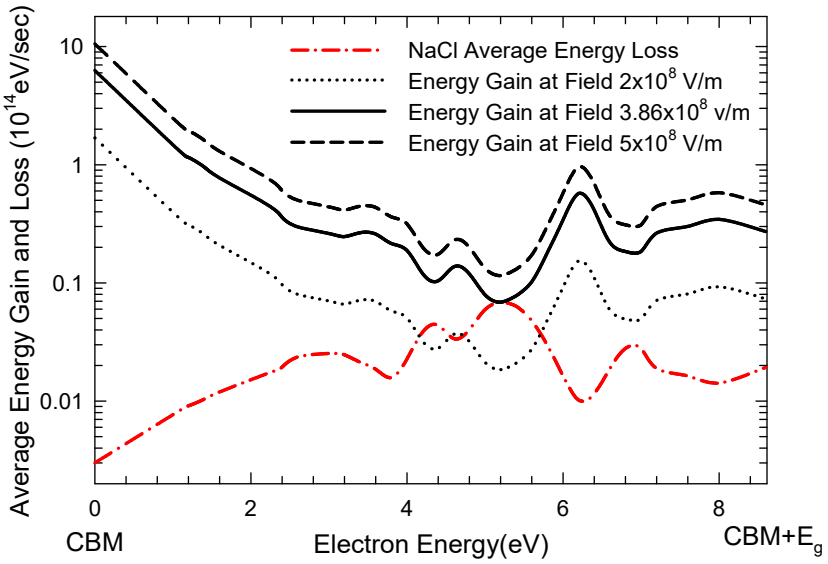

Figure 3.5 The average energy loss and energy gain at electric fields of 2×10^8 V/m, 3.86×10^8 V/m, and 5×10^8 V/m for NaCl as a function of electron energy. The electron energy scale is referenced to CBM. The intrinsic breakdown field of NaCl is estimated as the electric field for which the energy gain curve (black solid line) is greater than energy loss curve (red line) for all electron energies from the CBM to 8.61 eV above CBM, i.e., from the CBM to the CBM plus the bandgap (E_g) of NaCl.

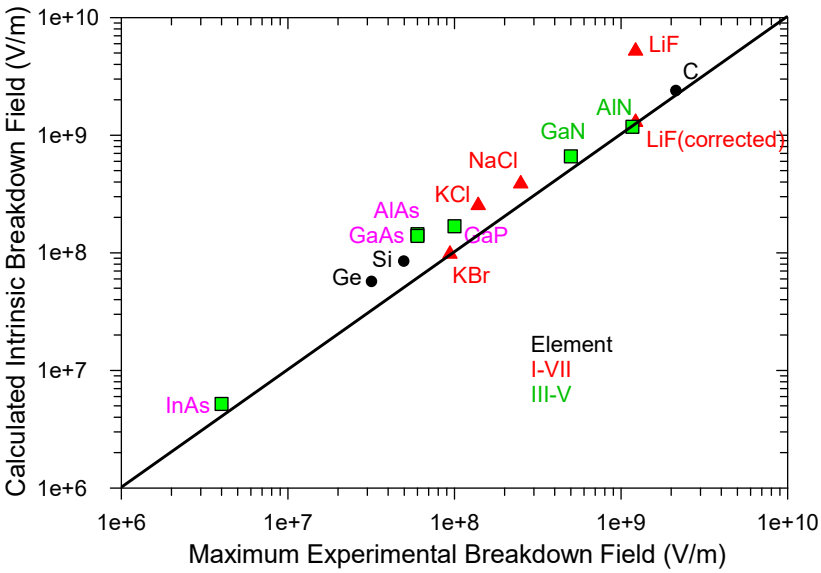

Figure 3.6 Comparison of the maximum experimental breakdown field and the calculated intrinsic breakdown field for a range of covalently bonded and ionic materials. The data are tabulated in Table 2. In the case of LiF, the enthalpy of formation (6.39 eV) is much lower than the bandgap (14.2 eV). Thus bond breakage will occur before impact ionization. The LiF (corrected) represents our result when the enthalpy of formation is used as impact ionization threshold instead of the bandgap. The symbols code for material type (element, etc.) while the text in the figures codes for material structure, i.e., (black) Diamond Structure: Ge, Si, C; (red) Rocksalt Structure: KBr, KCl, NaCl, LiF; (purple) Zincblende Structure: InAs, GaAs, GaP, AlAs; (green) Wurtzite Structure: AlN, GaN.

Figure 3.6 compares computations of intrinsic breakdown computed as described above with literature data for the intrinsic breakdown of many prototypical covalent bonded and ionic bonded materials. The data include elemental systems: Ge, Si, C (diamond cubic structure); I-VII compounds: KBr, KCl, NaCl, LiF (rocksalt structure); III-V compound: InAs, GaAs, GaP, AlAs (Zincblende Structure), and AlN, GaN (Wurtzite Structure). The groups of materials are represented by differing symbols in Figure 3.6. A major difficulty in obtaining agreement between theory and experiment for the intrinsic breakdown field is determining whether the experimental data represent intrinsic breakdown. Breakdown fields from the literature for a given material vary substantially as a result of material defects and the experimental technique employed. The maximum breakdown field from reported data provides the best estimate of intrinsic breakdown field. We note that the computed F_{bd} value represents the upper bound for intrinsic breakdown field. The best available breakdown data for

alkali halides are generated by optical breakdown measurements, which eliminate the influence of many extraneous factors such as electrode effects, interfaces, etc.

The case of LiF is interesting. If the usual criterion for intrinsic breakdown is used, that the energy gain is everywhere greater than the energy loss from the CBM to the CBM plus the bandgap, the predicted intrinsic breakdown field is much too high. However the enthalpy of formation for LiF is much less than the bandgap so that failure is likely to occur from bond breakage. When the enthalpy of formation is used in place of the bandgap, the computed intrinsic breakdown agrees very well with the measured data represented for LiF (corrected) Figure 3.6.

Table 3.1 For all systems studied, the calculated highest phonon frequency (in THz) and the breakdown field (in V/m) as per von Hippel's criterion are listed. The experimental bandgap (in eV), the highest observed breakdown field (in V/m), and the method adopted in such measurements are also listed. The computed LiF intrinsic breakdown is shown based the bandgap criterion, while the LiF(corrected) value in the is based on the bond energy criterion.

	Phonon Cutoff Frequency(THz)	Calculated Intrinsic F_{bd} (V/m)	Exp. E_g (eV)	Expt F_{bd} (V/m)
Ge	8.73	5.64×10^{7}	0.74[17]	[a] 3.2×10^{7} [23]
Si	15.3	8.39×10^{7}	1.17[17]	[a] 5×10^{7} [24]
C	37.9	2.37×10^{9}	5.48[17]	[b] 2.15×10^{9} [25]
KBr	5.23	9.75×10^{7}	7.81[18]	[c] 9.4×10^{7} [26]
KCl	6.88	2.53×10^{8}	8.51[18]	[c] 1.39×10^{8} [26]
NaCl	8.13	3.86×10^{8}	8.61[18]	[c] 2.5×10^{8} [1]
LiF	19.8	5.2×10^{9}	14.2[17]	[b] 1.22×10^{9} [27]
LiF (corrected)	19.8	1.29×10^{9}	14.2[17]	[b] 1.22×10^{9} [27]
AlAs	11.8	1.44×10^{8}	2.17[19]	[a] 6×10^{7}[19]
GaAs	8.82	1.39×10^{8}	1.43[20]	[a] 6×10^{7}[20]
GaP	12.2	1.68×10^{8}	2.26[21]	[a] 1.0×10^{8}[21]
InAs	7.73	5.19×10^{6}	0.354[21]	[a] 4×10^{6}[21]
AlN	27.6	1.18×10^{9}	6.23[22]	[a] 1.17×10^{9}[28]
GaN	23.3	6.6×10^{8}	3.2[17]	[a] 5×10^{8}[21]

a. Electrical breakdown, b. 1.06 μm laser breakdown, c. 10.6 μm laser breakdown

3.5 Comparison with Intrinsic Breakdown Measurement

Intrinsic breakdown refers to the electric field which will cause breakdown of a "perfect" material in a very short time, i.e., without the effects of high field aging. The measurement of

intrinsic breakdown is always problematic, as "perfection", even in crystalline materials, is difficult to achieve on a macroscopic basis. Electrode-material interfaces are never "perfect", and, in principle, the position of the electrode Fermi level within the band gap and relative to impurity states can affect the breakdown field [29]. Thus when metallic electrodes are employed, many tests must be carried out, and the intrinsic breakdown field is taken as the upper limit of the experimental data.

More recently, intrinsic breakdown has been measured using an intense optical field, which, for transparent materials, avoids electrode effects. The electric field of electromagnetic radiation can be related to its energy density (J/m^3) by the energy density of an electric field, $\varepsilon E^2/2$, where E is the optical electric field and, for an optical field, ε is the electronic component of the material dielectric constant, typically about $20\text{x}10^{-12}$ F/m (relative electronic dielectric constant of about 2.2) which results in an index of refraction of $n=\sqrt{2.2}=1.5$. The Power (W) or intensity (W/m^2) of a laser can be related to the energy density (ED, J/m^3) through

$$ED_{optical} = \frac{P n}{c A} = \frac{I n}{c} \tag{3.8}$$

where P is the power of the laser (W), I is intensity (W/m^2), n is the index of refraction of the dielectric, c is the speed of light in vacuum, and A is the area to which the optical beam is focused. If we equate this to the energy density from the electric field, we arrive at

$$E_{optical} = \sqrt{\frac{2P}{e_0 c A n}} = \sqrt{\frac{2I}{e_0 c n}} \ . \tag{3.9}$$

A 100 kW pulsed laser focused to an area of 10^{-10} m^2 can achieve an electric field in the range of 700 kV/mm, with the field increasing as the square root of the power. By focusing a pulsed laser into a transparent dielectric sample, the laser power (electric field) at which the samples is damaged can be determined by applying successively greater power pulses and inspecting the sample after each pulse. This approach allows a small volume to be tested, which minimizes the

likelihood of defects, and avoids electrode effects. Most such data have been generated with CO_2 lasers (10.6 μm) or YAG lasers (1.06 μm). The period of the light is given by $\tau=\lambda n/c$, where λ is the wavelength. Thus for 10.6 μm radiation in a medium with n=1.5, the period is about 50 fs ($50x10^{-15}$ s) while for 1.06 μm radiation, the period would be an order of magnitude shorter, at about 5 fs. Under high electric field conditions, in which an electron gains energy from the electric field and loses energy to the "lattice" (phonons), an electron has a characteristic time constant for coming to equilibrium. To first order, this can be taken as the mean time between electron-phonon scattering events which are likely to change both the energy and momentum (direction) of the electron. If the optical period is short compared to the mean time between scattering events, the reversal of the optical field between scattering events tends to reduce the energy transferred from the field to an electron. If the optical period is long compared to the mean time between scattering events, then the electric field is "quasistatic" in the context of scattering events, and the electric field for optically-induced breakdown will be similar to the DC breakdown field. The mean time between electron-phonon scatter events calculated by DFPT as shown above is sufficiently short that optically-induced breakdown, even at 1.06 μm, should be very close to the DC value.

In addition to laser-based measurements of transparent bulk materials, a great deal of work has been published on breakdown of thin SiO_2 films as related to gate oxides, some of which addresses intrinsic breakdown [5]. Since the thin films are usually part of electronic devices, current-voltage characteristics can be measured, and breakdown fields can also be measured relatively easily. The best available data for "intrinsic" breakdown field of polymers were measured by W. G. Oak [30] with care to eliminate extrinsic factors, e.g., electrode edge effects, thermal effects, conducting impurities, etc, which will be addressed in the next chapter.

3.6 Correlations of Intrinsic Breakdown and Other Properties

In order to develop an intuition for the fundamental chemical and physical factors that control intrinsic breakdown, we examined the correlation of several easily computable attributes with the

computed F_{bd} values. Our results indicate a clear correlation between F_{bd} and the material bandgap and the highest phonon frequency (i.e., the phonon cutoff frequency). As seen from Table 3.1, the breakdown strength tends to increase with bandgap and phonon cut-off frequency. The phonon cut-off frequencies are calculated from DPFT, while the bandgap is the experimental value from the literature. The dependence of intrinsic breakdown with these parameters is understandable intuitively, as a material with a greater bandgap has a greater threshold for impact ionization, and materials with greater phonon cutoff frequency tend to have greater average energy loss during each electron-phonon scattering event which leads to larger F_{bd} values. Figure 3.7 and Figure 3.8 plot the calculated intrinsic breakdown as a function of these two parameters from which we see that three correlation lines are formed for differing material groups, i.e. covalently bonded elements (Ge, Si and C), III-V compound semiconductors (InAs, GaAs, GaP, AlAs, AlN, GaN), and ionic bonded alkali halides (KBr, KCl, NaCl, LiF).

For a given bandgap, covalently bonded materials (Ge, Si and C) have the greater breakdown field, while for a given phonon cut-off frequency, ionic materials (alkali halides) have the greater breakdown field. Electron-phonon interaction is stronger in ionic (polar) materials than nonpolar materials which probably accounts for effect of phonon cut-off frequency. All the ionic materials have very large bandgap, and the breakdown field increases very rapidly (~4th power) with the bandgap. The covalently bonded materials, which tend not to be polar, have a greater range of bandgap, and the intrinsic breakdown field increases roughly as the square of the bandgap. The ionic materials tend to have lower phonon cutoff frequency than the covalent materials, but the intrinsic breakdown field increases more rapidly with cutoff frequency, probably because the ionic materials have strong interactions with a wider range of phonons, i.e., both polar and nonpolar, while the covalent materials have greater phonon cutoff frequency but the breakdown strength increases less rapidly with cutoff frequency, probably as a result of the reduced electron-phonon coupling in such materials.

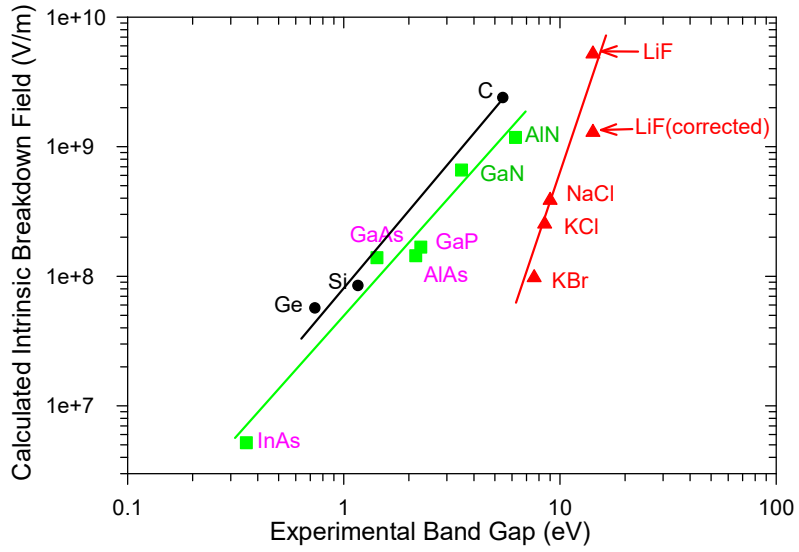

Figure 3.7 Correlation between the calculated intrinsic breakdown field and the experimental bandgap. Different correlation lines are formed for different groups of materials as indicated by different symbols in the figure.

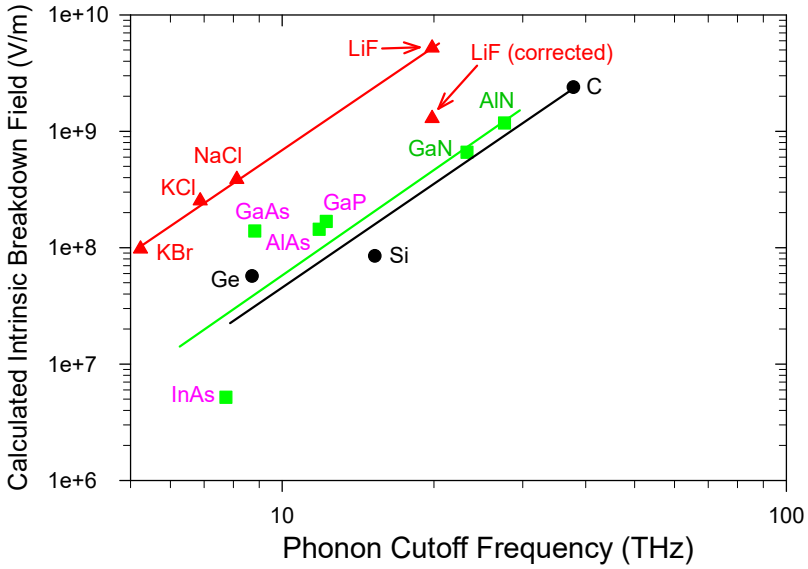

Figure 3.8 Correlation between the calculated intrinsic breakdown field (F_{bd}) and the phonon cutoff frequency. Different correlation lines are formed for different groups of materials as indicated by different symbols in the figure.

In conclusion, a highly predictive parameter-free first principles method for estimating the intrinsic breakdown field of insulators has been developed. The approach is based on the criterion that breakdown occurs when the average electron energy gain from the electric field exceeds

average energy loss to phonon collisions. Density functional perturbation theory and the direct integration of electronic scattering probabilities (due to phonons) over all possible final states is used to arrive at an estimate of intrinsic breakdown for a range of prototypical covalent and ionic systems. The computed intrinsic breakdown fields compare favorably with available experimental data. This work also establishes correlations between the breakdown field on the one hand and the bandgap and phonon cut-off frequencies on the other. These correlations, and the availability of first principles scattering rates, provide a logical basis to guide the design of materials more resistant to damage from large electric fields.

3.7 References

[1] M. Sparks, D. L. Mills, R. Warren, T. Holstein, A. A. Maradudin, L, J. Sham, E. Loh, Jr., and D. F. King, "Theory of electron-avalanche breakdown in solids", Phys. Rev. B, Vol. 24, pp.3519-3536, 1981.

[2] H. Frohlich, "Theory of Electrical Breakdown in Ionic Crystals", Proc. Roy. Soc. 160, pp.230-241, 1937.

[3] A. von Hippel, "Electric Breakdown of Solid and Liquid Insulators", J. App. Phys. Vol. 8, pp.815-832, 1937.

[4] E. Cartier and P. Pfluger, "Transport and Relaxation of Hot Conduction Electrons in an Organic Dielectric", Phys. Rev. B, Vol. 34 (12), pp. 8822-8827, 1986.

[5] D. Arnold, E. Cartier and D. J. Dimaria, "Theory of high-field electron transport and impact ionization in silicon dioxide", Phys. Rev. B, Vol. 49, pp.10278-10297, 1994.

[6] H.R. Zeller, P. Pfluger and J. Bernasconi, "High-Mobility States and Dielectric Breakdown in Polymeric Dielectrics", IEEE Trans Dielectr. Electr. Insul, Vol. 19, No. 3, 200-204, 1984.

[7] J. Sjakste, N. Vast, and V. Tyuterev, "Ab initio method for calculating electron-phonon scattering times in semiconductors: Application to GaAs and GaP," Phys. Rev. Lett., vol. 99, pp. 236405-1-4, 2007.

[8] O. D. Restrepo, K. Varga, and S. T. Pantelides, "First-principles calculations of electron mobilities in silicon: Phonon and Coulomb scattering", Appl. Phys. Lett., vol. 94, pp. 212103-1-3, 2009.

[9] K. M. Borysenko, J. T. Mullen, E. A. Barry, S. Paul, Y. G. Semenov, and J. M. Zavada, "First-principles analysis of electron-phonon interaction in graphene," Phys. Rev. B, vol. 81, pp.121412 (R) -1-4, 2010.

[10] Mott, N. F., "The conductivity of metals", Proc. Phys. Soc., Vol. 46 , 680, 1934.

[11] Schrieffer, J. R., "Theory of Superconductivity, Benjamin", New York, 1964.

[12] R. Stratton, "Progress in Dielectrics", vol. 3, J. B. Birks and J. Hart, Ed.New York, NY: Wiley, pp. 235–292, 1961.

[13] P. Giannozzi, S. Baroni, N. Bonini, M. Calandra, R. Car, C. Cavazzoni, D. Ceresoli, G. L. Chiarotti, M. Cococcioni, I. Dabo, A. Dal Corso, S. Fabris, G. Fratesi, S. de Gironcoli, R. Gebauer, U. Gerstmann, C. Gougoussis, A. Kokalj, M. Lazzeri, L. Martin-Samos, N. Marzari, F. Mauri, R. Mazzarello, S. Paolini, A. Pasquarello, L. Paulatto, C. Sbraccia, S. Scandolo, G. Sclauzero, A. P. Seitsonen, A. Smogunov, P. Umari, R. M. Wentzcovitch, "Quantum ESPRESSO: a modular and open-source software project for quantum simulations of materials", J. Phys. Condens. Matter 21, 395502 (2009). http://www.quantum-espresso.org/

[14] N. Jesse, G. Feliciano, M. Brad D., P. Cheol-Hwan, L. Steven G.; C. Marvin L. “EPW: A program for calculating the electron-phonon coupling using maximally localized Wannier functions”,Computer Physics Communications, Vol. 181, 12, pp. 2140-2148.
[15] Massimo V. Fischetti, “Monte Carlo Simulation of Transport in Technologically Significant Semiconductors of the Diamond and Zinc-Blende Structures-Part I: Homogeneous Transpor”,IEEE Trans. Electron Devices 38, 634 ,1991.
[16] J. N. Park, K. Rose, and K. E. Mortenson, “Avalanche Breakdown Effects in Near-Intrinsic Silicon and Germanium” , J. Appl. Phys. 38, 5343 ,1967.
[17] F. Tran and P. Blaha, “Accurate Band Gaps of Semiconductors and Insulators with a Semilocal Exchange-Correlation Potential”, Phys. Rev. Lett., Vol.102, pp.226401-1-4, 2009.
[18] R. T. Poole, J. G. Jenkin, J. Liesegang, and R. C. G. Leckey, “Electronic band structure of the alkali halides. I. Experimental parameters”, Phys. Rev. B. Vol.11, pp.5179-5189, 1975.
[19] Yu. A. Goldberg, Handbook on Semiconductor Parameters, Vol. 2, Chapter 1.
[20] M. N. Yoder, “Wide bandgap semiconductor materials and devices”, IEEE Trans. Electron Devices, Vol. 43, pp.1633-1636, 1996.
[21] L. M. Wang, “Relationship between Intrinsic Breakdown Field and Bandgap of Materials”, Proceedings of the 25th International Conference on Microelectronics, Belgrade, Serbia and Montenegro, pp. 576-579, 14–17 May 2006.
[22] I. Vurgaftman and J. R. Meyer, “Band parameters for III–V compound semiconductors and their alloys”, J. Appl. Phys., Vol. 89, pp. 5815-5875, 2001.
[23] S. L. Miller, “Avalanche Breakdown in Germanium”, Phys. Rev., Vol.99, pp.1234-1241, 1955.
[24] J. N. Park, K. Rose, and K. E. Mortenson, “Avalanche Breakdown Effects in NearIntrinsic Silicon and Germanium”, J. Appl. Phys. Vol.38, pp.5343-5351, 1967.
[25] P. Liu, R. Yen, and N. Bloembergen, “Dielectric Breakdown Threshold, Two-Photon Absorption, and Other Optical Damage Mechanisms in Dianmond”, IEEE J. Quantum Electron, Vol. QE-14, No.8, pp.574-576, 1978.
[26] E. Yablonovitch, “Optical Dielectric Strength of AlkaliHalide Crystals Obtained by Laser Induced Breakdown”, APPL. PHYS. LETT., Vol.19, pp.495-497, 1971.
[27] W. L. Smith, J. H. Bechtel, and N. Bloembergen, “Dielectric-breakdown threshold and nonlinear-refractive-index measurements with picosecond laser pulses”, Phys. Rev. B, Vol.12, pp.706-714, 1975.
[28] T. P. Chow, “SiC and GaN High-Voltage Power Switching. Devices”, Materials Science Forum, vol. 338-342, pp. 1155-1160, 2000.
[29] A. Huzayyin, S.A. Boggs, and R. Ramprasad, “Quantum Mechanical Study of Charge Injection at the Interface of Polyethylene and Platinum”. 2011 Annual Report of the IEEE Conference on Electrical Insulation and Dielectric Phenomena.
[30] W. G. Oakes, “The electric strength of some synthetic polymers”, Proceedings I.E.E., 96, Part I, 37, 1949.

CHAPTER 4
THE EFFECT OF DIPOLE SCATTERING ON INTRINSIC BREAKDOWN STRENGTH OF POLYMERS

4.1 The Effect of Dipoles on Intrinsic Breakdown

The effect on the breakdown field of small mole fractions of fluorine atoms incorporated into plasma-polymerized polyethylene has been studied by applying rectangular voltage pulses. The increased breakdown field after incorporation of fluorine atoms into the film for pulse widths less than 5 μs was explained on the basis of electron scattering by C-F dipoles [1]. Work of Austen and Pelzer [2] on polyethylene and vinylite showed that the dipoles act as additional scattering centers which increase the breakdown field at low temperature. The very high breakdown field of atomically flat, amorphous aromatic polythiourea films suggested that the randomly oriented dipoles (thiourea group) and the glass-phase structure provide strong scattering of charge carriers which results in greater breakdown field and reduced conductivity compared with nonpolar polymers [3]. Such experimental evidence demonstrates that dipoles play an appreciable role in determining the dielectric breakdown field of polar polymers. Fröhlich's early theoretical work demonstrated that polar groups in polymers act as scattering centers for hot electrons and thereby decrease the electron mean free path, which increases the breakdown field at low temperature[4]. Understanding the effect of dipole scattering on breakdown field at a fundamental level can provide guidance for the design of dielectrics with improved breakdown field.

The best available data for "intrinsic" breakdown field of polymers were measured by W. G. Oak [5] with care to eliminate extrinsic factors, e.g., electrode edge effects, thermal effects, conducting impurities, etc. The measured data are independent of thickness and ambient medium, with no obvious time effects. Figure 4.1 shows the measured intrinsic breakdown field of various polymers over the temperature range from -200^{o}C to 150^{o}C [5][6]. In general, the maximum breakdown fields are obtained in the low temperature region. At greater than 10 MV/m, the

breakdown field for polar polymers (solid lines) is greater than that for nonpolar polymers (dashed lines).

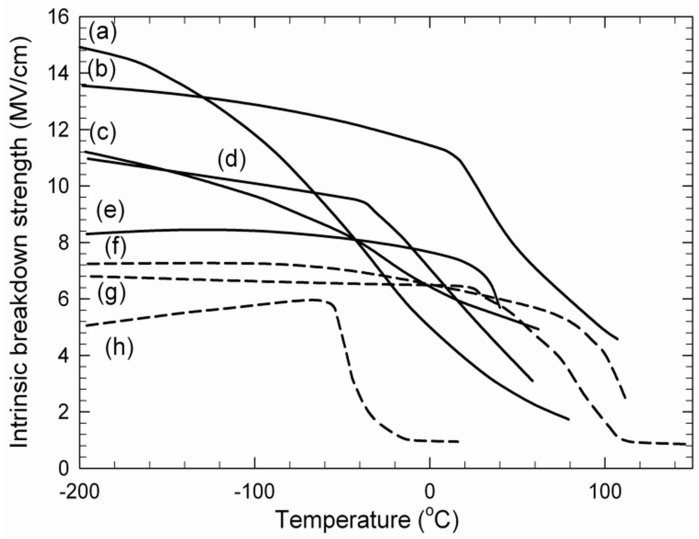

Figure 4.1 Temperature dependence of intrinsic breakdown field of various polymers with recessed specimens and dc voltage adapted from [5][6]. (a) Polyvinyl alcohol (PVA), (b) Polymethyl methacrylate (PMMA), (c) 55% Chlorinated Polyethylene, (d) 8% Chlorinated Polyethylene, (e) 1-1.5% Oxidized Polyethylene, (f) Polystyrene (PS), (g) Polyethylene (PE), (h) Polyisobutylene (PIB). Solid lines represent polar polymers and dashed lines represent nonpolar polymers.

4.2 Scattering Theory, Computations and Models

4.2.1 Hypothesis

Intrinsic breakdown has been explained in terms of electron avalanche theory, which depends on the presence and field induced multiplication of charge carriers. Avalanche multiplication occurs at high electric field when carriers acquire sufficient kinetic energy between collisions (scattering events) to cause impact ionization with relatively high probability. At sufficiently high field, carrier multiplication leads to irreversible damage and, ultimately, breakdown.

The intrinsic breakdown field increases with the scattering rate as field-induced energy gain is balanced by scattering-induced loss to a greater electric field. The greater energy loss can be expressed in terms of reduced mobility as a function of electric field. This leads to the hypothesis that materials with lower carrier mobility tend to have higher breakdown field. If more than one source of scattering is present, their effect can normally be combined, to a good approximation,

using Matthiessen's rule [7]. Since we are interested in the intrinsic breakdown field, which is an "intrinsic" material property, scattering induced by other sources such as chemical impurities, defects, and surface properties is ignored. In the present study, we consider the effect of dipole and phonon scattering, which can be expressed by

$$\frac{1}{\mu_{total}} = \frac{1}{\mu_{dipole}} + \frac{1}{\mu_{phonon}} \tag{4.1}$$

4.2.2 Mobility Limited by Dipole Scattering

Dipoles influence the electronic behavior of insulators in two ways. The first is creation of bound states (traps) [3][8]. Quantum mechanical analysis show that binding of electrons in the electric dipole field of a polar molecule can only occur when the molecule has a dipole moment larger than 1.625 Debye [3]. The binding energy of such states is in the range of 10^{-3} to 10^{-4} eV as predicted by Density Functional Theory (DFT) calculations, which is much smaller than the thermal energy at room temperature. As a result, the effect of such bound states should be negligible. Polaron binding energy calculations show that an extra electron injected into a polymer falls spontaneously into a bound state (trap), such traps are caused mainly by the conformational distortion of polymers (0.1 to 0.4 eV) or impurity states (0.2 to 2 eV), rather than states created by molecular dipoles [10][11].

The second way in which dipoles influence charge carrier mobility is through dipole scattering, i.e., the Coulomb field associated with the dipoles interacts with charge carriers to change their motion, which reduces electron mobility. Electrons experience dipole scattering as a result of the randomness of the dipole moment, since the matrix element for scattering in Fermi's golden rule vanishes for a time-independent periodic potential. Most polymers show long-range disorder as the degree of crystallinity of most polymers ranges from 5%~50%. The conformational disorder of polymers breaks the translational symmetry of the dipole potential, which makes dipole scattering relevant to polymers. The dipole scattering limited mobility can be derived in the relaxation time

approximation of the Boltzmann equation, which indicates that dipole limited mobility, μ_{dipole}, is proportional to the inverse dipole density and inverse square of the material polarization [12], i.e.,

$$\mu_{dipole} = C\frac{\varepsilon_r^2}{P^2 n_0} \tag{4.2}$$

where P is the dipole moment, n_0 is the dipole density, ε_r is the relative static dielectric constant, C is a constant given by

$$C = \frac{64\sqrt{2}\left(\hbar\varepsilon_0\right)^2 (\pi k_B T)^{1/2}}{3em^{*3/2}} \tag{4.3}$$

where $\hbar$ is the reduced Plank constant, ε_0 is the vacuum permittivity, k_B is Boltzmann's constant, e is the elementary charge, and m^* is the effective electron mass (approximated as free electron mass in this study). We can see that the dipole scattering limited mobility increases as the square root of temperature from above equations. A detailed derivation of dipole scattering limited mobility is presented in appendix A.

4.2.3 Mobility Limited by Phonon Scattering

Phonon scattering limited mobility results from collisions of electrons with the thermally vibrating nuclei. Electrons scatter from phonons by creating or destroying a phonon. Phonon scattering limited mobility characterizes how quickly an electron can move through a material when subjected to phonon scattering at electric field F, which is dependent on the average electron velocity, v_{avg}, as

$$\mu_{phonon} = F / v_{avg} \tag{4.4}$$

The main factor which determines the average electron velocity is the electron relaxation time, the reciprocal of which is the electron-phonon scattering rate, i.e., the number of scattering events per unit time, each of which changes the electron direction and/or energy. A first principles density functional perturbation theory (DFPT) based scheme for calculating electron-phonon scattering was discussed on Chapter 5 [13], which assumes the potential which generates scattering is the

result of perturbations of band energies caused by lattice displacements. As shown in equation (4.5), electrons scatter from state $\boldsymbol{k}$ (band j) to $\boldsymbol{k'}$ (band j'), while emitting or absorbing a phonon of wave vector $\boldsymbol{q}$ (band λ). Using Fermi's golden rule, the scattering rate can be evaluated by direct integration of electronic scattering probabilities over all possible final states. The electron-phonon coupling matrix elements, g, can be obtained directly in Quantum ESPRESSO [14], and the resulting data can be used to compute the electron-phonon scattering rate. The ± sign in equation (4.5) indicates whether a phonon is absorbed (+) or emitted (-) during scattering. The phonon occupation number, $n_{\boldsymbol{q}\lambda}$, given by the Bose-Einstein distribution, has a large effect on the temperature dependence of phonon scattering limited mobility.

Monte Carlo (MC) simulation, which is the most common approach to the study of charge transport, is used to evaluate the average electron velocity. The input parameter of the MC simulation is the electron-phonon scattering rate as a function of energy, which can be obtained by integrating the $\boldsymbol{k}$ dependent scattering rate from equation (4.5) over all directions [13]. The phonon involved in each scattering event is determined by a weighted random choice of phonon wave vector according to its contribution to total scattering rate. Whether a scattering event absorbs or emits a phonon is determined randomly based on the ratio contributed to the total scattering rate [15]. Detailed equations for calculating electron-phonon scattering rates are discussed in Chapter 3 and the MC scheme can be found in Chapter 5.

$$\frac{1}{\tau(\boldsymbol{kj})} = \frac{2\pi}{\hbar}\sum_{\boldsymbol{q}\lambda j'}\left|g^{\boldsymbol{q}\lambda}_{\boldsymbol{k}+\boldsymbol{q}j',\boldsymbol{k}j}\right|^2\left(n_{\boldsymbol{q}\lambda}+\frac{1}{2}\mp\frac{1}{2}\right)\delta(\varepsilon_{\boldsymbol{k}j}-\varepsilon_{\boldsymbol{k}+\boldsymbol{q}j'}\pm\hbar\omega_{\boldsymbol{q}\lambda}) \tag{4.5}$$

4.2.4 Computation Scheme of μ_{dipole} and μ_{phonon}

Calculations of dipole scattering were performed using density functional theory (DFT) in the local density approximation (LDA) using norm-conserving pseudopotentials, as implemented in Quantum-ESPRESSO. Variable cell relaxation calculations, including atomic and unit cell shape/size relaxation, were performed to determine structural properties of polymers studied. The supercells were relaxed

using a conjugate gradient algorithm until the forces on all atoms were smaller than 0.001(a.u) and energy changes were less than 0.0001(a.u). Sufficiently large Monkhorst-Pack k-point mesh and plane wave energy cutoffs were used for various polymers to produce converged results.

Three input parameters are needed to calculate dipole scattering limited mobility using equation (4.2), viz., dipole moment P, dipole denstiy n_0 and the dielectric constant ε_r. Polymer chains can rotate and fold easily; however, building blocks of polymers are assumed to be rigid, since they have constant bond length and bond angle. The dipole moment P is evaluated by taking the weighted average of the dipole moment in each building block of polymer. Dipole moment in each building block is evaluated by the vector sum of bond dipoles. The bond dipole moment of an X−Y bond is defined using Pauling's electronegativity (χ) as in equation (4.6) [16], where e is the elementary charge and d is the X−Y bond length. Dipole density $n_0=1/v_0$, where v_0 is the volume of a building unit of polymers. Accurate dielectric constant ε_r of a polymer is readily accessible through density functioal perturbation theory [17].

Table 4.1 Calculated bond length and bond dipole moments common in organic polymers

	C-H	O-C	O-H	Cl-C	F-C	N-C	N-H	O=C
d (Å)	1.11	1.41	0.980	1.79	1.36	1.45	1.03	1.23
P (Debye)	0.159	1.22	1.50	0.764	2.61	0.406	0.800	1.06

$$P_{bond} = ed\left(1-\exp\left[\frac{-(\chi_X-\chi_Y)^2}{4}\right]\right) \tag{4.6}$$

Taking polyvinyl alcohol (PVA) as an example, the structure of PVA proposed by Bunn [18] has two atactic chains in each unit cell, with 50% occupancy of hydroxyl groups as shown in Figure 4.2. The bond dipole moment can be evaluated easily using equation (4.6) with the bond length determined by geometry optimization using DFT (bond dipole moment of C-H 0.159 Debye, O-C 1.22 Debye, and O-H 1.50 Debye). The dipole moment P' of the CH_2 building block is 0.189 Debye, given that the two C-H bond dipoles have a H-C-H angle of 105.1 degrees. Dipole moment of the CHOH building block

P'' is 1.68 Debye, which is the vector sum of bond dipoles C-H, O-C and O-H. Given PVA has 50% occupancy of –OH sites, the average dipole moment *P* of PVA is 0.934 Debye. Dipole density n_0 is the reciprocal of the volume of each building unit v_0, which can be estimated from DFT calculation (v_0=22.5 Å^3). A dielectric constant of 3.65 is calculated from DFPT. Dipole limited mobility as a function temperature of PVA can be obtained using equation (4.2) and equation (4.3) (μ_{dipole}=3.28 at -200°C, and μ_{dipole}=6.65 at 27°C).

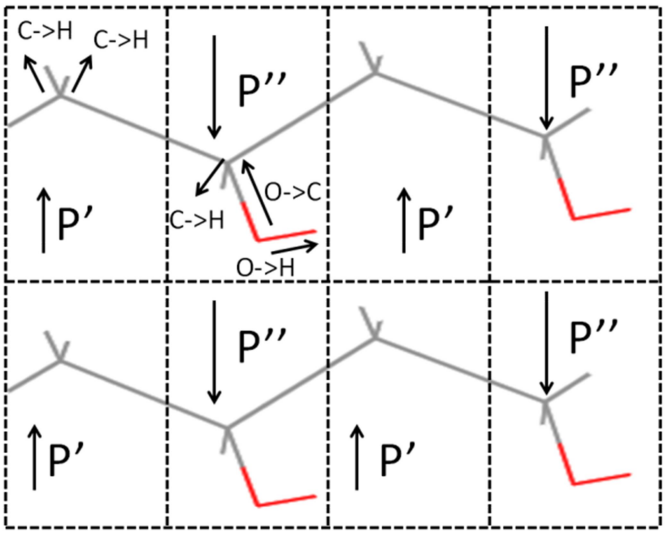

Figure 4.2 Schematic representation of polyvinyl alcohol (PVA). The dipole moment is the vector sum of bond dipoles in each building block, and the dashed lines define the boundaries of building blocks of volume v_0.

A 3D real space Monte Carlo simulation was performed to evaluate the phonon scattering limited mobility of electrons [15]. The simulation begins by putting 100 electrons with zero initial velocity over the surface at one end of the polymeric material, taken as z=0. The electrons are driven by the applied uniform field toward the opposite material surface. In moving through the material, electrons gain energy from the field and lose energy through collisions with phonons. The time interval *dt* between two consecutive collisions (which depends on the electron energy) is the reciprocal of electron-phonon scattering rate as a function of electron energy as calculated from DFPT [13]. The electron is assumed to travel a distance according to Newton's law during the time interval between collisions. At the end of free flight, an electron scatters through interaction with a phonon, with the

phonon involved in each scattering event determined stochastically from the phonon spectrum of the relevant polymer as calculated from DFPT. Conservation of momentum and energy determines the velocity after each scattering event. The trajectory of an electron is completed when its z coordinate reaches a preassigned value d, i.e., the thickness of the material (d=50 nm). Phonon scattering limited mobility can be evaluated by averaging the transient velocity of each step $\mu_{phonon} = F / v_{avg}$. Temperature influences phonon limited mobility greatly, as with increasing temperature the phonon density (phonons per unit volume) increases.

4.3 Temperature Dependence of Intrinsic Breakdown Field of Polymers

Electron mobilities of several polymers which can be modeled by DFT were calculated to investigate the correlation between electron mobility and intrinsic breakdown field. Computations for PVA use the crystal structure proposed by Bunn [18]with a monoclinic unit cell with two atactic chains. Each repeating monomer contains two hydroxyl sites, each with 50% occupancy. PE has an orthorhombic primitive unit cell composed of two chains, each of which is formed of two ethylene groups [22]. We use PE with carbonyl to model 1~1.5% oxidized PE, since carbonyl is the most common chemical impurity in PE. A 2x2x2 supercell is created based on the primitive unit cell of crystalline orthorhombic PE, and one of the CH_2 repeating units is replaced by carbonyl group ($C_{32}H_{62}O$), which results in about 1.56% carbonyl concentration. Likewise, one hydrogen atom replaced by chlorine atom in a 1x1x2 supercell ($C_8H_{15}Cl$) is used to model 8% chlorinated PE, and 55% chlorinated PE is modeled by $C_4H_4Cl_4$. PMMA, PS and PIB are relatively difficult to model in DFT because of their long side chains.

The experimental temperature dependence of the intrinsic breakdown field for various polar and nonpolar polymers is shown in Figure 4.1. In the high temperature region, the intrinsic breakdown field tends to decrease with temperature for all polymers, which is usually attributed to thermal breakdown, i.e., the thermal balance between Joule heating from conduction current and its dissipation. Investigations of statistical time lag, the direction of the breakdown path, and other

studies have determined that electronic process plays a dominant role in dielectric breakdown in the low temperature region, for which the curves of Figure 4.1 fall into two categories. For nonpolar polymers, the breakdown field increases slightly with temperature or is nearly independent of temperature, whereas for polar polymers, the breakdown field decreases with temperature. The variations in temperature dependence of intrinsic breakdown for polar and nonpolar polymers can be related to the dominant scattering mechanism.

Figure 4.3 shows the calculated electron mobility as a function of temperature for two typical polar (PVA) and nonpolar polymers (PE). Dipole scattering limited mobility increases with temperature, since at low temperature, a carrier has smaller thermal velocity, which results in a greater change in momentum when the carrier interacts with a dipole. Phonon scattering limited mobility decreases with temperature, as the phonon occupation factor is given by Bose-Einstein distribution. With increasing temperature, more phonon modes are excited and can participate in scattering events, which decreases electron mobility. Figure 4.3 indicates that for non-polar polymers such as PE, electron-phonon scattering limits the total mobility. In polar polymers like PVA, dipole scattering plays a significant role throughout the entire temperature range and dominates at low temperatures.

The positive temperature coefficient of breakdown field for nonpolar polymers can be explained by the dominance of electron-phonon scattering, the effect of which increases with temperature. The negative temperature coefficient of breakdown field for polar polymers can be explained by decreasing dipole-induced scattering as a function of temperature.

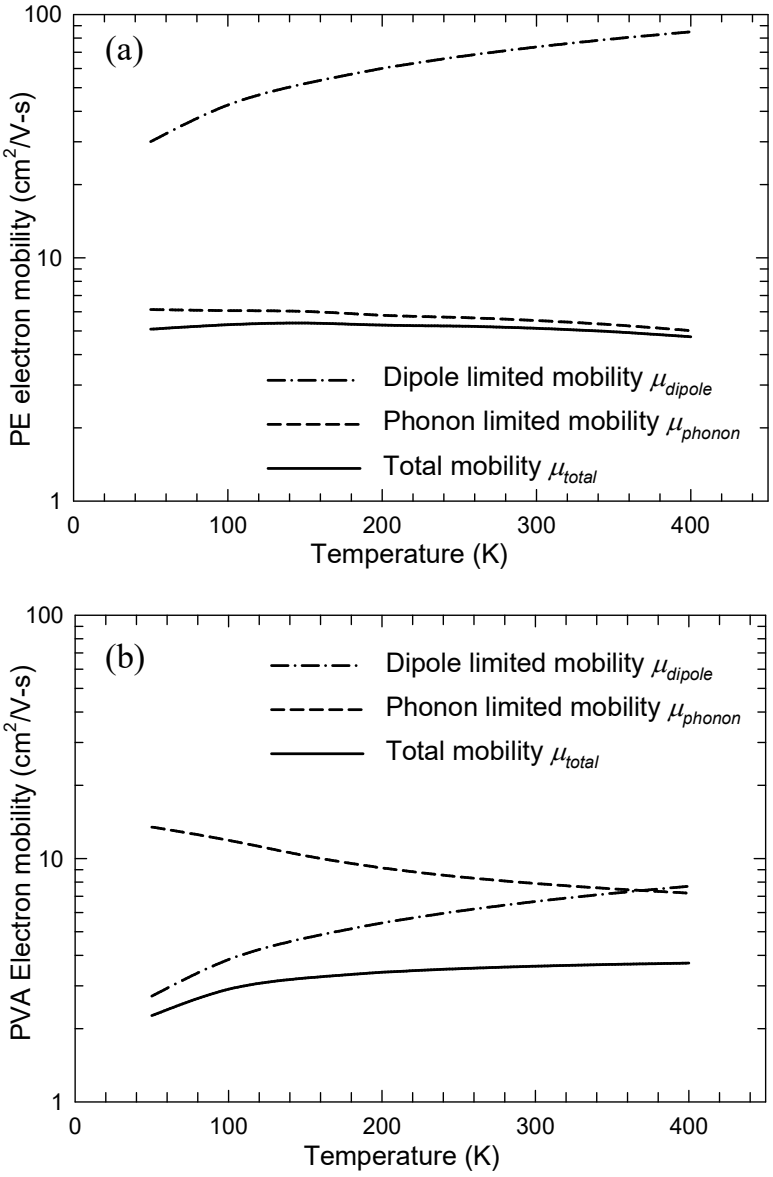

Figure 4.3(a) Electron mobility of PE and (b) Electron mobility of PVA. The dash-dot lines represent dipole scattering limited mobilities, dashed lines represent phonon scattering limited mobilities, and solid lines are the total electron mobilities.

4.4 Mobility of Selected Polymers and Comparison with Experiments

Table 4.2 provides the calculated dipole scattering limited mobility and phonon scattering limited mobility of various polymers at low temperature (-200 ^{o}C) and room temperature (27 ^{o}C). The calculated electron mobility in polymers is much greater than experimental data estimated from bulk conduction measurements (typically 10^{-10}-10^{-14} cm^2/Vs) [20]. Low field electron

transport, which results from hopping between localized states, is characterized by very low mobility. In the present context, electrons subject to dipole scattering and phonon scattering are in the conduction band as relevant to breakdown. The high mobility states (>1cm^2/Vs) required for avalanche formation in polyethylene are known to exist based on both theoretical [21] and experimental [22] research.

Table 4.2(a) Mobilities limited by dipole scattering and phonon scattering and correlation with intrinsic breakdown field of polymers at -200°C

	Properties at -200°C			
Various Polymers	μ_{dipole} (Vs/cm^2)	μ_{phonon} (Vs/cm^2)	$(\mu_{total})^{-1}$ (Vs/cm^2)	E_b (MV/cm)
g: Polyethylene	36.3	6.09	0.192	6.7
e: Oxidized Polyethylene(1~1.5%)	26.6	4.96	0.239	8.3
d: Chlorinated Polyethylene (8%)	23.1	4.74	0.254	10.9
c: Chlorinated Polyethylene (55%)	5.02	7.88	0.326	11.2
a: Polyvinyl alcohol	3.29	12.9	0.381	15

Table 4.2(b) Mobilities limited by dipole scattering and phonon scattering and correlation with intrinsic breakdown field of polymers at 27°C

	Properties at 27°C			
Various Polymers	μ_{dipole} (Vs/cm)	μ_{phonon} (Vs/cm^2)	$(\mu_{total})^{-1}$ (Vs/cm^2)	E_b (MV/m)
g: Polyethylene	73.5	2.51	0.412	6.4
e: Oxidized Polyethylene(1~1.5%)	53.8	1.99	0.521	7.05
d: Chlorinated Polyethylene (8%)	46.9	2.88	0.369	5.14
c: Chlorinated Polyethylene (55%)	10.2	3.88	0.356	5.76
a: Polyvinyl alcohol	6.66	7.89	0.277	3.62

The calculated dipole scattering limited mobility increases with temperature, whereas phonon scattering limited mobility decreases with temperature as discussed above. Dipole scattering plays a significant role in highly polar polymers with large dipole moment associated with each building block (e.g., hydroxyl group in PVA and C-Cl dipole in chlorinated polyethylene). Comparison of dipole scattering limited mobility for 8% and 55% chlorinated polyethylene indicates that large density of highly polar units which results in a large average dipole moment is important for effective dipole scattering. The above discussion indicates that scattering of carriers by dipoles is most important at low temperatures, where phonon-induced scattering is reduced. A large fraction of highly polar units in a polymer may extend this regime towards room temperature.

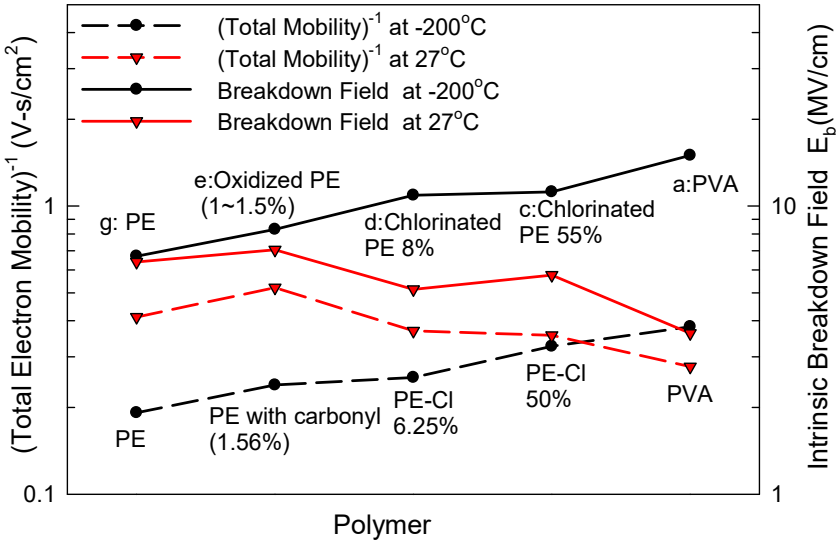

Figure 4.4 Correlation of reciprocal of the electron mobility (dashed lines) and intrinsic breakdown field (solid lines) of various polymers and at low temperature of -200°C (black lines) and room temperature of 27 °C (red lines)

Comparison of the electron mobility with experimental intrinsic breakdown data is based on plotting the reciprocal of total mobility together with intrinsic breakdown field of various polymers at both low temperature (-200°C) and room temperature (27°C), as shown in Figure 4.4. The intrinsic breakdown field (solid lines) tends to be proportional to the electron scattering rate as represented by the reciprocal of total electron mobility (dashed lines). The trends indicate that polymers with lower electron mobility (greater scattering) tend to have greater intrinsic breakdown

field. The analysis supports our hypothesis that greater scattering reduces electron mobility and thereby increases the dielectric breakdown field by balancing carrier energy gained from the electric field with energy loss to scattering to a greater electric field. Additional breakdown mechanisms, such as thermal breakdown and mechanical breakdown, may be relevant in the high temperature region. The inverse correlation of carrier mobility, as limited by dipolar and phonon scattering, and breakdown field of polymers is more likely in the low temperature region, for which dominant breakdown processes are electronic.

4.5 Systematic Assessment of Selected Dipolar Functional Groups

In an attempt to study the effect of dipoles on electron mobility on a systematic basis, we have calculated the dipole scattering limited mobility in seven polymers. We assume all seven polymers have eight building blocks (Figure 4.5) and have the two-chain crystal structure of PE. One of the eight building blocks, X, is subject it to systematic chemical substitution (X = CH_2, NH, CHCl, CO, CHOH, CHF, and CF_2). Table 4.3 lists the calculated dipole scattering limited mobility of the seven polymers at room temperature (27^{o}C), together with three input parameters needed to calculate μ_{dipole}, i.e., dielectric constant ε_r, dipole moment P, and dipole density n_0.

Table 4.3 Dipole limited mobility at 27 ^{o}C for seven polymers

X	CH_2	NH	CHCl	CO	CHOH	CHF	CF_2
Dielectric constant	2.98	3.20	2.96	3.28	4.00	3.07	3.07
Dipole Moment (Debye)	0.194	0.249	0.269	0.302	0.386	0.501	0.582
Dipole Density(1/ Å^3)	0.0625	0.0604	0.0500	0.0680	0.0654	0.0775	0.0757
μ_{dipole} (cm^2/Vs)	73.1	52.9	46.9	33.6	31.8	9.38	7.12

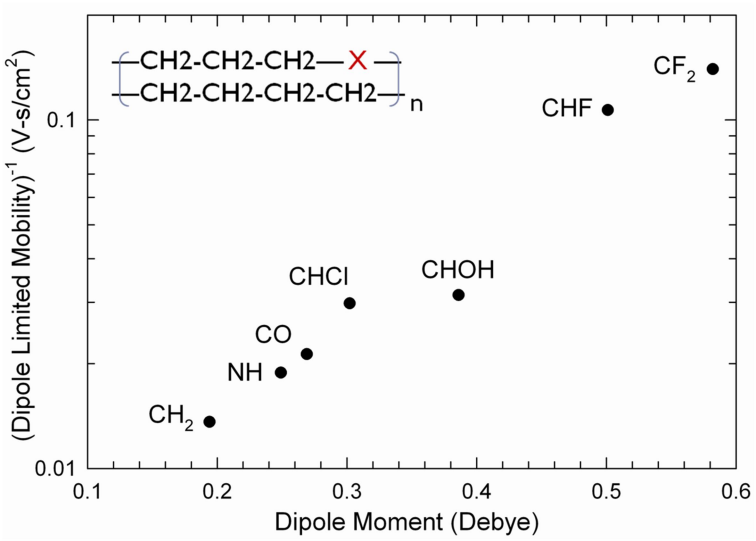

Figure 4.5 Reciprocal of dipole scattering limited mobility as a function of dipole moment for seven polymers subjected to systematic chemical modifications

As a result of the small fraction of polar functional groups introduced, the dielectric constant and the dipole density are similar for the substituted polymers. The dipole moment *P* is the most important parameter since $\mu_{dipole} \propto (P)^{-2}$. The reciprocal of dipole scattering limited mobility as a function of dipole moment is plotted in Figure 4.5, which indicates that for substitutions with large dipole moment, such as CF_2 and –OH, the electron mobility decreases greatly as a result of increased dipole-induced scattering. The calculations can identify promising chemical substitutions which may increase breakdown field through dipole scattering when introduced to polymer chains.

The above analysis supports the benefit of introducing dipoles into polymers to reduce the electron mobility and increase breakdown field, especially in the lower temperature region. By investigating the effect of dipole scattering and phonon scattering on carrier mobility in non-polar and polar polymers, a quantitative correlation between chemical composition and intrinsic breakdown strength of polymers can be established. The important findings of the present work can be summarized as follows:

1. Differing temperature dependent intrinsic breakdown field for polar and nonpolar polymers in low temperature region can be explained by the dominant scattering mechanism (dipoles or

phonons) in the framework of electronic break-down. Scattering of carriers by dipoles is most important at low temperatures, where phonon effects are reduced. A large fraction of highly polar units in a polymer may extend this regime toward room temperature.

2. Randomness of dipole moment is critical as carriers cannot experience dipole scattering in materials with translationally periodic potentials. Amorphous polymers with large dipoles distributed randomly along polymer chains are good candidates for high breakdown strength polymeric films.

3. Based on the inverse relationship of carrier mobility and intrinsic breakdown field, dipole scattering limited mobility can be used to evaluate the effect of dipole scattering on intrinsic breakdown field of polymers. Three parameters needed to calculate dipole scattering limited mobility, i.e., dielectric constant ε_r, dipole moment P, and dipole density n_0, are easily estimated and can be used for rapid screening to explore large chemical spaces for polymers with potential for high intrinsic breakdown field. Assessment of polymers subjected to systematic chemical modifications can identify promising functional groups containing dipoles which have the potential for high breakdown strength when introduced to polymers.

4.6 References

[1] T. Nakano. M. Fukuyama, H. Hayashi, K. Ishii and Y. Ohki, "Effect of polar groups on the electrical breakdown strength of plasma-polymerized films", IEEE Trans Dielectr. Electr. Insul, Vol. 25, No. 6, 1085, 1990.

[2] A. E. W. Austen, H. Pelzer, "Electric strength of vinylite and its temperature dependence", E.R.A. Report Ref. L/T 149, 1944.

[3] Shan Wu , Weiping Li , Minren Lin , Quinn Burlingame , Qin Chen , Andrew Payzant , Kai Xiao , and Q. M. Zhang, "Aromatic polythiourea dielectric with ultrahigh breakdown field strength, low dielectric loss and high electric energy density", Adv. Mater, 25, pp. 1734-1738, 2013

[4] H. Frohlich, "Theory of electrical breakdown in ionic crystals", Proc. Roy. Soc. 160, pp. 230, 1937.

[5] W. G. Oakes, "The electric strength of some synthetic polymers", Proceedings I.E.E., 96, Part I, 37, 1949.

[6] I. D. E. Ball, "The intrinsic electric strength of polyvinyl alcohol and its temperature variation", Proc. Inst. Engrs. Vol. 98(I), pp. 84-86, 1951.

[7] T. Ishihara and K. Kato, "Theoretical prediction of universal curves for carrier transport in Si/SiO2 (100) interface", J. Appl. Phys. 114, 053713, 2013.

[8] J. M. Lévy-Leblond , "Electron capture by polar molecules", Phys. Rev., Vol. 153 , pp. 1 – 4, 1967.

[9] J. M. Ugalde , C. Sarasola , “Bound electronic states in a statically screened electric-dipole potential”, Phys. Rev. A, Vol. 54 , pp. 2868 – 2873, 1996.
[10] S. Serra, S. Iarlori, E. Tosatti, S. Scandolo, M. C. Righi, G. E. Santoro, “Self-trapping vs. non-trapping of electrons and holes in organic insulators: polyethylene”, Chem. Phys. Lett., 360, pp. 487-493, 2002.
[11] Juraj Nozar, Stanislav Nespurek, Jakub Sebera, “Polaron binding energy in polymers: poly[methyl(phenyl) silylene]”, J Mol Model, 18, pp. 623-629, 2012.
[12] Wei Zhao and Debdeep Jena, “Dipole scattering in highly polar semiconductor alloys”, J. Appl. Phys., Vol. 96, pp. 2095-2101, 2004.
[13] Y. Sun, S. A. Boggs, R. Ramprasad, "The intrinsic electrical breakdown strength of insulators from first principles", Appl. Phys. Lett. 101, 132906, 2012.
[14] P. Giannozzi, etc, J.Phys.:Condens.Matter, 21, 395502 (2009). http://www.quantum-espresso.org
[15] Y. Sun, S. A. Boggs, R. Ramprasad, “Monte Carlo studies of hot electron transport in insulating films with nanocavities”, 2013 IEEE International Conference on Solid Dielectrics, pp. 611 – 614, July 2013.
[16] Pauling, L. General Chemistry; Dover Publications Inc.: New York, 1988.
[17] C. C. Wang, G. Pilania, and R. Ramprasad, "Dielectric properties of carbon-, silicon-, and germanium-based polymers: A first-principles study", Phys. Rev. B 87, 035103, 2013
[18] Bunn, C.W., “Crystal structure of polyvinyl alcohol”, Nature, 161, pp. 929-930, 1948.
[19] M. S. Miao, P. E. Van Camp, V. E. Van Doren, J. J. Ladik, J. W. Mintmire, "Conformation and Electronic Structure of Polyethylene: A Density-Functional Approach", Phys. Rev. B, Vol. 54, No. 15, pp. 10430-1043X, October 1996-I
[20] R. J. Fleming, “Space charge in Polymers, Particularly Polyethylene”, Brazilian Journal of Physics, Vol. 29, no. 2, June 1999.
[21] Zeller, H.R., Pfluger, P., and Bernascon, “High-Mobility states and dielectric breakdown in polymeric dielectrics”, IEEE Trans. Dielectr. Electr. Insul., Vol. EI-19(3), pp.200-204. 1984.
[22] Ritsko, “in electronic properties of polymers”, eds. Mort, J and Pfister, G. J. Wiley & Sons, New York, 1982. Chapter 2, pp. 13-57.

CHAPTER 5
MONTE CARLO STUDIES OF HOT ELECTRON TRANSPORT IN POLYETHYLENE (PE) FILMS WITH NANOCAVITIES

5.1 Introduction to Hot Electron Transport

The problem of hot electron transport and energy loss at high electric fields in insulators is of considerable interest for dielectric breakdown and hot carrier related dielectric degradation. The underlying mechanisms of breakdown and high field aging are complex, as many processes are involved, e.g., carrier injection, carrier recombination, and the effect of impurity states, impact ionization, etc.

The injection of carriers from an electrode depends on the location of the metal Fermi level in the polymer bandgap and the proximity of impurity states to the Fermi level. Recent computations on the interface between PE and Pt indicate that the Fermi level of the Pt is close to the center of the PE bandgap, and the barrier to injection of holes or electrons from the Fermi level into impurity states in the PE (including those caused by carbonyl at the Pt-PE interface) is in the range of 1 eV, i.e., similar to the measured activation energy for PE [1].

Injected electrons gain energy from the electric field. At sufficiently high field or in the presence of nanocavities at lower field, electrons can gain sufficient energy to create defects or to break chemical bonds. At low fields, the electrons will beare trapped by impurity states caused by chemical (~1 eV) or conformational “abnormalities” (~0.3 eV). With increasing field, the carrier energy will becomes great enough to avoid conformational traps and, eventually, chemical impurity state traps, at which point, the dominant energy loss is to phonons and through ionization resulting in electron multiplication. Recombination of electron-hole pairs can also release sufficient energy to cause polymer degradation. Recent experiments and modeling indicate that dc field-induced electroluminescence in PE can be interpreted on the basis of recombination [2].

Aging and breakdown can occur as a result of hot electrons, carrier recombination, thermal runaway, or a combination thereof.

In Chapter 3, we developed a first principles method to estimate the intrinsic breakdown strength field of materials based on the average electron model [3]. Implementation of Tthe average electron model is based on density functional perturbation theory (DFPT) and on the direct integration of electronic scattering probabilities over all possible final states, with no adjustable parameters. The computed intrinsic breakdown fields compare favorably with available experimental data. However, engineering breakdown is dominated by "extrinsic" factors such as imperfections (e.g., chemical impurities at the atomic level, and cavities at the nanoscopic to microscopic and macroscopic scales) as well as statistical variations in morphology and microstructure. A Monte Carlo simulation method is presented in this Chapter, and is used to examine the likely effect of cavities on high field aging and breakdown in polyethylene (PE) films as a first step down the path from intrinsic breakdown to engineering breakdown.

5.2 Monte Carlo Method

A summary of the Monte Carlo method with emphasis on implementation for the present study is provided in the flowchart of Figure 5.1. Appendix D gives Matlab code of the Monte Carlo simulation described below. An electrons with zero initial energy is injected into the insulating film at a randomly chosen position at one end of the film, taken as z=0. The electron is driven by the applied uniform field toward the opposite edge of the film, at $z=d$, d being the film thickness. In this study, the film thickness, d, is 50 nm. In moving through the film, the electron gains energy from the field and loses energy in collisions with the lattice vibrations, i.e., phonons.

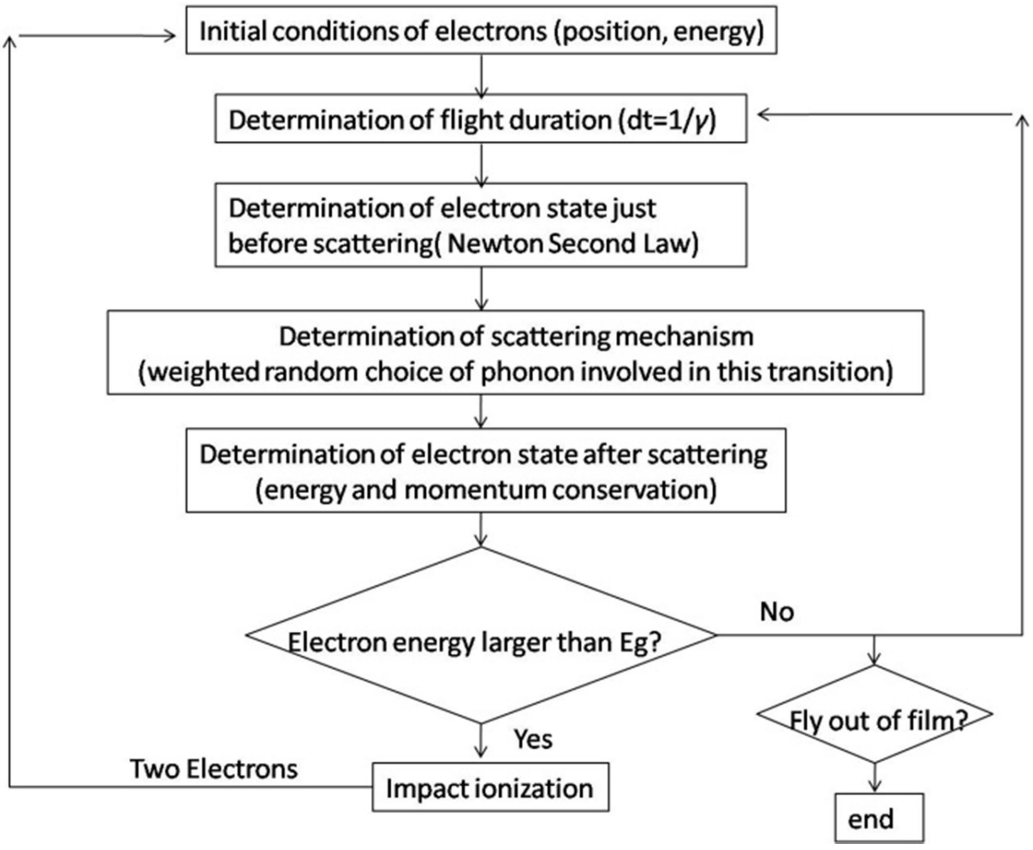

Figure 5.1 Flowchart of the MC simulation

An injected electron travels freely according to the electric field applied during a short time interval *dt*. Normally the time interval *dt* is determined stochastically in a Monte Carlo simulation [4]. Here, *dt* is the reciprocal of the electron-phonon scattering rate as a function of electron energy as calculated from DFPT [3]. Each electron is labeled with (**r, k**), where **r** is the position of the electron and **k** is its wave vector. During free flight, new **r** and **k** values are calculated according to Newton's second law:

$$\boldsymbol{k}(t+dt) = \boldsymbol{k}(t) + (eF/m^*)dt \tag{5.1}$$

$$\boldsymbol{r}(t+dt) = \boldsymbol{r}(t) + (\mathrm{h}\boldsymbol{k}/m^*)dt + (eF/2m^*)dt^2 \tag{5.2}$$

The effective electron mass, m^*, is taken as the free electron mass. The electron energy is related to its wave vector by the simple parabolic dispersion relation $E(\boldsymbol{k})=\hbar\boldsymbol{k}^2/2m^*$. Scattering is

determined by a weighted random choice of phonon wave vector $\boldsymbol{q}$ according to its contribution to total scattering rate ($\gamma = \sum \gamma_{q\lambda}$). Energy loss $\hbar\omega_{q\lambda}$ at each scattering event is determined by the phonon dispersion curve of crystalline PE calculated from DFPT. Final energy is determined by energy conservation (5.3). The ± sign indicates whether a phonon is absorbed (+) or emitted (-) during a scattering process. Whether a scattering event absorbs or emits a phonon is determined randomly based on the ratio contributed to the total scattering rate ($\gamma = \sum \gamma_{\pm}$).

$$E' = E \pm \hbar w_{ql} \tag{5.3}$$

Isotropic scattering is adopted since isotropic scattering is implicit in the average electron model [3]. The polar and azimuthal scattering angles (θ, φ) are determined by

$$\cos q = 2r_1 - 1, j = 2pr_2 \tag{5.4}$$

where r_1 and r_2 are random numbers between 0 and 1. In 3D simulations, the polar angle, θ, is a solid angle between initial and final electron wave vectors. At a sufficiently high electric field, the electron energy increases indefinitely until a threshold is reached at which the electron generates a second conduction electron by excitation across the bandgap, i.e., impaction ionization, which results in two electrons at the conduction band minimum (CBM) which are then subject to acceleration by the field [5].

5.3 Consistency with Average Electron Model

All simulations were performed in 3 dimensions, and results are projected onto xz planes for simplicity. Take NaCl as an example, Figure 5.2 (a) is a 3D electron trajectory at electric filed 2×10^8 V/m and Figure 5.2(b) is the 2D electron trajectory by projecting 3D electron trajectory on xz plane.

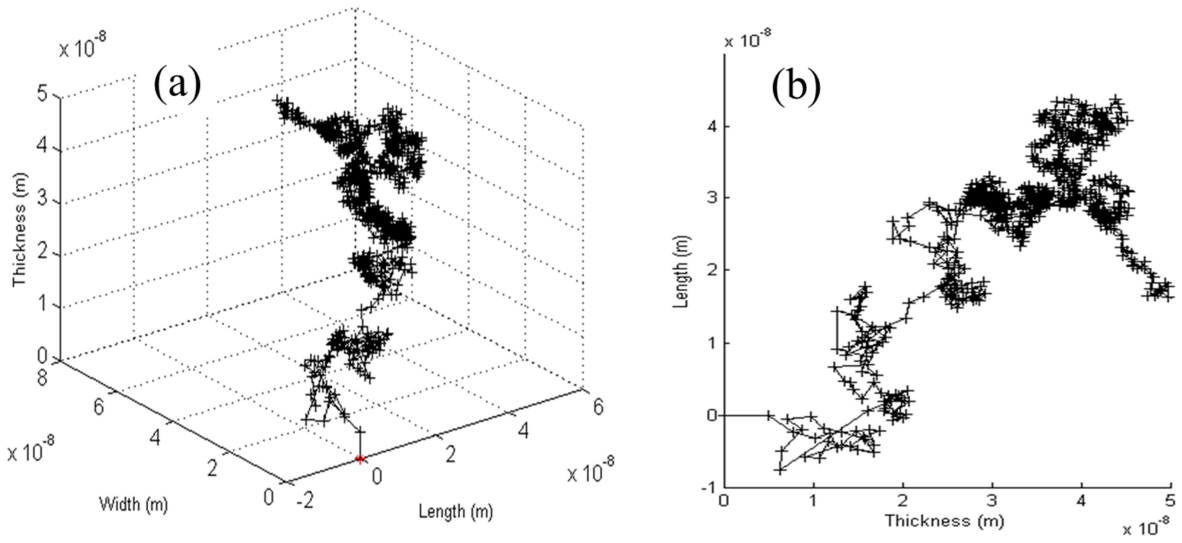

Figure 5.2 (a) 3D electron trajectory in NaCl at 2×10^8 V/m (b) 2D electron trajectorys projected onto xz plane in NaCl at 2×10^8 V/m

Comparing the results of average electron model [3][6] and MC model, we find that the two models are consistent in their description of electron energy distributions. Take the simulation results of sodium chloride as an example. Figure 5.3(a) is based on the average electron model. The red line represents average energy loss as a function of electron energy, while the black lines represent average energy gain at electric fields of 200, 386, and 500 MV/m. At an electric field 200MV/m, a low energy electron gains energy since the energy gain is greater than energy loss as shown by the black dotted curve and red curve. With increased electron energy, the energy gain decreases as the energy loss increases until at 4 to 6 eV, they equilibrate. Figure 5.3(b) shows the electron energy as a function of distance at the same field (200MV/m). We can see that the electron energy increases gradually and saturates at 4 to 6 eV in agreement with the average electron model.

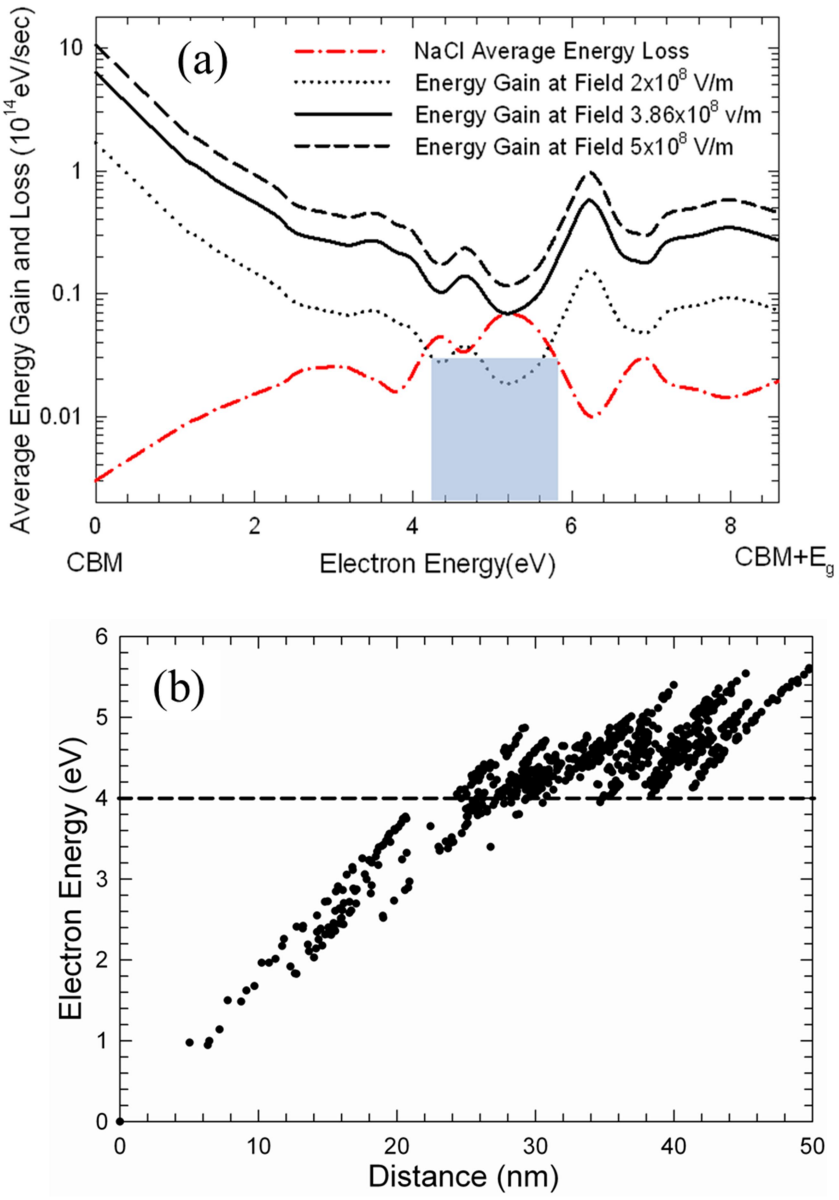

Figure 5.3 (a) Average electron model for NaCl. The red dotted curve is average energy loss, and the black gurves are energy gain at various electric fields as a function of electron energy. At electric field 200MV/m, electrons will equilibrate at 4 to 6 eV as confined in the blue box. (b) MC simulation of electron energy as a function of distance at the the same field (200MV/m), energy increases gradually and saturates at 4 to 6 eV.

5.4 MC Simulations of Crystalline PE

The Monte Carlo simulations based on the approach described in the previous section have been carried out for crystalline PE. Figure 5.4 and Figure 5.5 present the electron trajectories and the spatial evolution of the electron energy distribution respectively.

Figure 5.4 shows 2D projections of 3D electron trajectories for 10 initial electrons at four different electric fields, (a) F=500MV/m, (b) F=1 GV/m, (c) F=1.5 GV/m, and (d) F=2 GV/m. Colors represent successive "generations" of electrons genereated by impact ionization. At a sufficiently high electric field, an electron undergoes a random walk of progressively increadsing kinetic energy until it attains thereshold energy, at which the highly energetic electron from the conduction band excites another electron from the valence band to the conduction band generating an electron hole pair. The newly generated electron (second generation), caused by the high electric field, can attain sufficient energy to generate further carriers (third generation), and the repetition of this process leads to carrier multiplication and breakdown. No impact ionization occurs at 500 MV/m and 1 GV/m, and the electron energy distribution achieves steady state as the energy gain from the external electric field is balanced by energy loss from collisions with phonons. The energy loss is caused mainly by phonon collisions that result in an electron traveling "against" the field, i.e., being decelerated by it and giving up energy to the field. At 1.5 and 2 GV/m, the electrons gain sufficient energy to cause impacting ionization, as can be seen from Figure 5.4(c) and (d) which indicate that the electrons are multiplied by impact ionization as they travel through the films. The maximum "generation" of electrons after impact ionizations is 4 and 9 in Figure 5.4(c) and (d), respectively. The breakdown field for this model is in the range of 1.5 GV/mm, as impact ionization occurs at this field. The breakdown field determined from the MC model is not of great interest, since we used the electron phonon scattering rate calculated for a pure crystalline PE and the bandgap of 8.8eV [7]. Engineering breakdown and aging of PE occur at much lower fields, as technical PE is semi-crystalline and contains appreciable additives and chemical impurities which are sources of impurity states in the bandgap [8]. The experimental breakdown field of technical PE is in the range of 160 MV/m [9].

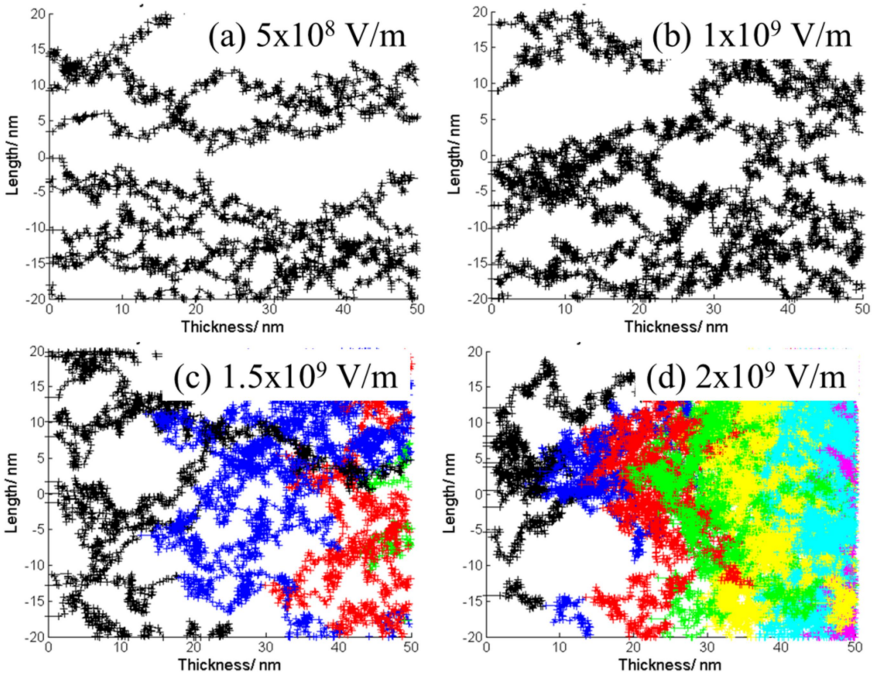

Figure 5.4 Trajectories of ten initial electrons projected onto the xz plane at electric fields of (a) 500 MV/m, (b) 1 GV/m, (c) 1.5GV/m, and (d) 2 GV/m. Colors represent successive "generations" of electrons generatged by impact ionization.

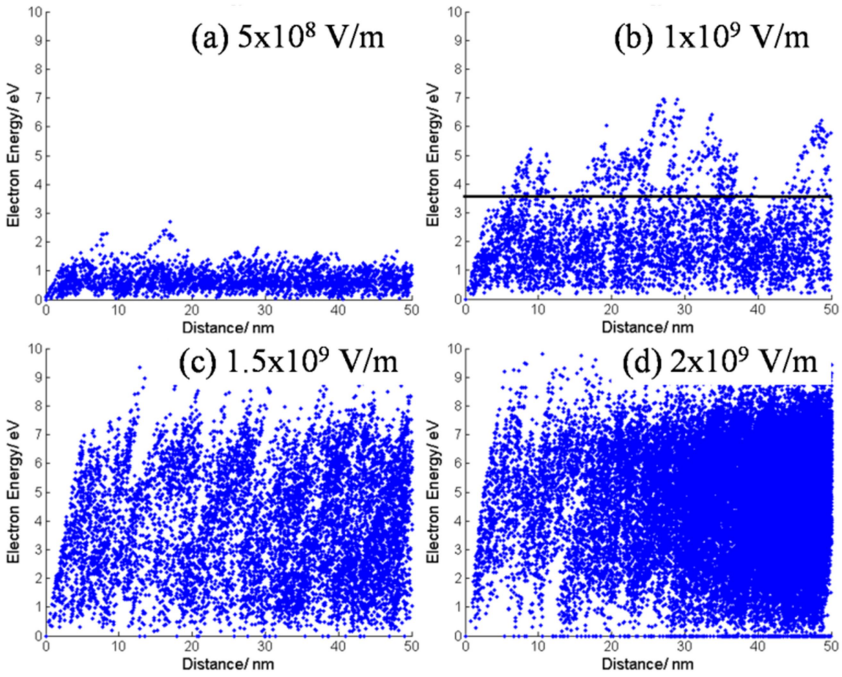

Figure 5.5 Electron energy as a function of distance along z axis at electric fields of (a) 500 MV/m, (b) 1 GV/m, (c) 1.5 GV/m, and (d) 2 GV/m. In moving through the film, the electron gains energy from the ekectric field and loses energy by scattering with phonons, the energy of each electron is recorded after each scattering event.

Figure 5.5 shows the spatial evolution of the electron energy and electron density distributions. Both the energy and number of electrons increase with electric field. In moving through the film, the electron gains energy from the electric field and loses energy by scattering with phonons, the energy of each electron is recorded after each scattering event. At low electric fields, energies of electrons reach equilibrium with statistical variation around that equilibrium. At sufficiently high electric fields, electrons udergo a random walk of progressively increasing kinetic energy. The slope of electron energy with respect to electron travel distance increase with the electric field applied. At 1 GV/m, significant electron heating occurs without impact ionization. The black line shows that substantial fraction of electrons have energy greater than 3 to 4 eV, which is comparable to C-H and C-C bond energies in organic molecules and suggests high field aging caused by bond cleavage [10]. In the linear hydrocarbon n-$C_{36}H_{74}$, strong evidence for a degradation threshold which corresponds to electron energies of 3 to 4 eV has been observed [11]. Given that electrons will be injected at one electrode and holes at the other, recombination will also release sufficient energy to break chemical bonds.

5.5 MC Simulations of PE with Nanocavities

Technical PE has about 50% crystallinity and a density in the range of 0.95 g/cm^3 which implies ~10% free volume in the amorphous regions. As well, technical PE contains appreciable chemical impurities, such as carbonyl, which create impurity states in the bandgap. The above considerations suggest the need to consider “extrinsic” factors such as physical disorder and chemical defects. The Monte Carlo scheme can include defects (whose scattering rates need to be computed independently) and voids (within which no scattering occurs), thereby providing a first principles pathway to go beyond intrinsic breakdown. Monte Carlo simulations with nanocavities are carried out in this study as the first step down the path toward engineering breakdown. Figure 5.6 is a

schematic of ~10% volume fraction of nanocavities in a film of 20 nm thickness (dimension 100×100×20 nm).

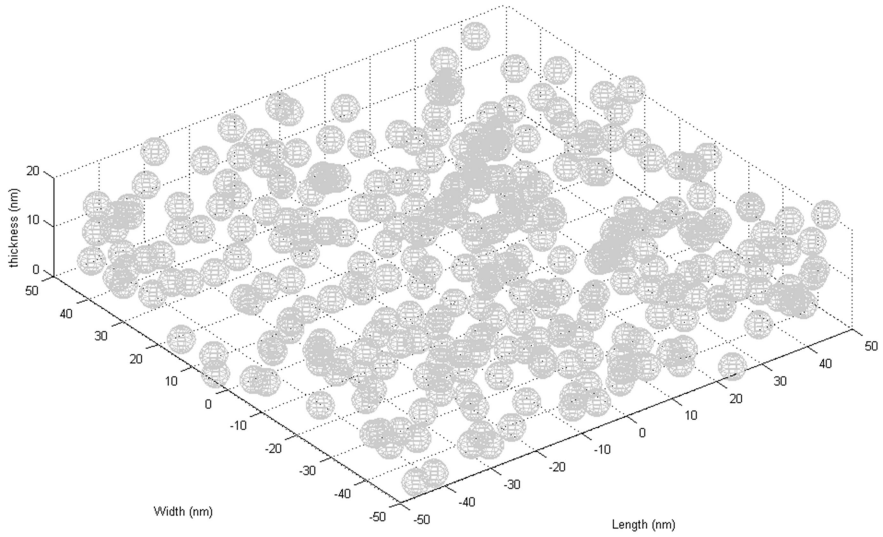

Figure 5.6 Schematic of 10% nanocavities in a film of 20 nm thickness, nanocavities are represented by gray surfaces.

Figure 5.7 shows electron trajectories through the film with no cavities and 10% volume fraction of cavities of various cavity radii at 500 MV/m. The effect of nanocavities on the energy distribution can be observed in Figure 5.8, where the energy of electrons passing through cavities increases linearly with distance, in some cases to energies which could cause bond cleavage, formation of carbonyl, etc., i.e., high field aging. The electron energy distribution indicates that the average electron energy increases substantially with cavity size at constant volume fraction, as might be expected. Future work will relate the electron energy distribution to the rate of bond cleavage within the dielectric.

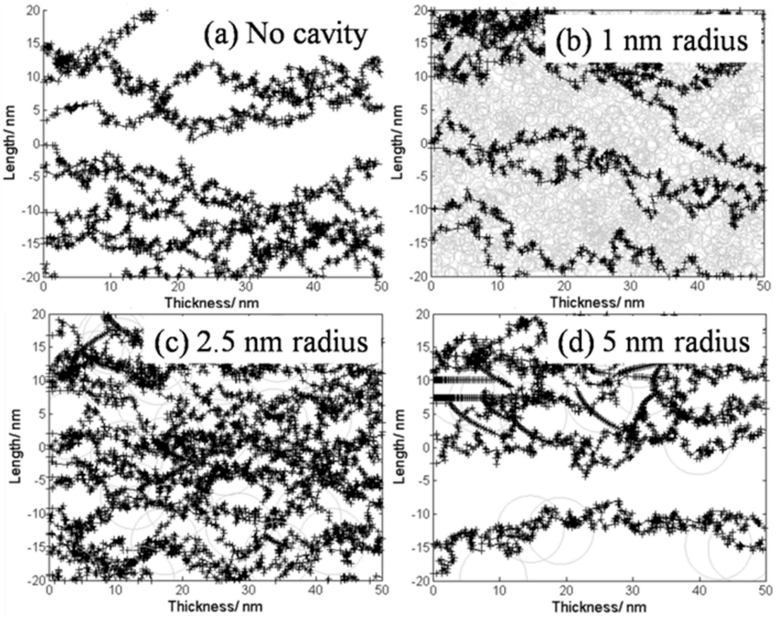

Figure 5.7 Projections of ten electrons trajectories in the PE film with 10% volume fraction nanocavities at a field of 500 MV/m. Nanocavities are indicated by gray circles: (a) no cavity, (b) 1 nm radius, (c) 2.5 nm radius, and (d) 5 nm radius.

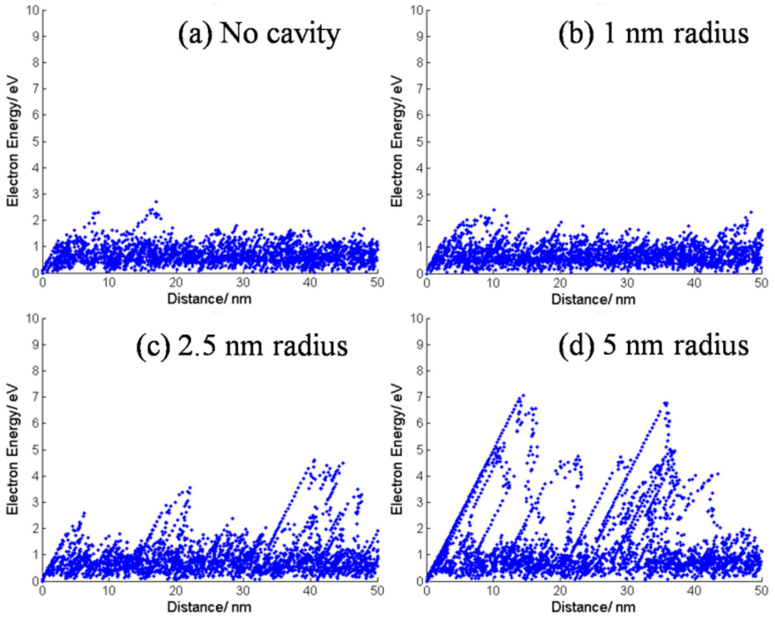

Figure 5.8 Electron energy as a function of distance along z axisin PE film with 10% volume fraction nanocavities at a field of 500 MV/m. A linear increase in energy with distance suggests that an electron is passing through a cavity: (a) no cavity, (b) 1 nm radius, (c) 2.5 nm radius, and (d) 5 nm radius.

Figure 5.9 provides the electron energy probability density distribution in PE film with 10% volume fraction nanocavities of various radii at 500 MV/m. With increasing cavity radius, the probability density broadens and flattens, as would be expected. Statistical configuration of nanocavities can be included to investigate the breakdown probability in this model as a future work.

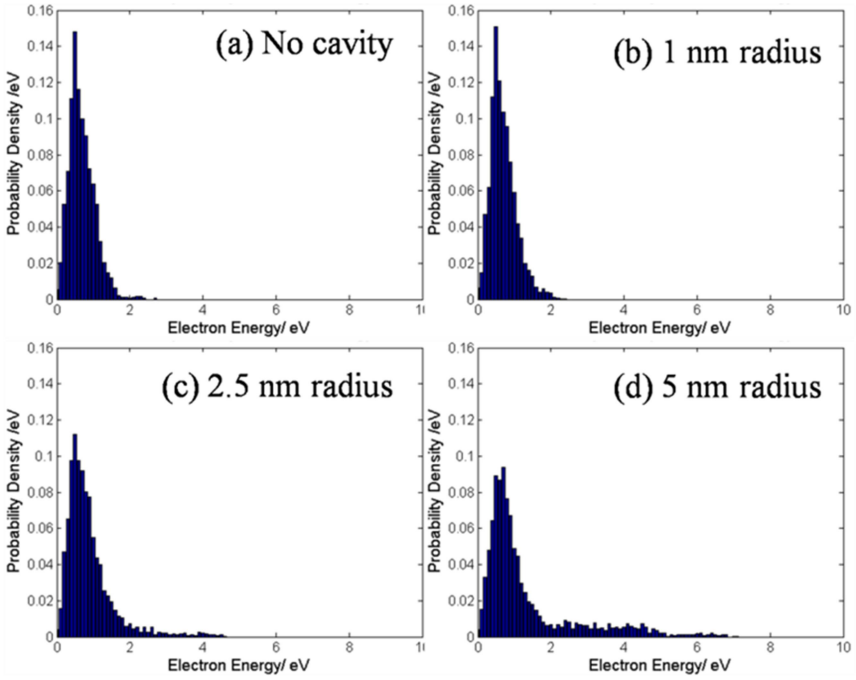

Figure 5.9 Probablity denstiy distribution of electron energy in PE film with 10% volume fraction of cavities of various radii at a field of 500 MV/m: (a) no cavity (b) 1 nm radius (c) 2.5 nm radius (d) 5 nm radius.

This chapter documents the development of MC simulations which are consistent with previous predictions of intrinsic breakdown based on average electron computations. Given that consistency, MC simulations can be used to examine the electron energy distributions as a function of electric field and the likely effect of nanocavities on high field aging and breakdown.

From the Monte Caro model, we have found, as expected, that at lower electrical fields, the electron energy gained from the external electric field is balanced by energy loss from collisions with phonons, and the electron energy distribution stablizes. At a higher electric fields, electrons reach energies at which they could break chemical bonds (3-4 eV) which suggests high field

degradation. We also observed the breakdown field insulating film (PE) by adding the effect of impaction ionization in the MC model. At breakdown field, electron energy gain is no longer balanced by energy loss which results in ionization and electron multiplication. Rapid electron multiplication causes sufficient electron density to damage the material.

Nanocavities have been added to PE as a first step down to the path of engineering “extrinsic breakdown”. By investigating PE with various radii nanocavities, we found that nanocavities increase the number of high energy electrons, which should accelerate the high field aging. Large radius nanocavities increase substantially the maximum electron energy at a given field. This suggests that larger nanocavities are likely to cause high field aging in their immediate vicinity.

Future work will include “extrinsic” factors other than nanocavities, such as the effect of density fluctuations in an amorphous polymer and the electron-phonon scattering rate in amorphous regions, which should be calculated differently from that in crystalline regions. The impurity states in the bandgap which decrease the threshold for impact ionization will also be included. Also impurity-induced traps can be formed during aging. All these effects should be included statistically to investigate high field aging and engineering breakdown of insulating films.

5.6 Reference

[1] A. Huzayyin, S.A. Boggs, and R. Ramprasad, "Quantum Mechanical Study of Charge Injection at the Interface of Polyethylene and Platinum". 2011 Annual Report of the IEEE Conference on Electrical Insulation and Dielectric Phenomena.

[2] S. Le Roy, G. Teyssedre and C. Laurent, "Charge Transport and Dissipative Processes in Insulating Polymers: Experiments and Model", IEEE Transactions on Dielectrics and Electrical Insulation, Vol. 12, No. 4, August 2005.

[3] Y. Sun, S. A. Boggs, and R. Ramprasad, "The intrinsic electrical breakdown strength of insulators from first principles," Appl. Phys. Lett. vol 101, 132906, 2012

[4] S. Baidyaroy, M. A. Lampert, and B. Zee, "Monte Carlo studies of hot-electron energy distributions in thin insulating films. I.Constant mean free path and a one-dimensional simulation," J. Appl. Phys. vol. 47, No.5, pp. 2013-2112, May 1976.

[5] M. Sparks, D. L. Mills, R. Warren, T. Holstein, A. A. Maradudin, L, J. Sham, E. Loh, Jr., and D. F. King, "Theory of electron-avalanche breakdown in solids", Phys. Rev. B, vol. 24, 3519, 1981.

[6] Y. Sun, C. Bealing, S. Boggs, and R. Ramprasad, "50+ years of intrinsic breakdown", Electrical Insulation Magazine, Vol. 29 , Issue: 2. pp: 8 – 15, 2013.

[7] D. Ceresoli, M. C. Righi, E. Tosatti, S. Scandolo, G, Santoro and S. Serra. "Exciton self-trapping in bulk polyethylene"J. Phys.: Condens. Matter, vol 17, 4621–4627, 2005.

[8] A. Huzayyin, S. Boggs and R. Ramprasad, "Quantum Mechanical Studies of Carbonyl Impurities in Dielectric Polyethylene", IEEE Trans. on Dielectrics and Electrical Insulation, Vol. 17, No. 3, pp.920-925, 2010.

[9] S.O. Pillai, Solid State Physics, New Age International, New Delhi, 2005.

[10] Cram D and Hammond G, Organic Chemistry, New York: McGraw-Hill, 1956

[11] Cartier E and Pfluger P, "Detection of Hot Electron-Induced Radiation Damage in Organic Dielectrics by Exoelectron Emission from Thin Films", IEEE Trans. Electr. Insul. EI-22, 123-128.

CHAPTER 6
SUMMARY AND FUTURE WORK

6.1 Summary

Next generation insulating materials require high dielectric constant, high breakdown field, low dielectric loss, and appropriate glass trasition temperature and morphology. A number of computational methods including classical, quantum mechanical, and modern data-driven statistical learning approaches is available to investigate those properties which provides screening strategies for rational design of new materials with desired properties. For example, screening for high dielectric constant materials can be performed with in Density Functional Theory (DFT), which can predict geometric details to within 1% of experiments and dielectric constant to within 5% of experiments. Molecular dynamics (MD) simulation based on empirical interatomic potentials or force fields can predict crystal structure, semicrystalline morphology and dielectric loss, although the latter is presently limited to loss in the GHz range.

The dielectric breakdown of insulating materials has been a subject of experimental and theoretical investigations for many decades as a result of its technical importance. However, engineering breakdown is very complex, as a wide range of instabilities can cause breakdown (impact ionization, thermal runaway, electrochemical deterioration, etc.). A predictive thory of dielectric breakown, as well a method for screening dielectrics for high electrical breakdown strength, is not available. In this thesis, a theoretical study of dielectric breakdown is carried out with the focus on the intrinsic breakdown. A preidctive parameter-free first principles method for estimating the intrinsic breakdown field of insulators has been developed. An improved understanding of the fundamental factors that control dielectric breakdown has been achieved, which provides search strategies for insulating materials (especially polymers) with a potential for high breakdown field. The important findings of this research work are summarized as follows:

A predictive, parameter-free, first principles method for estimating the intrinsic breakdown strength of insulators has been developed. This approach is based on the criterion that breakdown occurs when the average electron energy gain from the electric field exceeds average energy loss to phonon collisions. Density functional perturbation theory and the direct integration of electronic scattering probabilities (due to phonons) over all possible final states is used to arrive at an estimate of intrinsic breakdown for a range of prototypical covalent and ionic systems. The computed intrinsic breakdown fields compare favorably with available experimental data. This work also establishes correlations between the breakdown, field and bandgap and phonon cut-off frequencies. These correlations, and the availability of first principles scattering rates, provide a logical basis for guidance in designing materials more resistant to damage from large electric fields.

The benefit of introducing dipoles into polymers is obvious in the context of reduce the electron mobility and increase breakdown field, especially at lower temperatures. A theoretical analysis of electron scattering by dipoles and phonons is presented which provides the basis for explaining temperature dependence of breakdown field on the basis of the dominant scattering process as a function of temperature. By performing electron mobility calculations in non-polar and polar polymers, a quantitative correlation between chemical composition and intrinsic breakdown field can be established. Calculation of dipole scattering limited electron mobility can be used to assess the effect of dipole scattering on the intrinsic breakdown field of polymers. Randomness of dipole moment is critical, as carriers cannot experience dipole scattering in materials with translationally periodic potentials. Amorphous polymers with large dipoles distributed randomly along polymer chains are good candidates for high breakdown field polymeric films

A Monte Carlo simulation method was developed to examine the electron energy distributions as a function of electric field and the likely effect of nanocavities on high field aging and breakdown. Nanocavities increase the number of high energy electrons, which should accelerate the high field aging. The electrons with energy greater than the bandgap (8.8eV) trigger impact

ionization, which can lead to avalanche breakdown, while electrons with energy larger than 3-4eV can cause degradation of the dielectric. With the present of nanocavities, high field aging is likely to occur in the immediate vicinity of nanocavities. High field degradation may be more important than breakdown field.

6.2 Future Work

This thesis provides a better understanding of intrisic breakdown thoery had been achieved previously. However, prediction of engineering breakdown, which is is dominated by "extrinsic" factors, is still out of reach. In the following, research which may result in improved prediction of engineering breakdown is suggested.

1. The method developed for estimating the intrinsic breakdown field of dielectrics is applicable to crystalline materials and is computationally intensive, as it requires very dense sampling of both the electronic (k) and the phononic (q) reciprocal space grids, significantly more dense than required in standard DFT computations. For many polymers, the large number of atoms in the unit cell makes the computation more time-consuming. The lack of crystal information for new polymeric systems also makes the method less practical. A rapid screening method for high breakdown field materials needs to be developed. A method for predicting intirnsic breakdown of polymers based on a single-chain would be very useful for screening materials space.

2. Dipole scattering has been included in addition to phonon scattering in the context of intrinsic breakdown. Based on the inverse relationship of electron mobility and intrinsic breakdown field, a quantitative correlation between chemical composition and intrinsic breakdown field can be established by performing electron mobility calculations. The effect of dipole scattering needs to be included in a model for intrinsic breakdown field of amorphous materials. 3. The correlation of breakdown field with other properties can provide a basis for screening materials space for high electrical breakdown field materials by studying some of the easily computable or measurable attributes of the materials, e.g., bandgap, phonon density of states,

dipole moment, dipole density, etc. Establishing such a correlation requires analyzing data for large number of materials.

3. The greatest challenge going forward is to extend theory to provide reasonable predictions of engineering breakdown by including extrinsic factors such as free volume, the statistics of semicrystalline materials, impurity states in the band gap and at metal-dielectric interfacecs which influence charge transport, etc.

APPENDIX A
DIPOLE SCATTERING LIMITED MOBILITY DERIVATION

If the dipole moment in every unit cell was the same, there would be no scattering of electrons since the matrix element for scattering in Fermi's golden rule vanishes for a time-independent periodic potential. Electrons experience dipole scattering due to the randomness of dipole moment as shown in Figure A.1(a)[1][2].

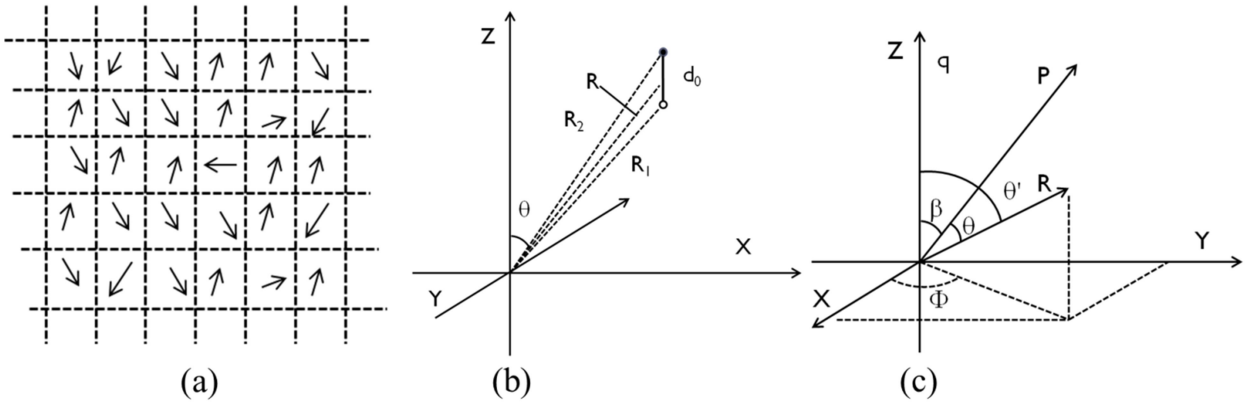

Figure A.1 (a) Random dipole distribution (b) Relative location of dipoles with respect to electron at the origin, where R_1 and R_2 are the distance of negative and positive charges from the origin, d_0 is the distance between two opposite charges in the dipole, R is the distance between the dipole center and the origin. (c) Coordinate system for Fourier transformation, P is the dipole moment, $\boldsymbol{q}=\boldsymbol{k}_2-\boldsymbol{k}_1$ is the wave vector and R is the real space vector.

In the coordinate system of Figure A.1 (b), the unscreened Coulomb potential at the origin is given by [1]

$$V_{UNS}(R,\theta)=\frac{e^2}{4\pi\varepsilon_s}\left[\frac{1}{R_1}-\frac{1}{R_2}\right]\approx\frac{eP\cos\theta}{4\pi\varepsilon_s R^2} \tag{A.1}$$

where P is the dipole moment defined as $P=ed_0$, $\varepsilon_s=\varepsilon_0\varepsilon_r$ is the dielectric constant, and θ is the angle between R and P. We can also directly get the screened potential for the dipole scattering

$$V_{SC}(R,\theta)=\frac{e^2}{4\pi\varepsilon_s}\left[\frac{e^{-R_1/L_D}}{R_1}-\frac{e^{-R_2/L_D}}{R_2}\right]\approx\frac{eP\cos\theta}{4\pi\varepsilon_s R^2}\left(1+\frac{R}{L_D}\right)e^{-R/L_D} \tag{A.2}$$

where L_D is the Debye screening length. As shown in Figure A.1(c), q direction is chosen as along z axis and P in the y-z plane, β is the angle between q and P. The Fourier transformation of this potential is evaluated in the wave vector (q) space [1],

$$V_{SC}(q) = \frac{eP\cos(\beta)}{\varepsilon_s q\left(1+1/q^2L_D^2\right)} \tag{A.3}$$

The momentum scattering rate is calculated from the relaxation time approximation of the Boltzmann equation as [1]

$$\frac{1}{\tau_m(k)} = n_0 \frac{\hbar k}{m^*} \frac{2\pi P^2\cos^2(\beta)}{\left(L_D k^2 a_0\right)^2 e^2}\left[4k^2L_D^2 - 2\ln\left(1+4k^2L_D^2\right) + \frac{4k^2L_D^2}{1+4k^2L_D^2}\right] \tag{A.4}$$

where $m^*=m_r m_0$, is the electron effective mass, $a_0=4\pi\hbar^2\varepsilon_s/m^*e^2 \approx 0.53\ (\varepsilon_r/m_r)$ Å is the effective Bohr radius, n_0 is the dipole concentration, and $\boldsymbol{k}$ is the electron wave vector. Angular averaging over random orientation of electron momentum yields $\langle\cos^2(\beta)\rangle=1/2$. The total momentum scattering time is found by the averaging procedure for a Fermi-Dirac distribution [1]

$$\tau_m(k) = \frac{2}{3}C' \frac{\int_0^\infty dE\left[AE' - 2\ln\left(1+AE'\right) + AE'\left(1+AE'\right)^{-1}\right]E^3\exp\left(E'-E_F\right)\left[1+\exp\left(E'-E_F\right)\right]^{-2}}{\int_0^\infty dE'\sqrt{E'}\left[1+\exp\left(E'-E_F\right)\right]^{-1}} \tag{A.5}$$

where $C' = 8\sqrt{\pi}(N_C/n_0)(L_D/d_0)^2(m^*a_0/\hbar)$ is a time constant characteristic of dipole scattering, and $A = 8m^*L_D^2k_BT/\hbar^2$ is a dimensionless factor. E' and E_F, carrier energy and Fermi energy are normalized by the thermal energy k_BT. A numerical evaluation of equation (A.5) is needed to get the dipole scattering limited mobility from Drude relation [3].

$$\mu = \frac{e\langle\tau_m\rangle}{m^*} \tag{A.6}$$

For strongly nongenerate carriers, momentum relaxation time in equation (A.5) can be cast into the form

$$\tau_m(k) = \tau_0(\frac{E}{k_B T})^2 \tag{A.7}$$

where τ_0 does not depend on carrier energy and is given by $\tau_0 = (\sqrt{\pi}\hbar / k_B T)(a_0 / d_0)^2 (N_C / n_0)$. So the mobility for strongly nongenerate carriers can be approximated using Maxwell-Boltzmann statistics as [1]

$$\mu = \frac{8}{3}\left(\frac{\hbar}{k_B T}\right)\left(\frac{e^3}{m^*}\right)\left(\frac{a_0}{P}\right)^2\left(\frac{N_C}{n_0}\right) \tag{A.8}$$

where P is the average dipole moment, n_0 is the dipole density $n_0=1/v_0$, where v_o is the volume of a unit cell. a_0 is the effective Bohr radius $a_0=4\pi\hbar^2\varepsilon_s/m^*e^2\approx 0.53(\varepsilon_r/m_r)$ Å, $m^*$is electron effective mass and N_c is the effective density of states calculated as

$$Nc = 2\left(\frac{2\pi m^* kT}{h^2}\right)^{3/2}. \tag{A.9}$$

From equations (A.8) (A.9) dipole scattering limited mobility can be easily estimated, the three parameters needed is average dipole moment per unit cell P, dipole denstiy n_0 and the dielectric constant ε_r.

$$\mu_{dipole} = C\frac{\varepsilon_r^2}{P^2 n_0} \tag{A.10}$$

$$C = \frac{64\sqrt{2}\left(\hbar\varepsilon_0\right)^2(\pi k_B T)^{1/2}}{3em^{*3/2}} \tag{A.11}$$

References

[1] Wei Zhao and Debdeep Jena, “Dipole scattering in highly polar semiconductor alloys”, J. Appl. Phys., Vol. 96, pp. 2095-2101, 2004.
[2] A. D. Boardman, “The theory of dipole scattering in semiconductors”, Proc. Phys. Soc., Vol. 85, pp.141-148, 1965.
[3] M. van Exter, D. Grischkowsky (1990). "Carrier dynamics of electrons and holes in moderately doped silicon". Phys. Rev. B 41 (17): 12140–12149.

APPENDIX B
EXAMPLE OF QUANTUM-ESPRESSO INPUT FILES

B.1 Calculation Procedure

This is an example of Quantum-ESPRESSO 4.3 input script files to calculate electron phonon scattering rate (Silicon). Minor input changes exist in later Quantum-ESPRESSO versions. A Monkhorst-pack k point mesh of 32×32×32 and q point mesh of 4×4×4 with 0.01 Ry Gaussian broadening is used in this calculation. Simple comment of each line is given after the symbol #. Detailed descriptions of the input data are available at the Quantum-ESPRESSO website and the documentation in the header of the main *.f90 file.

The calculation of electron-phonon scattering includes the following steps.

1. *Step1: A self-consistent calculation with a dense k-point grid. The dense grid must contain all k and k+q grid points used in the subsequent electron-phonon calculation and should be dense enough to produce accurate electron-phonon scattering coefficients. This example uses a (32 32 32) Monkhorst-Pack grid. The option "la2F=.true." instructs the code to save data into a file that is subsequently read during the electron-phonon calculation. All grids must be unshifted, i.e. include k= 0*
2. *Step2: A self-consistent calculation using a grid of coarse k points and a value of the gaussian broadening (0.01Ry is used here) that is suitable for good self-consistency and for the phonon calculation. This example uses a (16 16 16) Monkhorst-Pack grid.*
3. *Step3: Phonon and electron-phonon scattering rate and energy loss rate are calculated for the specified **q** vector. Specify "elph=.true." and the name of a file where the derivative of the potential is stored, "fildvscf". lambda.f90 read files 'filelph' produced by phonon (one for each q-point) sum over q-points to produce the electron-phonon scattering rate and energy loss rate.*

B.2 Sample Input File of Silicon

```
###############################################################################
```

```
##  "This example shows how to calculate electron-phonon scattering rate of Silicon"
#########################################################################################
# run from directory where this script is
cd `echo $0 | sed 's/\(.*\)\/.*/\1/'` # extract pathname
EXAMPLE_DIR=`pwd`

# check whether echo has the -e option
if test "`echo -e`" = "-e" ; then ECHO=echo ; else ECHO="echo -e" ; fi

# function to test the exit status of a job
. ../check_failure.sh

$ECHO
$ECHO "$EXAMPLE_DIR : starting"
$ECHO
$ECHO "This example shows how to calculate electron-phonon scattering rate of Silicon"

# set the needed environment variables
. ../environment_variables
# required executables and pseudopotentials
BIN_LIST="pw.x ph.x q2r.x matdyn.x lambda.x"
PSEUDO_LIST="Si.pz-vbc.UPF"

$ECHO
$ECHO "  executables directory: $BIN_DIR"
```

```
$ECHO "  pseudo directory:      $PSEUDO_DIR"
$ECHO "  temporary directory:   $TMP_DIR"
$ECHO "  checking that needed directories and files exist...\c"

# check for directories
for DIR in "$BIN_DIR" "$PSEUDO_DIR" ; do
   if test ! -d $DIR ; then
      $ECHO
      $ECHO "ERROR: $DIR not existent or not a directory"
      $ECHO "Aborting"
      exit 1
   fi
done
for DIR in "$TMP_DIR" "$EXAMPLE_DIR/results" ; do
   if test ! -d $DIR ; then
      mkdir $DIR
   fi
done
cd $EXAMPLE_DIR/results

# check for executables
for FILE in $BIN_LIST ; do
   if test ! -x $BIN_DIR/$FILE ; then
      $ECHO
      $ECHO "ERROR: $BIN_DIR/$FILE not existent or not executable"
```

```
      $ECHO "Aborting"
      exit 1
   fi
done

# check for pseudopotentials
for FILE in $PSEUDO_LIST ; do
   if test ! -r $PSEUDO_DIR/$FILE ; then
      $ECHO
      $ECHO "Downloading $FILE to $PSEUDO_DIR...\c"
          $WGET $PSEUDO_DIR/$FILE \
              http://www.quantum-espresso.org/pseudo/1.3/UPF/$FILE 2> /dev/null
   fi
   if test $? != 0; then
      $ECHO
      $ECHO "ERROR: $PSEUDO_DIR/$FILE not existent or not readable"
      $ECHO "Aborting"
      exit 1
   fi
done
$ECHO " done"

# how to run executables
PW_COMMAND="$PARA_PREFIX $BIN_DIR/pw.x $PARA_POSTFIX"
PH_COMMAND="$PARA_PREFIX $BIN_DIR/ph.x $PARA_POSTFIX"
```

```
Q2R_COMMAND="$PARA_PREFIX $BIN_DIR/q2r.x $PARA_POSTFIX"
MATDYN_COMMAND="$PARA_PREFIX $BIN_DIR/matdyn.x $PARA_POSTFIX"
LAMBDA_COMMAND="$BIN_DIR/lambda.x "
$ECHO
$ECHO "  running pw.x as: $PW_COMMAND"
$ECHO "  running ph.x as: $PH_COMMAND"
$ECHO "  running q2r.x as: $Q2R_COMMAND"
$ECHO "  running matdyn.x as: $MATDYN_COMMAND"
$ECHO "  running lambda.x as: $LAMBDA_COMMAND"
$ECHO

# clean TMP_DIR
$ECHO "  cleaning $TMP_DIR...\c"
rm -rf $TMP_DIR/*
$ECHO "  done"

# SCF at dense k-mesh
# la2F= true, save data into a file subsequently read during electron-phonon calculation
cat > si.scf.fit.in <<EOF
 &control
    calculation='scf',  # a string describing the task to be performed
    restart_mode='from_scratch', # task from previous interrupted calculation or from scratch
    prefix='si', #prepended to input/output filenames
    pseudo_dir = '$PSEUDO_DIR/', #directory containing pseudopotential files
    outdir='$TMP_DIR/', #input, temporary, output files are found in this directory
```

```
 /
 &system
    ibrav = 2, #Bravais-lattice index.
    celldm(1) =10.20704,# crystallographic constants (in BOHR)
    nat=  2, #number of atoms in the unit cell
    ntyp=1, #number of types of atoms in the unit cell
    ecutwfc =30.0,# wavefunctions kinetic energy cutoff (Ry), convergence should be #tested
    occupations='smearing', smearing='gaussian', degauss=0.01,
#gaussian smearing,  degauss is the value of the gaussian spreading (Ry)
    la2F = .true.,
# la2F= true, save data into a file subsequently read during electron-phonon calculation
    nbnd=8, # number of electronic states (bands) to be calculated.
 /
 &electrons
    conv_thr =  1.0d-8, # convergence threshold for self-consistency
    mixing_beta = 0.7, # mixing factor for self-consistency
 /
ATOMIC_SPECIES
 # label of the atom, mass of the atomic species and pseudopotential file for this species
 Si 28.086 Si.pz-vbc.UPF
ATOMIC_POSITIONS
# atomic positions specified here
Si 0.00 0.00 0.00
Si 0.25 0.25 0.25
K_POINTS {automatic}
```

```
# A Monkhorst-pack k point mesh of 32×32×32 is used for SCF calculation
32 32 32 0 0 0
EOF
$ECHO "  running the scf calculation with dense k-point grid...\c"
$PW_COMMAND  < si.scf.fit.in > si.scf.fit.out
check_failure $?
$ECHO "  done"
#
#  SCF at k-mesh for good self-consistency and for the phonon calculation.
#
cat > si.scf.in <<EOF
 &control
    calculation='scf'
    restart_mode='from_scratch',
    prefix='si',
    pseudo_dir = '$PSEUDO_DIR/',
    outdir='$TMP_DIR/'
 /
 &system
   ibrav = 2, celldm(1) =10.20704, nat=  2, ntyp=1,
   ecutwfc =30.0,
   occupations='smearing',
   smearing='gaussian',
   degauss=0.01,
   nbnd=8,
```

```
 /
 &electrons
   conv_thr =  1.0d-8
   mixing_beta = 0.7
 /
ATOMIC_SPECIES
Si  28.086  Si.pz-vbc.UPF
ATOMIC_POSITIONS
Si 0.00 0.00 0.00
Si 0.25 0.25 0.25
K_POINTS AUTOMATIC
16 16 16 0 0 0
EOF
$ECHO "  running the scf calculation...\c"
$PW_COMMAND < si.scf.in > si.scf.out
check_failure $?
$ECHO "  done"
#
# electron phonon calculation
cat > si.elph.in <<EOF
 Electron-phonon coefficients for Si
 &inputph
  tr2_ph=1.0d-12, # threshold for self-consistency.
  prefix='si', #prepended to input/output filenames
  fildvscf='sidv', # fildvscf file is where the potential variation is written for later use
```

```
 amass(1)=28.086, #atomic mass of each atomic type.
 outdir='$TMP_DIR/',# directory containing input, output, and scratch files;
 fildyn='si.dyn',# file where the dynamical matrix is written.
 elph=.true.,# electron-phonon is calculated by interpolation over the Brillouin Zone
 trans=.true.,# If .true. the phonons are computed.
 ldisp=.true. #If .true. the run calculates phonons for a grid of q-points
 nq1=4, nq2=4, nq3=4 # q points are specified by nq1, nq2, nq3
/
EOF
$ECHO "  running the el-ph calculation...\c"
$PH_COMMAND < si.elph.in > si.elph.out
check_failure $?
$ECHO "  done"
#
#   q2r calculates Interatomic Force Constants (IFC) in real space from dynamical
#   matrices produced by ph.x on a regular q-grid
cat > q2r.in <<EOF
 &input
zasr='simple', # type of Acoustic Sum Rules used for the Born effective charges.
fildyn='si.dyn',  # file where the dynamical matrix is written.
flfrc='si444.fc', # the name of output file containing force constant
la2F=.true.
 /
EOF
$ECHO "  running q2r...\c"
```

```
$Q2R_COMMAND < q2r.in > q2r.out
check_failure $?
$ECHO "  done"
# matdyn.x: produces phonon frequencies at a generic wave vector using the IFC file
#calculated by q2r.x; may also calculate phonon DOS, the electron-phonon coefficient λ,
#
cat > matdyn.in.freq <<EOF
 &input
    asr='simple', #indicates the type of Acoustic Sum Rule imposed
    amass(1)=28.086,# mass of the atomic species
    flfrc='si444.fc', # file produced by q2r containing force constants (needed)
    flfrq='si444.freq', # output file for frequencies
    la2F=.true., # if .true. interpolates also the el-ph coefficients.
    dos=.false.# if .true. calculate phonon Density of States (DOS)
 /
  19
  0.000 0.0 0.0     0.0
  0.125 0.0 0.0     0.0
  0.250 0.0 0.0     0.0
  0.375 0.0 0.0     0.0
  0.500 0.0 0.0     0.0
  0.750 0.0 0.0     0.0
  1.000 0.0 0.0     0.0
  0.825 0.125 0.125 0.0
  0.750 0.250 0.250 0.0
```

```
  0.625 0.375 0.375 0.0
  0.500 0.500 0.500 0.0
  0.325 0.325 0.325 0.0
  0.250 0.250 0.250 0.0
  0.125 0.125 0.125 0.0
  0.000 0.000 0.000 0.0
  0.125 0.125 0.000 0.0
  0.250 0.250 0.000 0.0
  0.325 0.325 0.000 0.0
  0.500 0.500 0.000 0.0
EOF
$ECHO "  running matdyn for frequency calculation...\c"
$MATDYN_COMMAND < matdyn.in.freq > matdyn.out.freq
check_failure $?
$ECHO "  done"
#
cat > matdyn.in.dos <<EOF
 &input
    asr='simple',  amass(1)=28.086,
    flfrc='si444.fc', # file produced by q2r containing force constants
    flfrq='si444.freq', # output file for frequencies
    la2F=.true., # if .true. interpolates also the el-ph coefficients.
    dos=.true. # if .true. calculate phonon Density of States (DOS)
    fldos='phonon.dos', # output file for phonon DOS
    nk1=10, nk2=10, nk3=10, # uniform q-point grid for DOS calculation
```

```
   ndos=50 # number of energy steps for DOS calculations
 /
EOF
$ECHO "  running matdyn for a2F(omega) calculation...\c"
$MATDYN_COMMAND < matdyn.in.dos > matdyn.out.dos
check_failure $?
$ECHO "  done"
#  lambda.f90 read files 'filelph' produced by phonon (one for each q-point)
# sum over q-points to produce the electron-phonon coefficients:
cat > lambda.in <<EOF
10  0.12  1    ! emax (something more than highest phonon mode in THz), degauss, smearing method
     8         ! Number of q-points for which electron phonon interaction is calculated,
      0.0000000  0.0000000  0.0000000   1.00  ! the first q-point, use kpoints.x program
     -0.2500000 -0.2500000  0.2500000   8.00  ! to calculate q-points and their weight
     -0.5000000 -0.5000000  0.5000000   4.00  !
      0.0000000  0.0000000  0.5000000   6.00  ! 4th q-point, qx,qy,qz
     -0.2500000 -0.2500000  0.7500000  24.00  !
     -0.5000000 -0.5000000  1.0000000  12.00  !
      0.0000000  0.0000000  1.0000000   3.00  !
     -0.5000000  0.0000000  1.0000000   6.00  ! the last q-point
elph. 0.000000. 0.000000. 0.000000 ! elph output file names,
elph.-0.250000. 0.250000.-0.250000 ! in the same order as the q-points before
elph. 0.500000.-0.500000. 0.500000
elph. 0.000000. 0.500000. 0.000000
```

```
elph. 0.750000.-0.250000. 0.750000
elph. 0.500000. 0.000000. 0.500000
elph. 0.000000.-1.000000. 0.000000
elph.-0.500000.-1.000000. 0.000000
0.10                    ! \mu the Coloumb coefficient in the modified
EOF
$ECHO "  running lambda.x for lambda calculation...\c"
$LAMBDA_COMMAND < lambda.in > lambda.out
check_failure $?
$ECHO "  done"
```

APPENDIX C
MODIFIED QUANTUM ESPRESSO ELPHON.F90 CODE

```
!
! Copyright (C) 2001-2008 Quantum ESPRESSO group
! This file is distributed under the terms of the
! GNU General Public License. See the file `License'
! in the root directory of the present distribution,
! or http://www.gnu.org/copyleft/gpl.txt .
!
!
!-----------------------------------------------------------------------
SUBROUTINE elphon()
  !---------------------------------------------------------------------
  !
  ! Electron-phonon calculation from data saved in fildvscf
  !
  USE kinds, ONLY : DP
  USE cell_base, ONLY : celldm, omega, ibrav
  USE ions_base, ONLY : nat, ntyp => nsp, ityp, tau, amass
  USE gvecs, ONLY: doublegrid
  USE fft_base, ONLY : dfftp, dffts
  USE noncollin_module, ONLY : nspin_mag
  USE dynmat, ONLY : dyn, w2
  USE qpoint, ONLY : xq
  USE modes,  ONLY : npert, nirr
  USE control_ph, ONLY : trans
  USE units_ph, ONLY : iudyn, lrdrho, iudvscf
  !
  IMPLICIT NONE
  !
  INTEGER :: irr, imode0, ipert, is
  ! counter on the representations
  ! counter on the modes
  ! the change of Vscf due to perturbations
  COMPLEX(DP), POINTER :: dvscfin(:,:,:), dvscfins (:,:,:)


  CALL start_clock ('elphon')

  !
  ! read Delta Vscf and calculate electron-phonon coefficients
  !
  imode0 = 0
  DO irr = 1, nirr
     ALLOCATE (dvscfin (dfftp%nnr, nspin_mag , npert(irr)) )
     DO ipert = 1, npert (irr)
        CALL davcio_drho ( dvscfin(1,1,ipert),  lrdrho, iudvscf, &
                           imode0 + ipert,  -1 )
     END DO
     IF (doublegrid) THEN
        ALLOCATE (dvscfins (dffts%nnr, nspin_mag , npert(irr)) )
        DO is = 1, nspin_mag
           DO ipert = 1, npert(irr)
```

```
               CALL cinterpolate (dvscfin(1,is,ipert),dvscfins(1,is,ipert),-1)
            ENDDO
         ENDDO
      ELSE
         dvscfins => dvscfin
      ENDIF
      CALL newdq (dvscfin, npert(irr))
      CALL elphel (npert (irr), imode0, dvscfins)
      !
      imode0 = imode0 + npert (irr)
      IF (doublegrid) DEALLOCATE (dvscfins)
      DEALLOCATE (dvscfin)
  ENDDO
  !
  ! now read the eigenvalues and eigenvectors of the dynamical matrix
  ! calculated in a previous run
  !
  IF (.NOT.trans) CALL readmat (iudyn, ibrav, celldm, nat, ntyp, &
       ityp, omega, amass, tau, xq, w2, dyn)
  !
  CALL stop_clock ('elphon')
  RETURN
END SUBROUTINE elphon
!
!-----------------------------------------------------------------------
SUBROUTINE readmat (iudyn, ibrav, celldm, nat, ntyp, ityp, omega, &
     amass, tau, q, w2, dyn)
  !-----------------------------------------------------------------------
  !
  USE kinds, ONLY : DP
  USE constants, ONLY : amconv
  IMPLICIT NONE
  ! Input
  INTEGER :: iudyn, ibrav, nat, ntyp, ityp (nat)
  REAL(DP) :: celldm (6), amass (ntyp), tau (3, nat), q (3), &
       omega
  ! output
  REAL(DP) :: w2 (3 * nat)
  COMPLEX(DP) :: dyn (3 * nat, 3 * nat)
  ! local (control variables)
  INTEGER :: ntyp_, nat_, ibrav_, ityp_
  REAL(DP) :: celldm_ (6), amass_, tau_ (3), q_ (3)
  ! local
  REAL(DP) :: dynr (2, 3, nat, 3, nat)
  CHARACTER(len=80) :: line
  CHARACTER(len=3)  :: atm
  INTEGER :: nt, na, nb, naa, nbb, nu, mu, i, j
  !
  !
  REWIND (iudyn)
  READ (iudyn, '(a)') line
  READ (iudyn, '(a)') line
  READ (iudyn, * ) ntyp_, nat_, ibrav_, celldm_
  IF ( ntyp.NE.ntyp_ .OR. nat.NE.nat_ .OR.ibrav_.NE.ibrav .OR. &
       ABS ( celldm_ (1) - celldm (1) ) > 1.0d-5) &
```

```
        CALL errore ('readmat', 'inconsistent data', 1)
DO nt = 1, ntyp
   READ (iudyn, * ) i, atm, amass_
   IF ( nt.NE.i .OR. ABS (amass_ - amconv*amass (nt) ) > 1.0d-5) &
      CALL errore ( 'readmat', 'inconsistent data', 1 + nt)
ENDDO
DO na = 1, nat
   READ (iudyn, * ) i, ityp_, tau_
   IF (na.NE.i.OR.ityp_.NE.ityp (na) ) CALL errore ('readmat', &
        'inconsistent data', 10 + na)
ENDDO
READ (iudyn, '(a)') line
READ (iudyn, '(a)') line
READ (iudyn, '(a)') line
READ (iudyn, '(a)') line
READ (line (11:80), * ) (q_ (i), i = 1, 3)
READ (iudyn, '(a)') line
DO na = 1, nat
   DO nb = 1, nat
      READ (iudyn, * ) naa, nbb
      IF (na.NE.naa.OR.nb.NE.nbb) CALL errore ('readmat', 'error reading &
           &file', nb)
      READ (iudyn, * ) ( (dynr (1, i, na, j, nb), dynr (2, i, na, j, nb) &
           , j = 1, 3), i = 1, 3)
   ENDDO
ENDDO
!
! divide the dynamical matrix by the (input) masses (in amu)
!
DO nb = 1, nat
   DO j = 1, 3
      DO na = 1, nat
         DO i = 1, 3
            dynr (1, i, na, j, nb) = dynr (1, i, na, j, nb) / SQRT (amass ( &
                 ityp (na) ) * amass (ityp (nb) ) ) / amconv
            dynr (2, i, na, j, nb) = dynr (2, i, na, j, nb) / SQRT (amass ( &
                 ityp (na) ) * amass (ityp (nb) ) ) / amconv
         ENDDO
      ENDDO
   ENDDO
ENDDO
!
! solve the eigenvalue problem.
! NOTA BENE: eigenvectors are overwritten on dyn
!
CALL cdiagh (3 * nat, dynr, 3 * nat, w2, dyn)
!
! divide by sqrt(mass) to get displacements
!
DO nu = 1, 3 * nat
   DO mu = 1, 3 * nat
      na = (mu - 1) / 3 + 1
      dyn (mu, nu) = dyn (mu, nu) / SQRT ( amconv * amass (ityp (na) ) )
   ENDDO
ENDDO
```

```
  !
  !
  RETURN
END SUBROUTINE readmat
!
!-----------------------------------------------------------------------
SUBROUTINE elphel (npe, imode0, dvscfins)
  !-----------------------------------------------------------------------
  !
  !      Calculation of the electron-phonon matrix elements el_ph_mat
  !         <\psi(k+q)|dV_{SCF}/du^q_{i a}|\psi(k)>
  !      Original routine written by Francesco Mauri
  !
  USE kinds, ONLY : DP
  USE fft_base, ONLY : dffts
  USE wavefunctions_module,  ONLY: evc
  USE io_files, ONLY: iunigk
  USE klist, ONLY: xk
  USE lsda_mod, ONLY: lsda, current_spin, isk
  USE noncollin_module, ONLY : noncolin, npol, nspin_mag
  USE wvfct, ONLY: nbnd, npw, npwx, igk
  USE uspp, ONLY : vkb
  USE el_phon, ONLY : el_ph_mat
  USE modes, ONLY : u
  USE units_ph, ONLY : iubar, lrbar, lrwfc, iuwfc
  USE eqv,      ONLY : dvpsi, evq
  USE qpoint,   ONLY : igkq, npwq, nksq, ikks, ikqs
  USE control_ph, ONLY : trans, lgamma
  USE mp_global, ONLY: intra_pool_comm
  USE mp,        ONLY: mp_sum

  IMPLICIT NONE
  !
  INTEGER :: npe, imode0
  COMPLEX(DP) :: dvscfins (dffts%nnr, nspin_mag, npe)
  ! LOCAL variables
  INTEGER :: nrec, ik, ikk, ikq, ipert, mode, ibnd, jbnd, ir, ig, &
       ios
  COMPLEX(DP) , ALLOCATABLE :: aux1 (:,:), elphmat (:,:,:)
  COMPLEX(DP), EXTERNAL :: zdotc
  !
  ALLOCATE (aux1    (dffts%nnr, npol))
  ALLOCATE (elphmat ( nbnd , nbnd , npe))
  !
  !  Start the loops over the k-points
  !
  IF (nksq.GT.1) REWIND (unit = iunigk)
  DO ik = 1, nksq
     IF (nksq.GT.1) THEN
        READ (iunigk, err = 100, iostat = ios) npw, igk
100     CALL errore ('elphel', 'reading igk', ABS (ios) )
     ENDIF
     !
     !  ik = counter of k-points with vector k
     !  ikk= index of k-point with vector k
```

```
     !  ikq= index of k-point with vector k+q
     !       k and k+q are alternated if q!=0, are the same if q=0
     !
     IF (lgamma) npwq = npw
     ikk = ikks(ik)
     ikq = ikqs(ik)
     IF (lsda) current_spin = isk (ikk)
     IF (.NOT.lgamma.AND.nksq.GT.1) THEN
        READ (iunigk, err = 200, iostat = ios) npwq, igkq
200     CALL errore ('elphel', 'reading igkq', ABS (ios) )
     ENDIF
     !
     CALL init_us_2 (npwq, igkq, xk (1, ikq), vkb)
     !
     ! read unperturbed wavefuctions psi(k) and psi(k+q)
     !
     IF (nksq.GT.1) THEN
        IF (lgamma) THEN
           CALL davcio (evc, lrwfc, iuwfc, ikk, - 1)
        ELSE
           CALL davcio (evc, lrwfc, iuwfc, ikk, - 1)
           CALL davcio (evq, lrwfc, iuwfc, ikq, - 1)
        ENDIF
     ENDIF
     !
     DO ipert = 1, npe
        nrec = (ipert - 1) * nksq + ik
        !
        !  dvbare_q*psi_kpoint is read from file (if available) or recalculated
        !
        IF (trans) THEN
           CALL davcio (dvpsi, lrbar, iubar, nrec, - 1)
        ELSE
           mode = imode0 + ipert
           ! TODO : .false. or .true. ???
           CALL dvqpsi_us (ik, u (1, mode), .FALSE. )
        ENDIF
        !
        ! calculate dvscf_q*psi_k
        !
        DO ibnd = 1, nbnd
           CALL cft_wave (evc(1, ibnd), aux1, +1)
           CALL apply_dpot(dffts%nnr, aux1, dvscfins(1,1,ipert), current_spin)
           CALL cft_wave (dvpsi(1, ibnd), aux1, -1)
        END DO
        CALL adddvscf (ipert, ik)

        !
        ! calculate elphmat(j,i)=<psi_{k+q,j}|dvscf_q*psi_{k,i}> for this
pertur
        !
        DO ibnd =1, nbnd
           DO jbnd = 1, nbnd
              elphmat (jbnd, ibnd, ipert) = zdotc (npwq, evq (1, jbnd), 1, &
                   dvpsi (1, ibnd), 1)
```

```
              IF (noncolin) &
                 elphmat (jbnd, ibnd, ipert) = elphmat (jbnd, ibnd, ipert)+ &
                   zdotc (npwq, evq(npwx+1,jbnd),1,dvpsi(npwx+1,ibnd), 1)
           ENDDO
        ENDDO
     ENDDO
     !
     CALL mp_sum (elphmat, intra_pool_comm)
     !
     !  save all e-ph matrix elements into el_ph_mat
     !
     DO ipert = 1, npe
        DO jbnd = 1, nbnd
           DO ibnd = 1, nbnd
              el_ph_mat (ibnd, jbnd, ik, ipert + imode0) = elphmat (ibnd, jbnd,
ipert)
           ENDDO
        ENDDO
     ENDDO
  ENDDO
  !
  DEALLOCATE (elphmat)
  DEALLOCATE (aux1)
  !
  RETURN
END SUBROUTINE elphel
!
!-----------------------------------------------------------------------
SUBROUTINE elphsum ( )
  !---------------------------------------------------------------------
  !
  !      Sum over BZ of the electron-phonon matrix elements el_ph_mat
  !      Original routine written by Francesco Mauri, modified by PG
  !      New version by  Malgorzata Wierzbowska
  !
  USE kinds,       ONLY : DP
  USE constants,   ONLY : pi, rytoev, degspin
  USE ions_base,   ONLY : nat, ityp, tau
  USE cell_base,   ONLY : at, bg
  USE lsda_mod,    ONLY: isk, nspin
  USE klist,       ONLY: nks, nkstot, xk, wk, nelec
  USE start_k,     ONLY: nk1, nk2, nk3
  USE symm_base,   ONLY: s, irt, nsym, invs
  USE noncollin_module, ONLY: nspin_lsda, nspin_mag
  USE wvfct,       ONLY: nbnd, et
  USE parameters,  ONLY : npk
  USE el_phon,     ONLY : el_ph_mat
  USE qpoint,      ONLY : xq, nksq
  USE modes,       ONLY : u, minus_q, nsymq, rtau
  USE dynmat,      ONLY : dyn, w2
  USE io_global,   ONLY : stdout, ionode, ionode_id
  USE mp_global,   ONLY : my_pool_id, npool, kunit, intra_image_comm
  USE mp,          ONLY : mp_bcast
  USE control_ph,  ONLY : lgamma, tmp_dir_phq, xmldyn
  USE save_ph,     ONLY : tmp_dir_save
```

```
  USE io_files,    ONLY : prefix, tmp_dir, seqopn
!!!!CRB
  USE mp_global,ONLY: intra_pool_comm,mpime,nproc,npool
!!!!CRB

  !
  IMPLICIT NONE
  ! epsw = 20 cm^-1, in Ry
  REAL(DP), PARAMETER :: Rytocm1 = 109737.57990d0, RytoGHz = 3.289828D6, &
       RytoTHz = RytoGHz/1000.d0, epsw = 20.d0 / Rytocm1, eps = 1.0d-6
  !
  INTEGER :: iuna2Fsave  = 40
  !
  REAL(DP), allocatable :: gam(:,:), lamb(:,:)
  !
  ! Quantities ending with "fit" are relative to the "dense" grid
  !
  REAL(DP), allocatable :: xkfit(:,:)
  REAL(DP), allocatable, target :: etfit(:,:), wkfit(:)
  INTEGER :: nksfit, nk1fit, nk2fit, nk3fit, nkfit, nksfit_real
  INTEGER, allocatable :: eqkfit(:), eqqfit(:), sfit(:)
  !
  integer :: nq, isq (48), imq
  ! nq :  degeneracy of the star of q
  ! isq: index of q in the star of a given sym.op.
  ! imq: index of -q in the star of q (0 if not present)
  real(DP) :: sxq (3, 48)
  ! list of vectors in the star of q
  !
  ! workspace used for symmetrisation
  !
  COMPLEX(DP), allocatable :: g1(:,:,:), g2(:,:,:), g0(:,:), gf(:,:,:)
  COMPLEX(DP), allocatable :: point(:), noint(:), ctemp(:)
  COMPLEX(DP) :: dyn22(3*nat,3*nat)
  !
  INTEGER :: ik, ikk, ikq, isig, ibnd, jbnd, ipert, jpert, nu, mu, &
       vu, ngauss1, nsig, iuelph, ios, i,k,j, ii, jj
  INTEGER :: nkBZ, nti, ntj, ntk, nkr, itemp1, itemp2, nn, &
       qx,qy,qz,iq,jq,kq
  INTEGER, ALLOCATABLE :: eqBZ(:), sBZ(:)
  REAL(DP) :: weight, wqa, w0g1, w0g2, degauss1, dosef, &
       ef1, lambda, gamma
  REAL(DP) :: deg(10), effit(10), dosfit(10), etk, etq
  REAL(DP), EXTERNAL :: dos_ef, efermig, w0gauss
  character(len=80) :: name
  LOGICAL  :: exst, xmldyn_save
  !
  COMPLEX(DP) :: el_ph_sum (3*nat,3*nat)

  COMPLEX(DP), POINTER :: el_ph_mat_collect(:,:,:,:)
  REAL(DP), ALLOCATABLE :: xk_collect(:,:), wk_collect(:)
  REAL(DP), POINTER :: wkfit_dist(:), etfit_dist(:,:)
  INTEGER :: nksfit_dist, rest, kunit_save
  INTEGER :: nks_real, ispin, nksqtot
!CRB
```

```
  COMPLEX(DP), allocatable :: gfcurr(:,:,:,:)
  COMPLEX(DP), allocatable :: www(:,:)
  Integer :: ieng,neng
  REAL(DP), allocatable, dimension( : ) :: w0g2curr
  Real( DP ) :: CBMeng,GAPeng,stepeng
  Character(36) :: filname
  Real( DP ),Allocatable,Dimension( :,:,: ) :: gamcurr,lamcurr,&
       gamcurrabs, lamcurrabs, &
       gamcurremi, lamcurremi
  Real( DP ),Allocatable,Dimension( :,: )   :: ecurrent , doscurrent
  Real( DP )                                :: nbose , kernl

! CRB: Read CBM, BG, and no. of energy intervals from file
  If( mpime.Eq.ionode_id )Then
     Open( Unit=4001, File='phin.aux' )
     Read( 4001,* ) CBMeng
     Read( 4001,* ) GAPeng
     Read( 4001,* ) neng
     Close( 4001 )
  End If
  CALL mp_bcast (CBMeng, ionode_id, intra_image_comm)
  CALL mp_bcast (GAPeng, ionode_id, intra_image_comm)
  CALL mp_bcast (neng, ionode_id, intra_image_comm)
! CRB: Set maximum energy as 1.1 * BG
  GAPeng = GAPeng * 1.1D0
! CRB: convert to Ry units:
  CBMeng  = CBMeng / RytoeV
  GAPeng  = GAPeng / RytoeV
! CRB: determine energy interval
  stepeng = GAPeng / DBLE( neng-1 )
  If( mpime.Eq.0 )Then
     Write( *,'(A)' ) "Scattering rates to be calculated at energies: "
     Do ieng=0,neng-1
        Write( *,'(I5,A,F10.5,A)' ) ieng+1,": ",&
             (CBMeng+DBLE(ieng)*stepeng)*RytoeV," eV"
     End Do
  End If

  !
  WRITE (6, '(5x,"electron-phonon interaction  ..."/)')
  ngauss1 = 0
  nsig = 10

!CRB: allocate arrays
  Allocate( ecurrent( neng,nsig ) , doscurrent( neng,nsig ) , w0g2curr( neng ) )
  Allocate( gfcurr(3*nat,3*nat,neng,nsig) , gamcurr(3*nat,neng,nsig) , &
       lamcurr(3*nat,neng,nsig) )
!CRB: gcabs,gcemi,lcabs,lcemi contain the absn,emisn rates and absn,emisn
energy loss rates, resp.
  allocate (gamcurrabs(3*nat,neng,nsig), lamcurrabs(3*nat,neng,nsig))
  allocate (gamcurremi(3*nat,neng,nsig), lamcurremi(3*nat,neng,nsig))

  Do ieng=1,neng
     ecurrent( ieng,: ) = CBMeng+DBLE(ieng-1)*stepeng
  End Do
```

```
  gfcurr(:,:,:,:) = 0.0D0


  ALLOCATE(xk_collect(3,nkstot))
  ALLOCATE(wk_collect(nkstot))
  IF (npool==1) THEN
!
!  no pool, just copy old variable on the new ones
!
     nksqtot=nksq
     xk_collect(:,1:nks) = xk(:,1:nks)
     wk_collect(1:nks) = wk(1:nks)
     el_ph_mat_collect => el_ph_mat
  ELSE
!
!  pools, allocate new variables and collect the results. All the rest
!  remain unchanged.
!
     IF (lgamma) THEN
        nksqtot=nkstot
     ELSE
        nksqtot=nkstot/2
     ENDIF
     ALLOCATE(el_ph_mat_collect(nbnd,nbnd,nksqtot,3*nat))
     CALL xk_wk_collect(xk_collect,wk_collect,xk,wk,nkstot,nks)
     CALL el_ph_collect(el_ph_mat,el_ph_mat_collect,nksqtot,nksq)
  ENDIF
  !
  ! read eigenvalues for the dense grid
  ! FIXME: this might be done from the xml file, not from a specialized file
  ! parallel case: only first node reads
  !
  IF ( ionode ) THEN
     tmp_dir=tmp_dir_save
     CALL seqopn( iuna2Fsave, 'a2Fsave', 'FORMATTED', exst )
     tmp_dir=tmp_dir_phq
     READ(iuna2Fsave,*) ibnd, nksfit
  END IF
  !
  CALL mp_bcast (ibnd, ionode_id, intra_image_comm)
  CALL mp_bcast (nksfit, ionode_id, intra_image_comm)
  if ( ibnd /= nbnd ) call errore('elphsum','wrong file read',iuna2Fsave)
  allocate (etfit(nbnd,nksfit), xkfit(3,nksfit), wkfit(nksfit))
  !
  IF ( ionode ) THEN
     READ(iuna2Fsave,*) etfit
     READ(iuna2Fsave,*) ((xkfit(i,ik), i=1,3), ik=1,nksfit)
     READ(iuna2Fsave,*) wkfit
     READ(iuna2Fsave,*) nk1fit, nk2fit, nk3fit
     CLOSE( UNIT = iuna2Fsave, STATUS = 'KEEP' )
  END IF
  !
  ! broadcast all variables read
  !
  CALL mp_bcast (etfit, ionode_id, intra_image_comm)
```

```
  CALL mp_bcast (xkfit, ionode_id, intra_image_comm)
  CALL mp_bcast (wkfit, ionode_id, intra_image_comm)
  CALL mp_bcast (nk1fit, ionode_id, intra_image_comm)
  CALL mp_bcast (nk2fit, ionode_id, intra_image_comm)
  CALL mp_bcast (nk3fit, ionode_id, intra_image_comm)
  !
  nkfit=nk1fit*nk2fit*nk3fit
  !
  ! efermig and dos_ef require scattered points and eigenvalues
  ! isk is neither read nor used. phonon with two Fermi energies is
  ! not yet implemented.
  !
  nksfit_dist  = ( nksfit / npool )
  rest = ( nksfit - nksfit_dist * npool )
  IF ( ( my_pool_id + 1 ) <= rest ) nksfit_dist = nksfit_dist + 1
  kunit_save=kunit
  kunit=1

#ifdef __MPI
  ALLOCATE(etfit_dist(nbnd,nksfit_dist))
  ALLOCATE(wkfit_dist(nksfit_dist))
  CALL poolscatter( 1, nksfit, wkfit, nksfit_dist, wkfit_dist )
  CALL poolscatter( nbnd, nksfit, etfit, nksfit_dist, etfit_dist )
#else
   wkfit_dist => wkfit
   etfit_dist => etfit
#endif
  !
  do isig=1,nsig
     !
     ! recalculate Ef = effit and DOS at Ef N(Ef) = dosfit using dense grid
     ! for value "deg" of gaussian broadening
     !
     deg(isig) = isig * 0.005d0
     !
!!$     effit(isig) = efermig &
!!$          ( etfit_dist, nbnd, nksfit_dist, nelec, wkfit_dist, &
!!$              deg(isig), ngauss1, 0, isk)
!!$     dosfit(isig) = dos_ef ( ngauss1, deg(isig), effit(isig), etfit_dist, &
!!$          wkfit_dist, nksfit_dist, nbnd) / 2.0d0
!CRB: DOS for current elec energy
     Do ieng=1,neng
         doscurrent(ieng,isig) = dos_ef ( ngauss1, deg(isig), &
             ecurrent(ieng,isig), etfit_dist, &
             wkfit_dist, nksfit_dist, nbnd) / 2.0d0
     End Do
!
  enddo
#ifdef __MPI
  DEALLOCATE(etfit_dist)
  DEALLOCATE(wkfit_dist)
#endif
  kunit=kunit_save
  allocate (eqkfit(nkfit), eqqfit(nkfit), sfit(nkfit))
  !
```

```
! map k-points in the IBZ to k-points in the complete uniform grid
!
nksfit_real=nksfit/nspin_lsda
call lint ( nsym, s, .true., at, bg, npk, 0,0,0, &
     nk1fit,nk2fit,nk3fit, nksfit_real, xkfit, 1, nkfit, eqkfit, sfit)
deallocate (sfit, xkfit, wkfit)
!
! find epsilon(k+q) in the dense grid
!
call cryst_to_cart (1, xq, at, -1)
qx = nint(nk1fit*xq(1))
if (abs(qx-nk1fit*xq(1)) > eps) &
     call errore('elphsum','q is not a vector in the dense grid',1)
if (qx < 0) qx = qx + nk1fit
if (qx > nk1fit) qx = qx - nk1fit
qy = nint(nk2fit*xq(2))
if (abs(qy-nk2fit*xq(2)) > eps) &
     call errore('elphsum','q is not a vector in the dense grid',2)
if (qy < 0) qy = qy + nk2fit
if (qy > nk2fit) qy = qy - nk2fit
qz = nint(nk3fit*xq(3))
if (abs(qz-nk3fit*xq(3)) > eps) &
     call errore('elphsum','q is not a vector in the dense grid',3)
if (qz < 0) qz = qz + nk3fit
if (qz > nk3fit) qz = qz - nk3fit
call cryst_to_cart (1, xq, bg, 1)
!
eqqfit(:) = 0
do i=1,nk1fit
   do j=1,nk2fit
      do k=1,nk3fit
         ik = k-1 + (j-1)*nk3fit + (i-1)*nk2fit*nk3fit + 1
         iq = i+qx
         if (iq > nk1fit) iq = iq - nk1fit
         jq = j+qy
         if (jq > nk2fit) jq = jq - nk2fit
         kq = k+qz
         if (kq > nk3fit) kq = kq - nk3fit
         nn = (kq-1)+(jq-1)*nk3fit+(iq-1)*nk2fit*nk3fit + 1
         eqqfit(ik) = eqkfit(nn)
      enddo
   enddo
enddo
!
! calculate the electron-phonon coefficient using the dense grid
!
nti  = nk1fit/nk1
ntj  = nk2fit/nk2
ntk  = nk3fit/nk3
nkBZ  = nk1*nk2*nk3
allocate (eqBZ(nkBZ), sBZ(nkBZ))
!
nks_real=nkstot/nspin_lsda
IF ( lgamma ) THEN
   call lint ( nsymq, s, minus_q, at, bg, npk, 0,0,0, &
```

```
         nk1,nk2,nk3, nks_real, xk_collect, 1, nkBZ, eqBZ, sBZ)
  ELSE
     call lint ( nsymq, s, minus_q, at, bg, npk, 0,0,0, &
          nk1,nk2,nk3, nks_real, xk_collect, 2, nkBZ, eqBZ, sBZ)
  END IF
  !
  allocate (gf(3*nat,3*nat,nsig))
  gf = (0.0d0,0.0d0)
!CRB correct for LO-TO splitting
  IF ((xq(1)==0.0d0).and.(xq(2)==0.0d0).and.(xq(3)==0.0d0))THEN
     write(6,'(5x,"correct w2 at q=0!!"/)')
     w2(3*nat)=5.83563E-6 !NaCl
  END IF

  !
  wqa  = 1.0d0/nkfit
  IF (nspin==1) wqa=degspin*wqa
  !
  do ibnd = 1, nbnd
     do jbnd = 1, nbnd
        allocate (g2(nkBZ*nspin_lsda,3*nat,3*nat))
        allocate (g1(nksqtot,3*nat,3*nat))
        do ik = 1, nksqtot
           do ii = 1, 3*nat
              do jj = 1, 3*nat
                 g1(ik,ii,jj)=CONJG(el_ph_mat_collect(jbnd,ibnd,ik,ii))* &
                      el_ph_mat_collect(jbnd,ibnd,ik,jj)
              enddo    ! ipert
           enddo    !jpert
        enddo   ! ik
        !
        allocate (g0(3*nat,3*nat))
        do i=1,nk1
           do j=1,nk2
              do k=1,nk3
                 do ispin=1,nspin_lsda
                    nn = k-1 + (j-1)*nk3 + (i-1)*nk2*nk3 + 1
                    itemp1 = eqBZ(nn)
                    if (ispin==2) itemp1=itemp1+nksqtot/2
                    g0(:,:) = g1(itemp1,:,:)
                    itemp2 = sBZ(nn)
                    call symm ( g0, u, xq, s, itemp2, rtau, irt, &
                         at, bg, nat)
                    if (ispin==2) nn=nn+nkBZ
                    g2(nn,:,:) = g0(:,:)
                 enddo
              enddo ! k
           enddo !j
        enddo !i
        deallocate (g0)
        deallocate (g1)
        !
        allocate ( point(nkBZ), noint(nkfit), ctemp(nkfit) )
        allocate ( www(nkfit,neng) )
        do jpert = 1, 3 * nat
```

```
           do ipert = 1, 3 * nat
              do ispin=1,nspin_lsda
              !
              point(1:nkBZ) = &
                  g2(1+nkBZ*(ispin-1):nkBZ+nkBZ*(ispin-1),ipert,jpert)
              !
              CALL clinear(nk1,nk2,nk3,nti,ntj,ntk,point,noint)
              !
              do isig = 1, nsig
                 degauss1 = deg(isig)
                 do ik=1,nkfit
                    etk = etfit(ibnd,eqkfit(ik)+nksfit*(ispin-1)/2)
                    etq = etfit(jbnd,eqqfit(ik)+nksfit*(ispin-1)/2)
                    w0g1 = w0gauss( (etq-etk) &
                                  / degauss1,ngauss1) / degauss1
                    Do ieng=1,neng
! CRB: Store value of smearing at current e energy
                       w0g2curr( ieng ) = w0gauss( (ecurrent(ieng,isig)-etk) &
                            / degauss1,ngauss1) / degauss1
                       www( ik,ieng ) = w0g2curr( ieng )
                    End Do
                    ctemp(ik) = noint(ik)* wqa * w0g1 ! * w0g2
                 enddo
!                 Do ik=1,nkfit
                    Do ieng=1,neng
                       gfcurr(ipert,jpert,ieng,isig) = &
                            gfcurr(ipert,jpert,ieng,isig) + &
                            Sum( ctemp(:) * www(:,ieng) )
                    End Do
!                 End Do
              enddo ! isig
              enddo ! ispin
           enddo    ! ipert
        enddo    !jpert
        deallocate (point, noint, ctemp, www)
        deallocate (g2)
        !
     enddo    ! ibnd
  enddo    ! jbnd

  deallocate (eqqfit, eqkfit)
  deallocate (etfit)
  deallocate (eqBZ, sBZ)
!
  allocate (gam(3*nat,nsig), lamb(3*nat,nsig))
  lamb(:,:) = 0.0d0
  gam (:,:) = 0.0d0
  lamcurr( :,:,: ) = 0.0D0
  lamcurrabs( :,:,: ) = 0.0D0
  lamcurremi( :,:,: ) = 0.0D0
  do isig= 1,nsig
     do nu = 1,3*nat
!CRB: set gamma for different values of elec energy
        Do ieng=1,neng
           gamcurr(nu,ieng,isig) = 0.0d0
```

```
           do mu = 1, 3 * nat
              do vu = 1, 3 * nat
                 gamcurr(nu,ieng,isig) = gamcurr(nu,ieng,isig) +
DBLE(conjg(dyn(mu,nu)) * &
                      gfcurr(mu,vu,ieng,isig) * dyn(vu,nu))
              enddo
           enddo
        end Do
        gamcurr(nu,:,isig) = gamcurr(nu,:,isig) *  pi !CRB /2.0d0
        !
        ! the factor 2 comes from the factor sqrt(hbar/2/M/omega) that appears
        ! in the definition of the electron-phonon matrix element g
        ! The sqrt(1/M) factor is actually hidden into the normal modes
        !
        ! gamma = \pi \sum_k\sum_{i,j} \delta(e_{k,i}-Ef) \delta(e_{k+q,j}-Ef)
        !         | \sum_mu z(mu,nu) <psi_{k+q,j}|dvscf_q(mu)*psi_{k,i}> |^2
        ! where z(mu,nu) is the mu component of normal mode nu (z = dyn)
        ! gamma(nu) is the phonon linewidth of mode nu
        !
        ! The factor N(Ef)^2 that appears in most formulations of el-ph
interact
        ! is absent because we sum, not average, over the Fermi surface.
        ! The factor 2 is provided by the sum over spins
        !
        if (sqrt(abs(w2(nu))) > epsw) then
           ! lambda is the adimensional el-ph coupling for mode nu:
           ! lambda(nu)= gamma(nu)/(pi N(Ef) \omega_{q,nu}^2)
           lamb(nu,isig) = gam(nu,isig)/pi/w2(nu)/dosfit(isig)
!CRB: redefine gamma (gamcurr) to be the scattering rate
!CRB: redefine lambda (lamcurr) to be the energy-loss rate
           nbose = 1.0D0/(exp(sqrt(w2(nu))*526.2917D0)-1.0D0)
           Do ieng=1,neng
              kernl = gamcurr(nu,ieng,isig)/doscurrent(ieng,isig)
           ! lamcurr is in units (10E12) eV s^(-1)
           ! Absn --> elecn GAINS energy, Emsn --> elecn LOSES energy
           ! elecn energy LOSS rate = Emsn - Absn
           ! propl. to (n+1) - (n) = 1
              lamcurr(nu,ieng,isig)=&    !
                   kernl*pi*RytoTHz*RytoeV

              lamcurrabs(nu,ieng,isig)=& ! (n)
                   nbose*&
                   kernl*pi*RytoTHz*RytoeV

              lamcurremi(nu,ieng,isig)=& ! (n+1)
                   (nbose+1.0D0)*&
                   kernl*pi*RytoTHz*RytoeV
!
           ! gamcurr is in units (10E-14) s^(-1)
              gamcurr(nu,ieng,isig)=& ! (2n+1)
                   (2.0D0*nbose+1.0D0)*&
                   kernl*pi*RytoTHz/sqrt(w2(nu))

              gamcurrabs(nu,ieng,isig)=& ! (n)
                   (nbose)*&
```

```
                  kernl*pi*RytoTHz/sqrt(w2(nu))

               gamcurremi(nu,ieng,isig)=& ! (n+1)
                    (nbose+1.0D0)*&
                    kernl*pi*RytoTHz/sqrt(w2(nu))

            End Do
         else
            lamb(nu,isig) = 0.0d0
            lamcurr( nu,:,isig ) = 0.0D0
            lamcurrabs( nu,:,isig ) = 0.0D0
            lamcurremi( nu,:,isig ) = 0.0D0
            gamcurr( nu,:,isig ) = 0.0D0
            gamcurrabs( nu,:,isig ) = 0.0D0
            gamcurremi( nu,:,isig ) = 0.0D0
         endif
!CRB:         gam(nu,isig) = gam(nu,isig)*RytoGHz
      enddo  !nu
   enddo  ! isig
   !
   do isig= 1,nsig
      WRITE (6, 9000) deg(isig), ngauss1
!CRB write gamcurr( nu ) for all energies, values of sigma
      Do ieng=1,neng
         WRITE (6, 9005) dosfit(isig), ecurrent(ieng,isig) * rytoev
         do nu=1,3*nat
            WRITE (6, 9099) nu, lamcurr(nu,ieng,isig), gamcurr(nu,ieng,isig)
         enddo
      End Do
!CRB
   enddo
   ! Isaev: save files in suitable format for processing by lambda.x
   write(name,'(A5,f9.6,A1,f9.6,A1,f9.6)') 'elph.',xq(1),'.',xq(2),'.',xq(3)
   open(12,file=name, form='formatted', status='unknown')

   write(12, "(5x,3f14.6,2i6)") xq(1),xq(2),xq(3), nsig, 3*nat
   write(12, "(6e14.6)") (w2(i), i=1,3*nat)

!CRB: Save also values of absn and emisn rates and energy-loss rates
   open(2012,file='Absn-Rates.dat', form='formatted', status='unknown')
   write(2012, "(5x,3f14.6,2i6)") xq(1),xq(2),xq(3), nsig, 3*nat
   write(2012, "(6e14.6)") (w2(i), i=1,3*nat)
   open(2013,file='Emsn-Rates.dat', form='formatted', status='unknown')
   write(2013, "(5x,3f14.6,2i6)") xq(1),xq(2),xq(3), nsig, 3*nat
   write(2013, "(6e14.6)") (w2(i), i=1,3*nat)
!CRB

   do isig= 1,nsig
      WRITE (12, 9000) deg(isig), ngauss1
!CRB write gamcurr( nu ) for all energies, values of sigma
      Do ieng=1,neng
         WRITE (12, 9005) dosfit(isig), ecurrent(ieng,isig) * rytoev
         WRITE (2012, 9005) dosfit(isig), ecurrent(ieng,isig) * rytoev
         WRITE (2013, 9005) dosfit(isig), ecurrent(ieng,isig) * rytoev
         do nu=1,3*nat
```

```
           WRITE (12, 9099) nu, lamcurr(nu,ieng,isig), gamcurr(nu,ieng,isig)
           WRITE (2012, 9099) nu, lamcurrabs(nu,ieng,isig),
gamcurrabs(nu,ieng,isig)
           WRITE (2013, 9099) nu, lamcurremi(nu,ieng,isig),
gamcurremi(nu,ieng,isig)
        enddo
     End Do
!CRB
  enddo
  close (unit=12,status='keep')
  close (unit=2012,status='keep')
  close (unit=2013,status='keep')
  ! Isaev end
  deallocate (gam)
  deallocate (lamb)
  write(stdout,*)
  !
  !    Prepare interface to q2r and matdyn
  !
  call star_q (xq, at, bg, nsym, s, invs, nq, sxq, isq, imq, .TRUE. )
  !
  do isig=1,nsig
     write(name,"(A7,I2)") 'a2Fq2r.',50 + isig
     if (ionode) then
        iuelph = 4
        open(iuelph, file=name, STATUS = 'unknown', FORM = 'formatted', &
             POSITION='append')
     else
        !
        ! this node doesn't write: unit 6 is redirected to /dev/null
        !
        iuelph =6
     end if
     dyn22(:,:) = gf(:,:,isig)
     write(iuelph,*) deg(isig), effit(isig), dosfit(isig)
     IF ( imq == 0 ) THEN
        write(iuelph,*) 2*nq
     ELSE
        write(iuelph,*) nq
     ENDIF
     xmldyn_save=xmldyn
     xmldyn=.FALSE.
     call q2qstar_ph (dyn22, at, bg, nat, nsym, s, invs, &
          irt, rtau, nq, sxq, isq, imq, iuelph)
     xmldyn=xmldyn_save
     if (ionode) CLOSE( UNIT = iuelph, STATUS = 'KEEP' )
  enddo
  deallocate (gf)
  DEALLOCATE(xk_collect)
  DEALLOCATE(wk_collect)
  IF (npool /= 1) DEALLOCATE(el_ph_mat_collect)

  !
9000 FORMAT(5x,'Gaussian Broadening: ',f7.3,' Ry, ngauss=',i4)
9005 FORMAT(5x,'DOS =',f10.6,' states/spin/Ry/Unit Cell at Ef=', &
```

```
          &       f10.6,' eV')
9006 FORMAT(5x,'double delta at Ef =',f10.6)
9010 FORMAT(5x,'lambda(',i2,')=',f8.4,'   gamma=',f8.2,' GHz')
9099 FORMAT(5x,'Eng loss rate (',i2,')= ',f16.8, ' (10^12) eV/s',&
          '   Scatt. rate = ',f16.8,' (10^14) Hz')
  !
  RETURN
END SUBROUTINE elphsum

!-----------------------------------------------------------------------
SUBROUTINE elphsum_simple
  !-----------------------------------------------------------------------
  !
  !      Sum over BZ of the electron-phonon matrix elements el_ph_mat
  !      Original routine written by Francesco Mauri
  !      Rewritten by Matteo Calandra
  !-----------------------------------------------------------------------
  USE kinds, ONLY : DP
  USE constants, ONLY : pi, ry_to_cmm1, rytoev
  USE ions_base, ONLY : nat, ityp, tau,amass,tau, ntyp => nsp, atm
  USE cell_base, ONLY : at, bg, ibrav, celldm
  USE fft_base,  ONLY: dfftp
  USE symm_base, ONLY : s, sr, irt, nsym, time_reversal, invs
  USE klist, ONLY : xk, nelec, nks, wk
  USE wvfct, ONLY : nbnd, et
  USE el_phon
  USE mp_global, ONLY : me_pool, root_pool, inter_pool_comm, npool,
intra_pool_comm
  USE io_global, ONLY : stdout
  USE klist, only : degauss,ngauss
  USE control_flags, ONLY : modenum, noinv
  USE units_ph,       ONLY :iudyn
  USE io_files,  ONLY : prefix
  USE qpoint, ONLY : xq, nksq
  USE dynmat, ONLY : dyn, w2
  USE modes, ONLY : u,rtau, irgq, nsymq,irotmq, minus_q
  USE control_ph, only : lgamma
  USE lsda_mod, only : isk,nspin, current_spin,lsda
  USE mp,        ONLY: mp_sum
  !
  IMPLICIT NONE
  REAL(DP), PARAMETER :: eps = 20_dp/ry_to_cmm1 ! eps = 20 cm^-1, in Ry
  !
  INTEGER :: ik, ikk, ikq, isig, ibnd, jbnd, ipert, jpert, nu, mu, &
       vu, ngauss1, nsig, iuelph, ios, iuelphmat,icnt,i,j,rrho,nt,k
  INTEGER :: na,nb,icar,jcar,iu_sym,nmodes
  INTEGER :: iu_Delta_dyn,iu_analdyn,iu_nonanaldyn
  INTEGER :: io_file_unit
  !   for star_q
  INTEGER :: nsymloc, sloc(3,3,48), invsloc(48), irtloc(48,nat), &
             nqloc, isqloc(48), imqloc
  REAL(DP) :: rtauloc(3,48,nat), sxqloc(3,48)
  !   end of star_q definitions
  REAL(DP) :: weight, w0g1, w0g2, w0gauss, wgauss,degauss1, dosef, &
       ef1, phase_space, lambda, gamma, wg1, w0g,wgp,deltae
```

```
  REAL(DP), EXTERNAL :: dos_ef, efermig
  REAL(DP) xk_dummy(3)
  COMPLEX(DP), allocatable :: phi(:,:,:,:),phi_nonanal(:,:,:,:)
  COMPLEX(DP), allocatable :: dyn_mat_r(:,:),zz(:,:)
  CHARACTER(len=20) :: char_deg
  CHARACTER(len=1) :: char_ng
  character(len=80) :: filelph
  CHARACTER(len=256) ::  file_elphmat
  !
  COMPLEX(DP) :: el_ph_sum (3*nat,3*nat), dyn_corr(3*nat,3*nat)

  INTEGER, EXTERNAL :: find_free_unit

  nmodes=3*nat

  write(filelph,'(A5,f9.6,A1,f9.6,A1,f9.6)') 'elph.',xq(1),'.',xq(2),'.',xq(3)

  ! parallel case: only first node writes
  IF ( me_pool /= root_pool ) THEN
     iuelph = 0
  ELSE
     !
     iuelph = find_free_unit()
     OPEN (unit = iuelph, file = filelph, status = 'unknown', err = &
          100, iostat = ios)
100  CALL errore ('elphon', 'opening file '//filelph, ABS (ios) )
     REWIND (iuelph)
     !
  END IF

  WRITE (iuelph, '(3f15.8,2i8)') xq, nsig, 3 * nat
  WRITE (iuelph, '(6e14.6)') (w2 (nu) , nu = 1, nmodes)


  ngauss1=0
  DO isig = 1, el_ph_nsigma
     !     degauss1 = 0.01 * isig
     degauss1 = el_ph_sigma * isig
     write(stdout,*) degauss1
     el_ph_sum(:,:) = (0.d0, 0.d0)
     phase_space = 0.d0
     !
     ! Recalculate the Fermi energy Ef=ef1 and the DOS at Ef, dosef = N(Ef)
     ! for this gaussian broadening
     !
     ! Note that the weights of k+q points must be set to zero for the
     ! following call to yield correct results
     !

     ef1 = efermig (et, nbnd, nks, nelec, wk, degauss1, el_ph_ngauss, 0, isk)
     dosef = dos_ef (el_ph_ngauss, degauss1, ef1, et, wk, nks, nbnd)
     ! N(Ef) is the DOS per spin, not summed over spin
     dosef = dosef / 2.d0
     !
     ! Sum over bands with gaussian weights
```

```
      !

      DO ik = 1, nksq

         !
         ! see subroutine elphel for the logic of indices
         !
         IF (lgamma) THEN
            ikk = ik
            ikq = ik
         ELSE
            ikk = 2 * ik - 1
            ikq = ikk + 1
         ENDIF
         DO ibnd = 1, nbnd
            w0g1 = w0gauss ( (ef1 - et (ibnd, ikk) ) / degauss1, ngauss1) &
                 / degauss1
            xk_dummy(:)=xk(:,ikk)
            call cryst_to_cart(1,xk_dummy,at,-1)
            DO jbnd = 1, nbnd
               w0g2 = w0gauss ( (ef1 - et (jbnd, ikq) ) / degauss1, ngauss1) &
                    / degauss1
               ! note that wk(ikq)=wk(ikk)
               weight = wk (ikk) * w0g1 * w0g2
               DO jpert = 1, 3 * nat
                  DO ipert = 1, 3 * nat
                     el_ph_sum (ipert, jpert) = el_ph_sum (ipert, jpert)  +
weight * &
                          CONJG (el_ph_mat (jbnd, ibnd, ik, ipert) ) * &
                          el_ph_mat (jbnd, ibnd, ik, jpert)
                  ENDDO
               ENDDO
               phase_space = phase_space+weight
            ENDDO
         ENDDO

      ENDDO

      ! el_ph_sum(mu,nu)=\sum_k\sum_{i,j}[ <psi_{k+q,j}|dvscf_q(mu)*psi_{k,i}>
      !                                  x <psi_{k+q,j}|dvscf_q(nu)*psi_{k,i}>
      !                                  x \delta(e_{k,i}-Ef) \delta(e_{k+q,j}
      !
      ! collect contributions from all pools (sum over k-points)
      !

!      CALL poolreduce (2 * 3 * nat * 3 * nat, el_ph_sum)
!      CALL poolreduce (1, phase_space)
      call mp_sum ( el_ph_sum , inter_pool_comm )
      call mp_sum ( phase_space , inter_pool_comm )

      !
      ! symmetrize el_ph_sum(mu,nu) : it transforms as the dynamical matrix
      !

      CALL symdyn_munu (el_ph_sum, u, xq, s, invs, rtau, irt, irgq, at, &
```

```
          bg, nsymq, nat, irotmq, minus_q)
     !
     WRITE (6, 9000) degauss1, ngauss1
     WRITE (6, 9005) dosef, ef1 * rytoev
     WRITE (6, 9006) phase_space
     IF (iuelph.NE.0) THEN
        WRITE (iuelph, 9000) degauss1, ngauss1
        WRITE (iuelph, 9005) dosef, ef1 * rytoev
     ENDIF

     DO nu = 1, nmodes
        gamma = 0.0
        DO mu = 1, 3 * nat
           DO vu = 1, 3 * nat
              gamma = gamma + DBLE (CONJG (dyn (mu, nu) ) * el_ph_sum (mu, vu)&
                   * dyn (vu, nu) )
           ENDDO
        ENDDO
        write(819+mu,*) gamma
        gamma = pi * gamma / 2.d0
        write(6,*) 'gamma*pi/2=',gamma
        !
        ! the factor 2 comes from the factor sqrt(hbar/2/M/omega) that appears
        ! in the definition of the electron-phonon matrix element g
        ! The sqrt(1/M) factor is actually hidden into the normal modes
        !
        ! gamma = \pi \sum_k\sum_{i,j} \delta(e_{k,i}-Ef) \delta(e_{k+q,j}-Ef)
        !         | \sum_mu z(mu,nu) <psi_{k+q,j}|dvscf_q(mu)*psi_{k,i}> |^2
        ! where z(mu,nu) is the mu component of normal mode nu (z = dyn)
        ! gamma(nu) is the phonon linewidth of mode nu
        !
        ! The factor N(Ef)^2 that appears in most formulations of el-ph
interact
        ! is absent because we sum, not average, over the Fermi surface.
        ! The factor 2 is provided by the sum over spins
        !
        IF (SQRT (ABS (w2 (nu) ) ) > eps) THEN
           ! lambda is the adimensional el-ph coupling for mode nu:
           ! lambda(nu)= gamma(nu)/(pi N(Ef) \omega_{q,nu}^2)
           lambda = gamma / pi / w2 (nu) / dosef
        ELSE
           lambda = 0.0
        ENDIF
        ! 3.289828x10^6 is the conversion factor from Ry to GHz
        WRITE (6, 9010) nu, lambda, gamma * 3.289828d6
        IF (iuelph.NE.0) WRITE (iuelph, 9010) nu, lambda, gamma * &
             3.289828d6
     ENDDO
  ENDDO


9000 FORMAT(5x,'Gaussian Broadening: ',f7.3,' Ry, ngauss=',i4)
9005 FORMAT(5x,'DOS =',f10.6,' states/spin/Ry/Unit Cell at Ef=', &
          &       f10.6,' eV')
9006 FORMAT(5x,'double delta at Ef =',f10.6)
```

```
9010 FORMAT(5x,'lambda(',i2,')=',f8.4,'   gamma=',f8.2,' GHz')
  !
  !
  IF (iuelph.NE.0) CLOSE (unit = iuelph)
  RETURN



     !          call star_q(x_q(1,iq), at, bg, nsym , s , invs , nq, sxq, &
     !               isq, imq, .FALSE. )


END SUBROUTINE elphsum_simple




!-----------------------------------------------------------------------
FUNCTION dos_ef (ngauss, degauss, ef, et, wk, nks, nbnd)
  !-----------------------------------------------------------------------
  !
  USE kinds, ONLY : DP
  USE mp_global, ONLY : inter_pool_comm, intra_pool_comm
  USE mp,        ONLY : mp_sum
  IMPLICIT NONE
  REAL(DP) :: dos_ef
  INTEGER :: ngauss, nbnd, nks
  REAL(DP) :: et (nbnd, nks), wk (nks), ef, degauss
  !
  INTEGER :: ik, ibnd
  REAL(DP), EXTERNAL :: w0gauss
  !
  !     Compute DOS at E_F (states per Ry per unit cell)
  !
  dos_ef = 0.0d0
  DO ik = 1, nks
     DO ibnd = 1, nbnd
        dos_ef = dos_ef + wk (ik) * w0gauss ( (et (ibnd, ik) - ef) &
             / degauss, ngauss) / degauss
     ENDDO
  ENDDO
  !
  !    Collects partial sums on k-points from all pools
  !
  CALL mp_sum ( dos_ef, inter_pool_comm )
  !
  RETURN
END FUNCTION dos_ef

!a2F
subroutine lint ( nsym, s, minus_q, at, bg, npk, k1,k2,k3, &
     nk1,nk2,nk3, nks, xk, kunit, nkBZ, eqBZ, sBZ)
  !-----------------------------------------------------------------------
  !
  ! Find which k-points of a uniform grid are in the IBZ
```

```
!
use kinds, only : DP
implicit none
integer, intent (IN) :: nks, nsym, s(3,3,48), npk, k1, k2, k3, &
     nk1, nk2, nk3, kunit, nkBZ
logical, intent (IN) :: minus_q
real(kind=DP), intent(IN):: at(3,3), bg(3,3), xk(3,npk)
integer, INTENT(OUT) :: eqBZ(nkBZ), sBZ(nkBZ)
!
real(kind=DP) :: xkr(3), deltap(3), deltam(3)
real(kind=DP), parameter:: eps=1.0d-5
real(kind=DP), allocatable :: xkg(:,:), xp(:,:)
integer ::  i,j,k, ns, n, nk
integer :: nkh
!
! Re-generate a uniform grid of k-points xkg
!
allocate (xkg( 3,nkBZ))
!
if(kunit < 1 .or. kunit > 2) call errore('lint','bad kunit value',kunit)
!
! kunit=2: get only "true" k points, not k+q points, from the list
!
nkh = nks/kunit
allocate (xp(3,nkh))
if (kunit == 1) then
   xp(:,1:nkh) = xk(:,1:nkh)
else
   do j=1,nkh
      xp(:,j) = xk(:,2*j-1)
   enddo
end if
do i=1,nk1
   do j=1,nk2
      do k=1,nk3
         n = (k-1) + (j-1)*nk3 + (i-1)*nk2*nk3 + 1
         xkg(1,n) = dble(i-1)/nk1 + dble(k1)/2/nk1
         xkg(2,n) = dble(j-1)/nk2 + dble(k2)/2/nk2
         xkg(3,n) = dble(k-1)/nk3 + dble(k3)/2/nk3
      end do
   end do
end do

call cryst_to_cart (nkh,xp,at,-1)

do nk=1,nkBZ
   do n=1,nkh
      do ns=1,nsym
         do i=1,3
            xkr(i) = s(i,1,ns) * xp(1,n) + &
                     s(i,2,ns) * xp(2,n) + &
                     s(i,3,ns) * xp(3,n)
         end do
         do i=1,3
            deltap(i) = xkr(i)-xkg(i,nk) - nint (xkr(i)-xkg(i,nk) )
```

```
            deltam(i) = xkr(i)+xkg(i,nk) - nint (xkr(i)+xkg(i,nk) )
          end do
          if ( sqrt ( deltap(1)**2 + &
                      deltap(2)**2 + &
                      deltap(3)**2 ) < eps .or. ( minus_q .and. &
            sqrt ( deltam(1)**2 +  &
                   deltam(2)**2 +  &
                   deltam(3)**2 ) < eps ) ) then
            eqBZ(nk) = n
            sBZ(nk) = ns
            go to 15
          end if
        end do
     end do
     call errore('lint','cannot locate  k point  xk',nk)
15   continue
  end do

  do n=1,nkh
     do nk=1,nkBZ
        if (eqBZ(nk) == n) go to 20
     end do
     !  this failure of the algorithm may indicate that the displaced grid
     !  (with k1,k2,k3.ne.0) does not have the full symmetry of the lattice
     call errore('lint','cannot remap grid on k-point list',n)
20   continue
  end do

  deallocate(xkg)
  deallocate(xp)

  return
end subroutine lint
```

APPENDIX D
MONTE CARLO SIMULATION MATLAB CODE

```
%%%%%%%%%%%%%%%%%%%%%%%%%%%%%%%%%%%%%%%%%%%%%%%%%%%
% Monte Carlo Simulation of Crystalline PE with 10% nano-cavities%%%%%%%%%%%%
%%%%%%%%%%%%%%%%%%%%%%%%%%%%%%%%%%%%%%%%%%%%%%%%%%%%cl
ear all;
global aaaa n m e Energyf nelectron_right nelectron_max Original_data ...,
    nanocavity center_x center_y center_z n_nano radius_nano Eg
    %r_n radius of nano_cavity
    %x0_n y0_n z0_n Cartesian center of nano cavity
load('D:\LAPTOP ying work\MonteCarlo Matlab\ying MC code pe\MC PE Original data.mat')
nanocavity=0; % if no nano cavity exists, set nanocavity==0
%nanocavity=1; % if there exists nano cavity, set nanocavity==1
Original_data=MC_PE_Original_data; % where phonon frequencies stored
nstep=20000; % maximum step number
nelectron_start=5; % number of start electrons
nelectron_max=10000; %maximum electrons numbers
nelectron_right=0;   %number of the electrons which go through the film
%%%%%%%%%%%%%%%%%%%%%%%%%%%%%%%%%%%%%%%%
m=9.109e-31; %mass of free electron
e=1.602e-19; %element charge
F=1e9; % electric field
Eg=8.8;% experimental bandgap of PE
L1=2e-8; % L1, L2, L3 dimensions of film
L2=2e-8;
```

```
L3=5e-8;
filmthickness=L3; %film thickness
%%%%%%%%%%%%%%%%%%%%%%%%%%%%%%%%%%%%%%%%%%%%%%%%%%%%%%%%%%%%%%%%%%%%%%%ini
tial_K=1;
struc.F=F;
struc.m=m;
struc.e=e;
struc.filmthickness=filmthickness;
struc.taomax=3.2491e-015;
struc.nstep=nstep;
struc.initial_K=initial_K;
struc.generation=0;
struc.order=0;
n=0;
%initiate variables x,y,z,vx,vy,vz,v
split_number=zeros(1,nelectron_start);
% set random initial position
x=L1*(2*rand(nelectron_start,nstep)-1); %random x position
y=L2*(2*rand(nelectron_start,nstep)-1); %random y position
% x=zeros(nelectron_start,nstep);  % zero x position
% y=zeros(nelectron_start,nstep);  % zero y position
z=zeros(nelectron_start,nstep); % zero z position
% set initial velocity of electrons as zero
vx=zeros(nelectron_start,nstep);
vy=zeros(nelectron_start,nstep);
```

```
vz=zeros(nelectron_start,nstep);
v=zeros(nelectron_start,nstep);
%%%%%%%%%%%%%%%%%%%%%%%%%%
%Nano-Cavity parameters
%%%%%%%%%%%%%%%%%%%%%%%%%%%%%%%%%%%%%%%%%%
V_film=2*L1*2*L2*L3;
ratio_nano=0.1;  % 10% nano cavity
radius_nano=2.5e-9;
V_nano=4*pi*radius_nano^3/3;
n_nano=V_film*ratio_nano/V_nano;
if nanocavity==1
for i=1:n_nano
[x_n,y_n,z_n] = sphere(10);
center_x(i)=L1*(2*rand(1)-1);
center_y(i)=L2*(2*rand(1)-1);
center_z(i)=L3*(rand(1));
end
end
%set the initial energy of start electron
% iniE=5; %set initial energy5eV
% vz(:,1)=sqrt(2*(iniE*e)/m);
% v(:,1)=sqrt(2*(iniE*e)/m);
for i=1:nelectron_start
   [x_step,y_step,z_step,vx_step,vy_step,vz_step,v_step,split_number(i),length]= ...,
      oneelectron(x(i,1),y(i,1),z(i,1),vx(i,1),vy(i,1),vz(i,1),v(i,1),struc,split_number(i));
```

```
    x(i,1:length)=x_step;
    y(i,1:length)=y_step;
    z(i,1:length)=z_step;
    vx(i,1:length)=vx_step;
    vy(i,1:length)=vy_step;
    vz(i,1:length)=vz_step;
    v(i,1:length)=v_step;
    if nelectron_right >= nelectron_max
        break;
    end
end
%display maximum generation%%%%%%%%%%%%%%
[I,L]=size(aaaa);
 for i=1:L
    maxgene(i)=aaaa(i).gene;
     maxgene=max(maxgene(:));
end
 disp(' maximum generation is ');
 disp(maxgene);
% draw nano_cavity in 3D figure
%%%%%%%%%%%%%%%%%%%%%%%%%%%%%%%%%%%%%%%%
figure(1); %3D figure
lightGrey = 0.8*[1 1 1]; % It looks better if the lines are lighter
%center=rand(n_nano,3);
if nanocavity==1
```

```
for i=1:n_nano
[x_n,y_n,z_n] = sphere(10);
x_n = x_n*radius_nano + center_x(i);
y_n = y_n*radius_nano + center_y(i);
z_n = z_n*radius_nano + center_z(i);
surface(1e9*x_n,1e9*y_n,1e9*z_n,'FaceColor', 'none','EdgeColor',lightGrey);
end
end
daspect([1,1,1]);
% draw electron trajectory in 3D; different generation use different color
%%%%%%%%%%%%%%%%%%%%%%%%%%%%%%%%%%%%%%%%%%%%%%%%%%%%%%%%%%%%%%%%%%%%%%%
 Colorpool = {'k','b','r','g','y','c','m',[.5 .6 .7],[.8 .2 .6], ...,
    'k','b','r','g','y','c','m',[.5 .6 .7],[.8 .2 .6], ...,
    'k','b','r','g','y','c','m',[.5 .6 .7],[.8 .2 .6], ...,
    'k','b','r','g','y','c','m',[.5 .6 .7],[.8 .2 .6]};
 for i=1:L
 figure(1); %draw 3D trajectory
 hold on ;
plot3(1e9*aaaa(i).para(1,:),1e9*aaaa(i).para(2,:),1e9*aaaa(i).para(3,:),'color',Colorpool{aaaa(i).
gene},'marker','+');
 plot3(0,0,0,'r*');
 grid on;
 view(3);
end
title('3D trajectories of electrons in PE','FontSize', 14);
```

```
set(gca,'FontSize',12);
%axis([-20 20 -20 20 0 50]);
xlabel('length/ nm','FontSize', 14);
ylabel('width/ nm','FontSize', 14);
zlabel('thickness/ nm','FontSize', 14);
%%%%%%%%%%%%%%%%%%%%%%%%%%%%%%%%%%%%%%%%%%%%%%%%%%%%%%%%%%%%%%%%%%%%%%%%%%%%%%%%
%2D draw nano cavity%%%%%%%%%%%%%%%%%%%%
figure(2); %2D
if nanocavity==1
for i=1:n_nano
 th = 0:pi/1000:2*pi;
 x_2d = radius_nano * cos(th) + center_x(i);
 z_2d= radius_nano * sin(th) + center_z(i);
 plot(1e9*z_2d,1e9*x_2d,'Color',lightGrey);
 hold on;
end
end
daspect([1,1,1]);
%2D draw trajectoreis%%%%%%%%%%
[I,L]=size(aaaa);
 Colorpool = {'k','b','r','g','y','c','m',[.5 .6 .7],[.8 .2 .6], ...,
    'k','b','r','g','y','c','m',[.5 .6 .7],[.8 .2 .6], ...,
    'k','b','r','g','y','c','m',[.5 .6 .7],[.8 .2 .6], ...,
    'k','b','r','g','y','c','m',[.5 .6 .7],[.8 .2 .6]};
for i=1:L
```

```
    figure(2);%2D trajectory
    hold on;
    plot(1e9*aaaa(i).para(3,:),1e9*aaaa(i).para(1,:),'color',Colorpool{aaaa(i).gene},'marker','+');
end
figure(2); %2D
title('2D Projection of 3D Electron Path in PE','FontSize', 14);
set(gca,'FontSize',12)
xlabel('Thickness/ nm','FontSize', 14);
ylabel('Length/ nm','FontSize', 14);
%axis([0 50 -20 20]);
%%%%%%%%%%%%%%%%%%%%%%%%%%%%%%%%%%%%%%%%%%%%%%%%%%%%%%%
%plot energy vs distance figure(3)
[I,L]=size(aaaa);
for i=1:L
    figure(3);
    hold on;
    plot(1e9*aaaa(i).para(3,:),aaaa(i).para(8,:),'.');
end
figure(3);
xlabel('Distance/ nm','FontSize', 14);
ylabel('Electron Energy/ eV','FontSize', 14);
title('Electron Enenrgy vs Distance','FontSize', 14);
set(gca,'FontSize',12);
%axis([0 50 0 10]);
%plot histogram of electron energy
```

```
figure(4);
[I,L]=size(aaaa);
energycount=zeros(0);
for i=1:L
    energycount=cat(2,energycount,aaaa(1,i).para(8,:));
end
% energycount=[aaaa(1,1).para(8,:),aaaa(1,2).para(8,:),aaaa(1,3).para(8,:)];
 energyspan=0:0.1:10;
[nenergy,xout] = hist(energycount,energyspan);
sumn=sum(nenergy);
bar(xout,nenergy/sumn);
%histfit(energycount);
%[muhat,sigmahat] = normfit(energycount)
xlabel('Electron Energy/ eV','FontSize', 14);
ylabel('Probability Density /eV','FontSize', 14);
title('Probability Density of Electron Energy','FontSize', 14);
set(gca,'FontSize',12);
axis([0 10 0 0.16]);
%legend('Histogram','FontSize', 14);
%figure 5 plot the average electron energy vs distance
figure(5);
[I,L]=size(aaaa);
energycount=zeros(0);
distancecount=zeros(0);
velocitycount=zeros(0);
```

```
for i=1:L
   energycount=cat(2,energycount,aaaa(1,i).para(8,:));
   distancecount=cat(2,distancecount,aaaa(1,i).para(3,:));
   mean_energy=mean(energycount);
end
% find average velocity
for i=1:L
   velocitycount=cat(2,velocitycount,aaaa(1,i).para(7,:));
   mean_velocity=mean(velocitycount(velocitycount~=0));
end
disp(' average velocity is ');
disp(mean_velocity);
ave_1=mean(energycount(find(distancecount<5e-9)));
ave_2=mean(energycount(find(5e-9<=distancecount & distancecount<10e-9)));
ave_3=mean(energycount(find(10e-9<=distancecount & distancecount<15e-9)));
ave_4=mean(energycount(find(15e-9<=distancecount & distancecount<20e-9)));
ave_5=mean(energycount(find(20e-9<=distancecount & distancecount<25e-9)));
ave_6=mean(energycount(find(25e-9<=distancecount & distancecount<30e-9)));
ave_7=mean(energycount(find(30e-9<=distancecount & distancecount<35e-9)));
ave_8=mean(energycount(find(35e-9<=distancecount & distancecount<40e-9)));
ave_9=mean(energycount(find(40e-9<=distancecount & distancecount<45e-9)));
ave_10=mean(energycount(find(45e-9<=distancecount & distancecount<50e-9)));
distance_ave=[2.5 7.5 12.5 17.5 22.5 27.5 32.5 37.5 42.5 47.5];
ave_energy=[ave_1 ave_2 ave_3 ave_4 ave_5 ave_6 ave_7 ave_8 ave_9 ave_10];
bar(distance_ave,ave_energy);
```

```
hold on;
disp(' mean electron energy is ');
disp(mean_energy);
mean_energy=mean_energy*ones(11);
distance_ave=[0 5 10 15 20 25 30 35 40 45 50];
plot(distance_ave,mean_energy,'r','LineWidth',2.5);
set(gca,'FontSize',12)
xlabel('Distance/ nm','FontSize', 14);
ylabel('Average Electron Energy/ eV','FontSize', 14);
title('Average Electron Enenrgy vs Distance','FontSize', 14);
%%%%%%%%%%%%%%%%%%%%%%%%%%%%%%%%%%%%%%%%%%%%%%%%%%%
%Function oneelectron.m calculate the behavior of one electron
function
[X,Y,Z,VX,VY,VZ,V,Split_number,j]=oneelectron(x,y,z,vx,vy,vz,v,struc,split_number)
global aaaa n Energyf nelectron_right nelectron_start nelectron_max nanocavity center_x
center_y center_z Eg;
% pass constant%%%%%%%%%
e=struc.e;
F=struc.F;
m=struc.m;
a=F*e/m;
filmthickness=struc.filmthickness;
taomax=struc.taomax;
K=struc.initial_K;
order=struc.order;
```

```
Nstep=struc.nstep;
temp=[1:36*30];
%give initial value
X(1)=x;
Y(1)=y;
Z(1)=z;
VX(1)=vx;
VY(1)=vy;
VZ(1)=vz;
V(1)=v;
Energy(1)=0.5*m*V(1)^2;
EnergyE(1)=0.5*m*V(1)^2/e;
%%%%%%%%%%%%%%%%%%%%%%%%%%%%%%%%%%%%%%%%%%%%%%%
if Z(1)==0;  %if start moving from the start point z=0
   Split_number=0;
else
   Split_number=split_number;
end
   for j=1:Nstep
 % move freely inside nano-cavity
      if nanocavity==1
       [IN_OUT]=nano_cavity(X(j),Y(j),Z(j));
        while IN_OUT==1
           tao=taomax/2;
           [X(j+1),Y(j+1),Z(j+1),VX(j+1),VY(j+1),VZ(j+1),V(j+1),E]= ...,
```

```
        NextPosition(X(j),Y(j),Z(j),VX(j),VY(j),VZ(j),V(j),tao,a);
        j=j+1;
        [IN_OUT]=nano_cavity(X(j),Y(j),Z(j));
        %disp(' inside the nano cavity ');
      end
    end
  %%%%%%%%%%%%%%%%%%%%%%%%%%%%%%%%%%%%%%%%%%%%%
     if nelectron_right >= nelectron_max
        break;
     end
%%%%%%%%%%%%%%%%%%%%%%%%%%%%%%%%%%%%%%%%%%%%%%%%%
% scattering rate data
rate_seg=[307.78  951.12  1038.8  1226  1269.6  1918.5  2305.6  2815.9  2037.4  2580.8  2580.8
2580.8];
  EnergyE_temp=0.5*m*V(j)^2/e;
  Ecurr=round(EnergyE_temp);
  index=floor(Ecurr+1);
  taomax=1e-14/rate_seg(index);
  tao=taomax;
     [X(j+1),Y(j+1),Z(j+1),VX(j+1),VY(j+1),VZ(j+1),V(j+1),E]= ...,
        NextPosition(X(j),Y(j),Z(j),VX(j),VY(j),VZ(j),V(j),tao,a);
     Energy(j+1)=0.5*m*V(j+1)^2;
     EnergyE(j+1)=E;
 %when electron fly out of films
     if Z(j+1)>=filmthickness
```

```
        nelectron_right=nelectron_right+1;
        Energyf(nelectron_right)=Energy(j+1)/e;
        j=j+1;
        generation=Split_number+1;
        n=n+1;
        Mother(1,:)=X;
        Mother(2,:)=Y;
        Mother(3,:)=Z;
        Mother(4,:)=VX;
        Mother(5,:)=VY;
        Mother(6,:)=VZ;
        Mother(7,:)=V;
        Mother(8,:)=0.5*m*V.^2/e;
        aaaa(n).para=Mother;
        aaaa(n).gene=generation;
        break;
    end
% impact ionization happens when electron energy larger than bangap
    if EnergyE(j+1)>=Eg
     Split_number=Split_number+1;
        generation=Split_number;
        n=n+1;
        Mother(1,1:j+1)=X;
        Mother(2,1:j+1)=Y;
        Mother(3,1:j+1)=Z;
```

```
            Mother(4,1:j+1)=VX;
            Mother(5,1:j+1)=VY;
            Mother(6,1:j+1)=VZ;
            Mother(7,:)=V;
            Mother(8,:)=0.5*m*V.^2/e;
            aaaa(n).para=Mother;
            aaaa(n).gene=generation;
            %Nelectron=2;   %%%%%store x y z
            [aaa,bbb,ccc,ddd,eee,fff,ggg]=twoelectrons(X(j+1),Y(j+1),Z(j+1),struc,Split_number);
            j=j+1;
            break;
        end
%if electron fly out of film, record the final electron energy
% end of free flight, scattering happens;
        if EnergyE(j+1)>0 && EnergyE(j+1)< Eg
% determine the polar angle and energy after scattering VX(j+1),VY(j+1),VZ(j+1)
[vx_prime,vy_prime,vz_prime]=scatter_old(VX(j+1),VY(j+1),VZ(j+1));
            VX(j+1)=vx_prime;
            VY(j+1)=vy_prime;
            VZ(j+1)=vz_prime;
            EnergyE(j+1)=0.5*m*(vx_prime^2+vy_prime^2+vz_prime^2)/e;
            V(j+1)=sqrt(2*(EnergyE(j+1)*e)/m);
%               Thta(j+1)=thta_V(index);
%               Phi(j+1)=2*pi*rand(1);
        elseif EnergyE(j+1)<=0
```

```
        %order=order+1;
%           Thta_change(j+1)=0;
%           Phi(j+1)=0;
        j=j+1;    %length
        n=n+1;
        generation=Split_number+1;
        Son(1,1:j)=X;
        Son(2,1:j)=Y;
        Son(3,1:j)=Z;
        Son(4,1:j)=VX;
        Son(5,1:j)=VY;
        Son(6,1:j)=VZ;
        Son(7,1:j)=V;
        Son(8,1:j)=VZ;
        aaaa(n).para=Son;
        aaaa(n).gene=generation;
        break;
      %elseif EnergyE(j+1)>=Eg*e change here
        elseif EnergyE(j+1)>=Eg
        Split_number=Split_number+1;
        generation=Split_number;
        n=n+1;
        Mother(1,1:j+1)=X;
        Mother(2,1:j+1)=Y;
        Mother(3,1:j+1)=Z;
```

```
        Mother(4,1:j+1)=VX;
        Mother(5,1:j+1)=VY;
        Mother(6,1:j+1)=VZ;
        Mother(7,1:j+1)=V;
        Mother(8,1:j+1)=0.5*m*V.^2;
        aaaa(n).para=Mother;
        aaaa(n).gene=generation;
        %Nelectron=2;   %%%%%store x y z
        [aaa,bbb,ccc,ddd,eee,fff]=twoelectrons(X(j+1),Y(j+1),Z(j+1),struc,Split_number);
        j=j+1;
        break;
    end
end
```